PLACE IN RETURN BOX to remove this checkout from your record.
TO AVOID FINES return on or before date due.
MAY BE RECALLED with earlier due date if requested.

DATE DUE	DATE DUE	DATE DUE

5/08 K:/Proj/Acc&Pres/CIRC/DateDue.indd

LAYER-BY-LAYER MODIFICATION OF MEMBRANES FOR ION SEPARATIONS AND CATALYSIS

By

Lu Ouyang

A DISSERTATION

Submitted to
Michigan State University
in partial fulfillment of the requirements
for the degree of

DOCTOR OF PHILOSOPHY

Chemistry

2009

ABSTRACT

LAYER-BY-LAYER MODIFICATION OF MEMBRANES FOR ION SEPARATIONS AND CATALYSIS

By

Lu Ouyang

Layer-by-layer (LBL) adsorption of polycations and polyanions enables the formation of functional thin films containing charged materials ranging from polymer electrolytes to metal nanoparticles and viruses. This adsorption method is applicable to a variety of substrates including flat surfaces, colloids, and membrane pores. This dissertation examines the use of LBL adsorption to modify membranes for specific applications in ion separations and catalysis.

To simultaneously achieve high permeability and selectivity in ion separations, composite membranes contain a thin, selective layer on a thicker porous support that provides mechanical stability. Polyelectrolyte multilayer films adsorbed on porous ultrafiltration membranes present an ultrathin, selective skin that can be tailored for selective removal of multivalent ions in the presence of monovalent ions. Deposition conditions such as the type of terminating layer, the number of bilayers deposited, and the pH and ionic strength of the polyelectrolyte deposition solutions allow for optimization of film properties for selected ion separations. Specifically, five bilayers of poly(styrenesulfonate)/poly(allylamine hydrochloride) (PSS/PAH) on porous alumina supports allow a solution flux of 0.85 $m^3/(m^2\ day)$ at 4.8 bar and exhibit 95% rejection of $MgCl_2$ along with a Na^+/Mg^{2+} selectivity of 22. Films with 4.5 bilayers of PSS/poly(diallyldimethylammonium chloride) (PDADMAC) deposited on alumina

supports show a 98% rejection of phosphate, a chloride/phosphate selectivity of 48, and a solution flux of 2.4 $m^3/(m^2\ day)$. Both membranes exhibit higher fluxes and selectivities than commercially available nanofiltration membranes.

Metal nanoparticles are attractive catalysts due to their high surface area to volume ratio and unique electronic properties. However, their high surface energy often leads to aggregation, which greatly reduces catalytic activity. Alternating adsorption of polyelectrolytes and metal nanoparticles is a simple and effective method to load flat sheet and hollow fiber membranes with metal nanoparticles without nanoparticle aggregation. Catalytic, immobilized nanoparticles such as Au and Pd allow the use of such membranes as catalytic reactors. Hollow fiber membrane reactors coated with films of Au nanoparticle/polyelectrolyte show high catalytic activity in the reduction of 4-nitrophenol with $NaBH_4$, and >99% initial conversion of 4-nitrophenol by HCOONa also takes place in flat sheet membranes containing Pd nanoparticles. However, a slight conversion decline over time takes place in both cases. This conversion decline probably stems from catalyst fouling by byproducts of 4-aminophenol oxidation.

Overall, LBL adsorption provides a simple, versatile method for modifying a variety of porous substrates to create functional membranes. Deposition of polyelectrolyte films on the surface of porous support yields composite membranes for ion separations, whereas adsorption of metal nanoparticle/polyelectrolyte films in porous supports gives catalytic membrane reactors. Further work is needed, however, to decrease the time and processing required in the LBL method and to increase the stability of membrane reactors prepared through LBL deposition.

To my family, for all their love and support

ACKNOWLEDGEMENTS

First and foremost, I would like to thank my advisor, Dr. Merlin Bruening, for his support and guidance during my graduate study. I learned a lot from him, not only about how to be a good scientist, but also about how to be a nice person. I appreciate his patience and encouragement, without which I will not able to finish this degree or dissertation.

I would also like to thank past and present members in the Bruening group. I am especially grateful to Dr. Malaisamy Ramamoorthy and Dr. David M. Dotzauer for their generous help and direct involvement in my research projects. I would also like to express my gratitude to Dr. Lei Sun, Dr. Srividhya Kidambi, Fei Xu, Dr. Jinhua Dai and Dr. Matthew D. Miller for their help and suggestions in my graduate study.

I want to thank Dr. Jean-Francois Lahitte for being my co-advisor and his generous help when I was working in the Chemical Engineering Laboratory at University Paul Sabatier in Toulouse, France. I would also like to thank Dr. Jorge Macanás, who is a great scientist and remarkable colleague to work with.

Lastly, I want to give my special gratitude to my family for all their support and especially my husband, Tao, for his love and encouragement.

TABLE OF CONTENTS

LIST OF TABLES

LIST OF FIGURES

LIST OF SCHEMES

LIST OF ABBREVIATIONS

AFM	Atomic Force Microscopy
AAS	Atomic Absorption Spectroscopy
AuNP	Au Nanoparticle
CP	Coprecipitation
DP	Deposition-Precipitation
EDC	N-(3-dimethylaminopropyl)-N'-ethylcarbodiimide
FESEM	Field Emission Scanning Electron Microscopy
FT-IR	Fourier Transform-Infrared Spectroscopy
GA	Glucoamylase
GOD	Glucose Oxidase
ICP-OES	Inductively Coupled Plasma Optical Emission Spectroscopy
LB	Langmuir-Blodgett
LBL	Layer-by-Layer
MF	Microfiltration
NF	Nanofiltration
NPS	Nanoporous Polymer Spheres
OTS	N-octadecyltrichlorosilane
PAA	Poly(acrylic acid)
PAH	Poly(allylamine hydrochloride)
PAN	Poly(acrylonitrile)
PDADMAC	Poly(diallyldimethylammonium chloride)
PdNP	Pd Nanoparticle

PEI	Poly(ethylenimine)
PEMs	Polyelectrolyte Multilayer Films
PEO	Poly(ethylene oxide)
PES	Poly(ethersulfone)
PET	Poly(ethylene terephthalate)
PMMA	Poly(methyl methacrylate)
PS	Polystyrene
PSS	Poly(tyrenesulfonate)
PSSMA	Poly(4-styrenesulfonic acid-co-maleic acid)
PVC	Poly(vinyl chloride)
PVP	Poly(vinyl pyrrolidone)
PVS	Poly(vinylsulfate)
QCM	Quartz Crystal Microbalance
RO	Reverse Osmosis
SAM	Self assembled monolayer
TALH	Titanium (IV) bis(ammonium lactate) dihydroxide

Chapter 1 Introduction and Background

This dissertation describes the growth of polyelectrolyte multilayer films (PEMs) using layer-by-layer (LBL) adsorption on and in porous supports to form high-flux nanofiltration (NF) membranes and membrane reactors that employ immobilized metal nanoparticles as catalysts. These studies build on previous research and recent developments in the preparation of thin films through LBL adsorption. To put my research in perspective, this introduction first describes the importance of functional thin films and two well-developed thin film preparation methods that have been used for more than 50 years. Subsequently, I focus on the film-formation technique employed in this dissertation, LBL adsorption. This method was developed in the 1990s and has attracted extensive research interest during the past two decades due to its simplicity and versatility. The discussion of the LBL method includes the driving forces involved in assembly, the applicability of this technique to substrates of different geometries, and recent developments in optimization of the LBL process. Because my work aims at using LBL adsorption to create nanofiltration and catalytic membranes, I also present applications of the LBL method in these areas. Finally, I give a brief outline of this dissertation.

1.1. Functional Thin Films

1.1.1. Applications of Functional Thin Films

Functional thin films have important practical applications in a number of areas including separation membranes, sensors, and solar cells. Thus, optimization of the

methods for preparation of functional thin films could potentially improve the efficiency of a wide range of practical devices. Ultrathin films with thicknesses on the nm scale are particularly attractive because their minimal thickness allows the use of relatively expensive materials and may also improve device performance. In the case of sensors, a thinner sensing layer usually results in a lower response time,[1] whereas in separation membranes, ultrathin membrane skins allow high permeation rates.[2] Because fabrication of ultrathin film on solid surfaces is vital for creating devices ranging from membranes to transistors, various methods have been developed for thin film preparation.[3]

1.2. Methods for Preparing Ultrathin Functional Films

A partial list of strategies for thin film fabrication includes spin-coating,[4-9] physical/chemical vapor deposition,[10-16] electrospray deposition,[17-21] sol-gel processing,[22-26] sputtering,[27-29] and pulsed laser deposition.[30-33]. Here, I focus on three methods for forming ultrathin organic films with thicknesses on nanometer scale. Two of them, the Langmuir-Blodgett (LB) technique and adsorption of self-assembled monolayer (SAMs), are well established and have been widely used for more than 50 years. The other strategy, LBL adsorption emerged in the 1990s and progressed rapidly due to the ease of film formation and film versatility.

1.2.1. Langmuir-Blodgett (LB) Technique

1.2.1.1. History and Background of the LB Technique

The Langmuir-Blodgett (LB) technique yields ordered monomolecular films with a densely packed structure and precisely controlled thickness.[34] Irving Langmuir initiated work in this area in the early 1900s while studying the structure of monolayers of

amphiphilic species, molecules with a polar head group and a long hydrocarbon tail, at the air-water interface.[35] Specifically, he dissolved amphiphilic molecules in a water-immiscible organic solvent and carefully cast this solution onto a clean water surface. A disordered layer of amphiphiles formed on the water after the solvent evaporated. Compression of the molecules through the movement of a barrier across the surface (Figure 1.1) forced the molecules to pack closely and form a monolayer with the hydrophobic tails of the molecules aligned in the same direction.

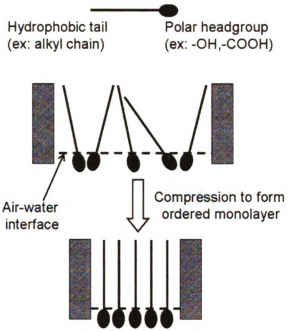

Figure 1.1. Formation of a monolayer of amphiphilic molecules at the air-water interface.

Blodgett, together with Langmuir, found that once the amphiphilic molecules attain the desired organization, the monolayer can be transferred from the air-water interface to solid substrates (e.g., glass, mica, silica or quartz) by simply immersing the substrate vertically through the organized monolayer.[36] In the case of a hydrophobic substrate, the monolayer transfers to the solid surface via hydrophobic interactions

between the alkyl chain and the substrate. During withdrawal of the hydrophobic substrate from the subphase, hydrophilic interactions drive the formation of the second layer (Figure 1.2). Further dipping can lead to deposition of multilayer films.[37]

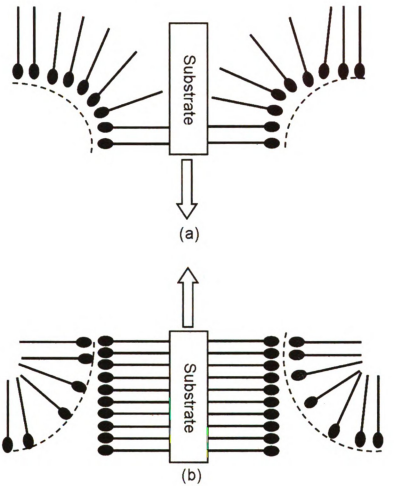

Figure 1.2. Formation of Langmuir-Blodgett films. (a) a single monolayer being transferred to a hydrophobic support on a down-trip. (b) transfer of a second monolayer on an up-trip to form a bilayer. (The dashed lines represent the air-water interface.) (Redrawn from *Biosens. Bioelectron.* **2005,** *21,* 1-20.)

Different dipping schemes result in the three types of Langmuir-Blodgett multilayer films shown in Figure 1.3.[38] Y-type multilayer films are the most common

and form on either hydrophilic or hydrophobic substrates. Because head-head or tail-tail interactions drive the film formation, Y-type films are typically more stable than X- or Z-type films. In contrast, X- and Z-type multilayer films can only form on hydrophobic and hydrophilic substrates, respectively. In some cases, the spacing between the hydrophilic headgroups in X- and Z-type films shows similar packing to that of Y-type films, even when the films have been transferred by an X- or Z-method. This might be due to the molecular rearrangement during or shortly after the film deposition.

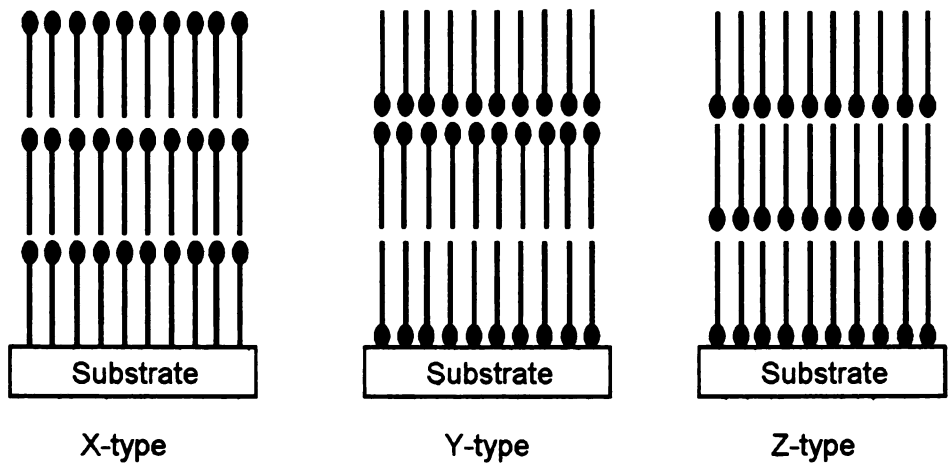

Figure 1.3. Three possible film architectures in Langmuir-Blodgett films. From left to right: X-type films on a hydrophobic substrate, Y-type films on a hydrophilic substrate and Z-type films on a hydrophilic substrate. (Redrawn from *Chem. Rev.* **2004,** *104,* 5479-5501.)

1.2.1.2. Advantages of the LB Method

Although it is one of the earliest strategies for fabricating a supramolecular assembly, the LB approach offers several advantages over other techniques. First, the LB method allows precise control over film thickness at the molecular level.[39] Second, this technique affords homogeneous deposition of a monolayer over relatively large surface

areas. Finally, the LB method can provide multilayered film structures with a defined sequence of composition along with ordered molecular arrangement and orientation.[40] Although this technique was traditionally limited to depositing organic amphiphilic molecules, LB films composed of a wide variety of inorganic complexes with interesting magnetic and conducting properties can be prepared.[38,39] This increased versatility expanded the potential applications of the LB method to areas such as biosensors, semiconductors, optics and electronics.[1,38,39,41,42]

1.2.2. Self-Assembled Monolayers (SAMs)

Although the LB technique is more than 70 years old, it still requires special equipment for film fabrication, and the weak interactions between the film and the substrate limit the chemical and mechanical stability of LB films.[3,43-45] Self-assembled monolayers (SAMs) attach to solid surfaces through relatively strong interactions (physisorption, chemisorption, or covalent bond formation), and are therefore generally more stable than LB films.[34,45-47]

1.2.2.1. History of SAMs

Bigelow first noted the self-assembly of organic monolayers in the 1950s when he found that long chain alkylalcohols adsorb on clean glass surfaces.[48] A few years later, Shafrin and Zisman discovered similar adsorption of long-chain alkylamines on Pt substrates.[49] However, these layers formed via physisorption and could be easily removed from the substrate.[1] Allara and Nuzzo later formed more robust films through chemisorption, where deprotonated fatty acids bound strongly to alumina surfaces,[50] and soon thereafter SAMs formed by covalent bonding appeared.

1.2.2.2. SAMs Formed via Covalent Bonding to a Surface

There are two primary groups of SAMs based on strong chemisorption. The first group, initially developed by Sagiv and coworkers, utilizes silane chemistry to link the monolayer to the surface.[51,52] Well-packed monolayers form on various substrates (such as clean glass, poly(vinyl alcohol), oxidized polyethylene, and evaporated alumina) through simple immersion of the substrate in an organic solution containing n-octadecyltrichlorosilane (OTS). Scheme 1.1 shows the chemistry behind the film formation, which includes hydrolysis of the Si-Cl bonds, adsorption on the substrate via –OH groups, and condensation polymerization of the silanol groups.

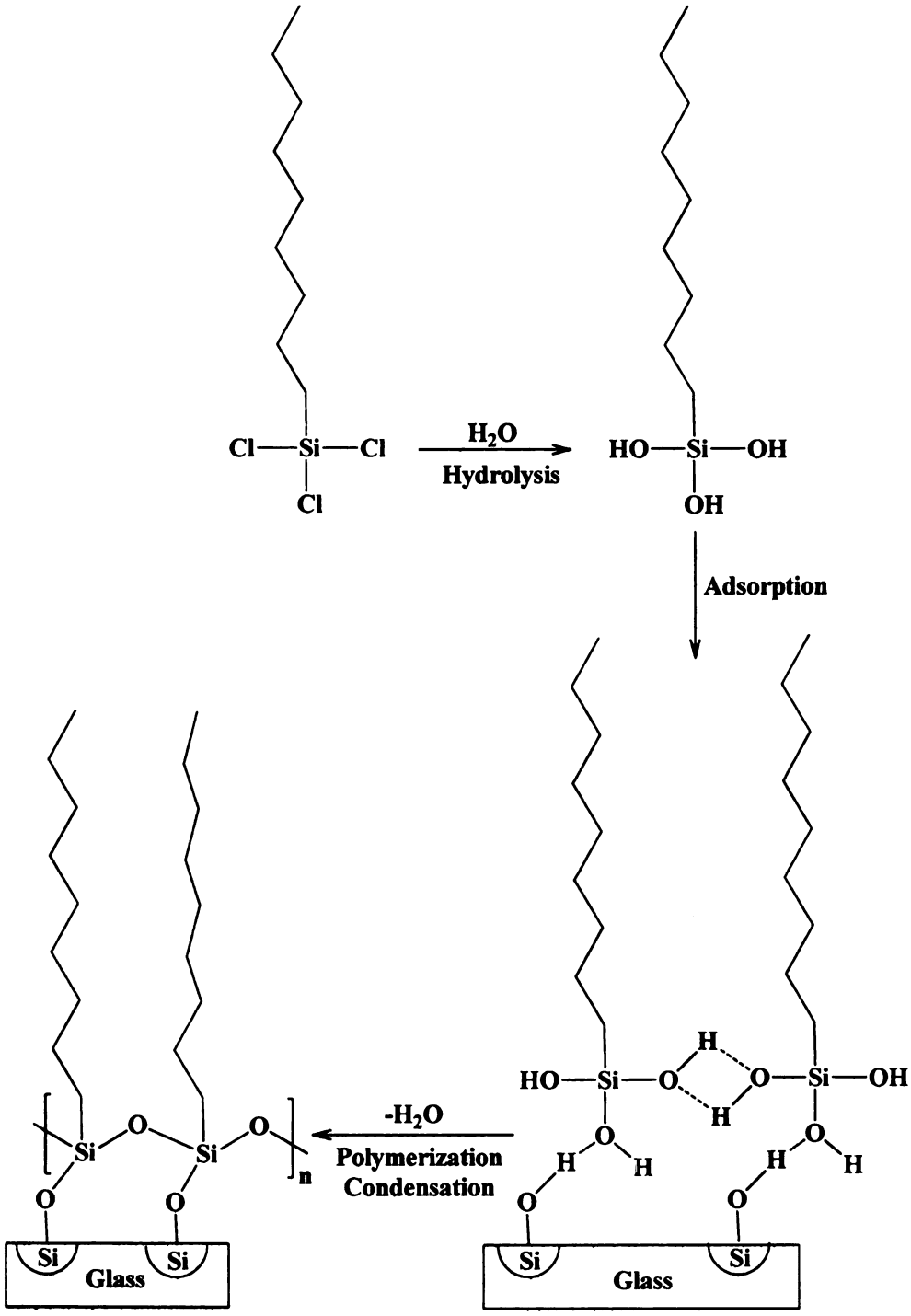

Scheme 1.1. Formation of an OTS SAM on a glass substrate. (Redrawn from *J. Am. Chem. Soc.* **1980,** *102,* 92-98.)

The other extensively studied method for formation of covalently immobilized SAMs is adsorption of sulfur-containing compounds (alkane thiols and alkyl sulfides) on gold substrates.[53-56] Sulfur compounds are highly reactive towards noble metals, and alkane thiols have high affinity for a variety of substrates including gold,[54-56] silver,[57-59] copper,[58] palladium,[60,61] and platinum.[62] The strong interaction between thiols and these metals makes it possible to generate well-defined and relatively stable SAMs.

Monolayers formed by adsorption of alkane thiols on gold (Scheme 1.2) comprise the most extensively studied SAMs. Gold is the most commonly used substrate for several reasons. First, binding to the surface occurs through interactions between "soft" gold and sulfur atoms, whereas many other functional groups (acids, amines, etc.) are relatively "hard" and do not have a strong affinity for the gold surface.[1] This allows the incorporation of other functional groups into these SAMs without disruption of the gold-sulfur interaction. Second, gold is easy to clean and reasonably stable under standard laboratory conditions. The interaction between gold and sulfur is strong enough to displace weakly bound impurities. In addition, gold-coated substrates are amenable to a wide range of SAM characterization techniques including ellipsometry, reflectance fourier transform-infrared spectroscopy (FT-IR), quartz crystal microbalance (QCM) gravimetry, and electrochemical methods.[63]

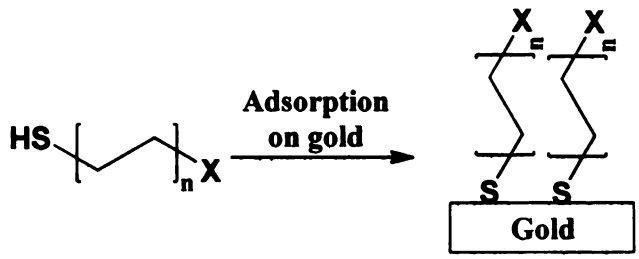

(X=CH_3, COOH, NH_2, etc.)

Scheme 1.2. Formation of a gold-supported alkane thiol SAM with terminal functional groups.

Formation of alkane thiol SAMs typically occurs by immersion of a cleaned gold substrate in an alcoholic solution of thiol and removal of weakly adsorbed molecules by rinsing with alcohol.[45] Adsorption times vary from minutes to days, depending on the nature and concentration of the thiol solution. Kinetic studies of this type of SAM formation indicate that there are two adsorption steps.[1,55] The initial step, which is well described by diffusion-controlled Langmuir adsorption, depends on the thiol concentration. This step takes place in several minutes and includes an oxidative addition of S-H to the gold surface followed by a reductive elimination of the hydrogen.[64] In the second step, which lasts several hours, the alkyl side chains assemble together to maximize Van der Waal's interactions and form two-dimensional crystalline structures. Molecules with long alkyl chains such as hexadecanethiol lead to well-packed quasi-crystalline monolayers while molecules with short alkyl chain form liquid-like monolayers.[1,64]

1.2.2.3. Advantages of SAMs

As Figure 1.4 shows, the formation of SAMs is driven by strong interactions such as covalent bond formation between the functionalized headgroup and the substrate

surface, as well as hydrophobic interactions between the hydrocarbon backbones of the absorbent molecules. Thus, SAMs are reasonably stable.[40] The ease of preparation and highly ordered film structure make SAMs promising candidates for modification of surface properties including wetting, frictional coefficient, and susceptibility to corrosion.[65-68] More importantly, SAMs can incorporate a wide range of functional groups both in the alkyl chain and at the chain endgroups. This enables the formation of surfaces capable of specific interactions.[64,69] All these unique features make SAMs attractive in the areas of sensors, wetting and lubrication control, and biomolecular and molecular electronic devices.[45,46,63,69,70] In some cases, the combination of LB and SAM techniques yields highly ordered and thermodynamically stable thin films that take advantage of assets of both methods.[34,44]

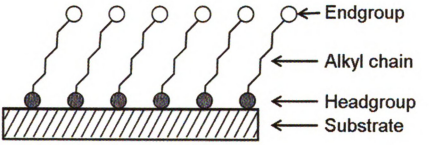

Figure 1.4. Structure of a SAM. The shaded and open circles indicate chemisorbing headgroups and free endgroups, respectively. (Reproduced with permission from *Prog. Surf. Sci.* **2000**, *65*, 151-257.)

1.2.3. Layer-by-Layer (LBL) Assembly

Layer-by-layer (LBL) film formation technique involves alternating adsorption of interacting materials. In the early 1990s, Decher developed electrostatic methods for the

formation of polymeric multilayer films,[71-73] but other interactions can also facilitate LBL film formation. Below I discuss films prepared using different interactions.

1.2.3.1. Driving Forces Involved in LBL Assembly

1.2.3.1.1. LBL Assembly Based on Electrostatic Interactions

LBL adsorption of polyelectrolytes is one of the easiest surface modification methods because it simply involves exposure of substrates to oppositely charged species, with water rinses between each deposition step. Many water-soluble and multiply charged species such as polymeric electrolytes,[71,73-76] proteins,[77-80] colloidal nanoparticles,[81-84] DNA,[85-87] and dye molecules[86,88,89] can be incorporated in LBL films.

Figure 1.5 illustrates the formation of polyelectrolyte-colloid bilayers on a negatively charged substrate. Specifically, the negatively charged solid substrate is initially placed in a dilute solution of polycations, and multiple polyelectrolyte-surface interactions result in the formation of a thin layer of polycation. This process is entropically favored because the polyvalent attachment of a single polycation molecule to the surface releases many counter-ions (both cations and anions) into the solution.[90] Overcompensation of the surface charge by the polycation leads to a positive surface,[91] and the modified substrate is then rinsed with water and subsequently immersed in a solution of negatively charged colloids. Adsorption of the colloid takes place and again reverses the surface charge. After another water rinse, one "bilayer" of the polycation-colloid film is present on the substrate, and this process can be repeated until the desired number of bilayers or film thickness has been reached.[1,3,90,92,93]

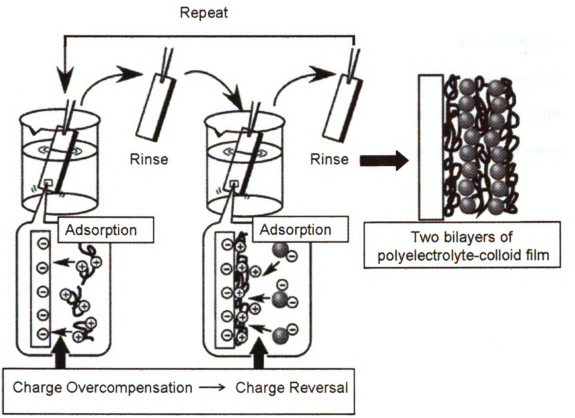

Figure 1.5. LBL assembly of polyelectrolyte-colloid bilayers through electrostatic interactions. (Reproduced by permission of the PCCP Owner Societies from *Phys. Chem. Chem. Phys.* **2007**, *9*, 2319-2340.)

1.2.3.1.2. LBL Assembly via Hydrogen Bonding

Stockton and Rubner[94] and Zhang and coworkers[95] introduced hydrogen bonding as a driving force for LBL assembly in 1997. In this method, alternating adsorption of polymers with hydrogen bond donors and polymers with hydrogen bond acceptors results in film formation. Stockton and Rubner examined the LBL adsorption of polyaniline and a variety of neutral water-soluble polymers, including poly(vinyl pyrrolidone) (PVP), poly(vinyl alcohol), poly(acrylamide), and poly(ethylene oxide) (PEO).[94] Figure 1.6

shows the structures of these polymers. FT-IR studies confirm that hydrogen bonding drives the film formation. The non-hydrogen-bonded N-H stretch of pure polyaniline appears at about 3380 cm^{-1}, while the hydrogen-bonded N-H stretch has an energy of about 3310 cm^{-1}. The appearance of pronounced peaks at 3304 and 3300 cm^{-1}, for polyaniline/PVP and polyaniline/PEO systems, respectively, suggests that a large fraction of the N-H groups in polyaniline is involved in the hydrogen bonding.[94]

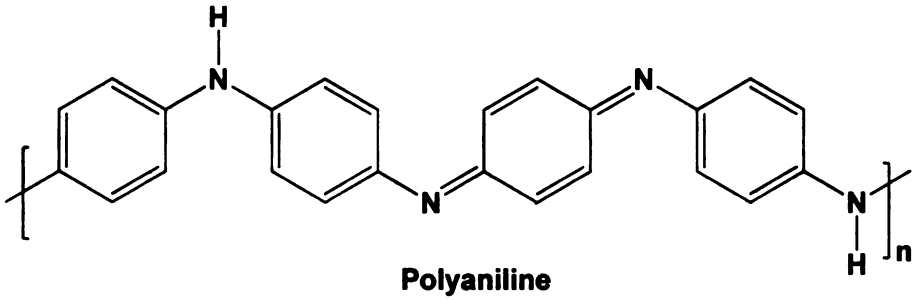

Polyaniline

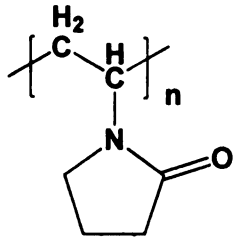

Poly(vinyl pyrrolidone)

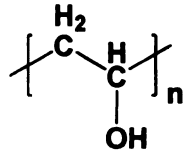

Poly(vinyl alcohol)

Poly(acrylamide)

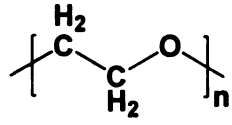

Poly(ethylene oxide)

Figure 1.6. Structure of polymers used in LBL assembly based on hydrogen bonding.[93,94]

Zhang and coworkers demonstrated the fabrication of LBL films through hydrogen bonding using poly(acrylic acid) (PAA) as a hydrogen bond donor and poly(4-vinylpyridine) as a hydrogen bond acceptor as shown in Scheme 1.3.[92] Adsorption of

PAA layers was performed using solutions at pH 3.28 to suppress ionization of the carboxylic acid groups. UV-vis spectrophotometry suggests linear film growth, and FT-IR spectroscopy confirms that the film growth occurs due to hydrogen bonding. However, films only form when the carboxylic groups of PAA are mostly protonated to allow PAA to serve as a hydrogen bond donor.[92]

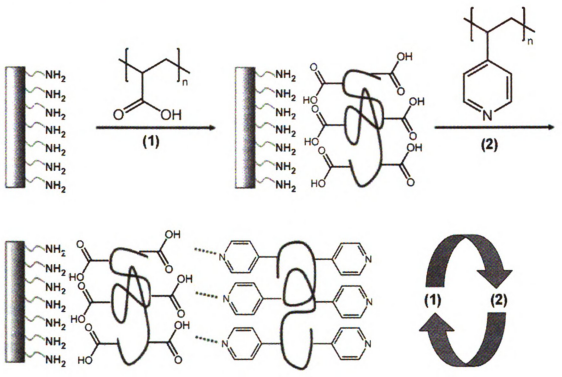

Scheme 1.3. Fabrication of LBL films via hydrogen bonding between poly(acrylic acid) and poly(4-vinylpyridine). (Reproduced by permission of The Royal Society of Chemistry from *Chem. Commun.* **2007,** 1395-1405.)

Hydrogen bonds are more sensitive to changes in their environment than electrostatic interactions, and LBL films formed via hydrogen bonding may only be stable under certain conditions. Sukhishvili and Granick studied the stability of hydrogen-bonded LBL films of poly(methacrylic acid) (PMAA) and poly(vinyl

pyrrolidone) at different pH values, and found that these films dissolve at pH values higher than 6.9.[96,97] Dissolution occurs due to ionization of the carboxylic groups in PMAA, which introduces an unacceptably large electric charge within the film.[96] Similar phenomena appear in other LBL assemblies formed through hydrogen bonding,[97] and dissolution under specific conditions enables the formation of responsive films that might prove useful in biomedical applications.[93]

1.2.3.1.3. LBL Assembly Based on Covalent Bonding

The use of covalent interactions as a basis for the LBL method should significantly improve film stability, which is advantageous for most applications. In 1997, Crooks and coworkers reported one of the first examples of multilayer polymer films formed through covalent bonding.[98,99] LBL reactions of poly(maleic anhydride)-co-poly(methyl vinyl ether) (Grantrez™) with amine-terminated dendrimers gave films on glass, Si, and Au-coated Si substrates. These covalently assembled films had a thickness of ~15 nm per bilayer. Due to the presence of ionizable amine and carboxylic groups, these materials exhibited pH-switchable permselectivity that allowed exclusion of cations and anions at low and high pH, respectively.[98,99]

Kohli and Blanchard reported the covalent growth of multilayer films of diphenylmethane derivatives using urea interlayer linking chemistry.[100] Alternating addition of diisocyanates and diamines (Scheme 1.4) afforded a controlled linear film growth, with a total thickness of 9.8 nm for 7-bilayer films.[100] Kohli and Blanchard later demonstrated the compatibility of covalent and ionic interactions in LBL growth, which might prove useful in the formation of ultrathin conducting and insulating layers.[101]

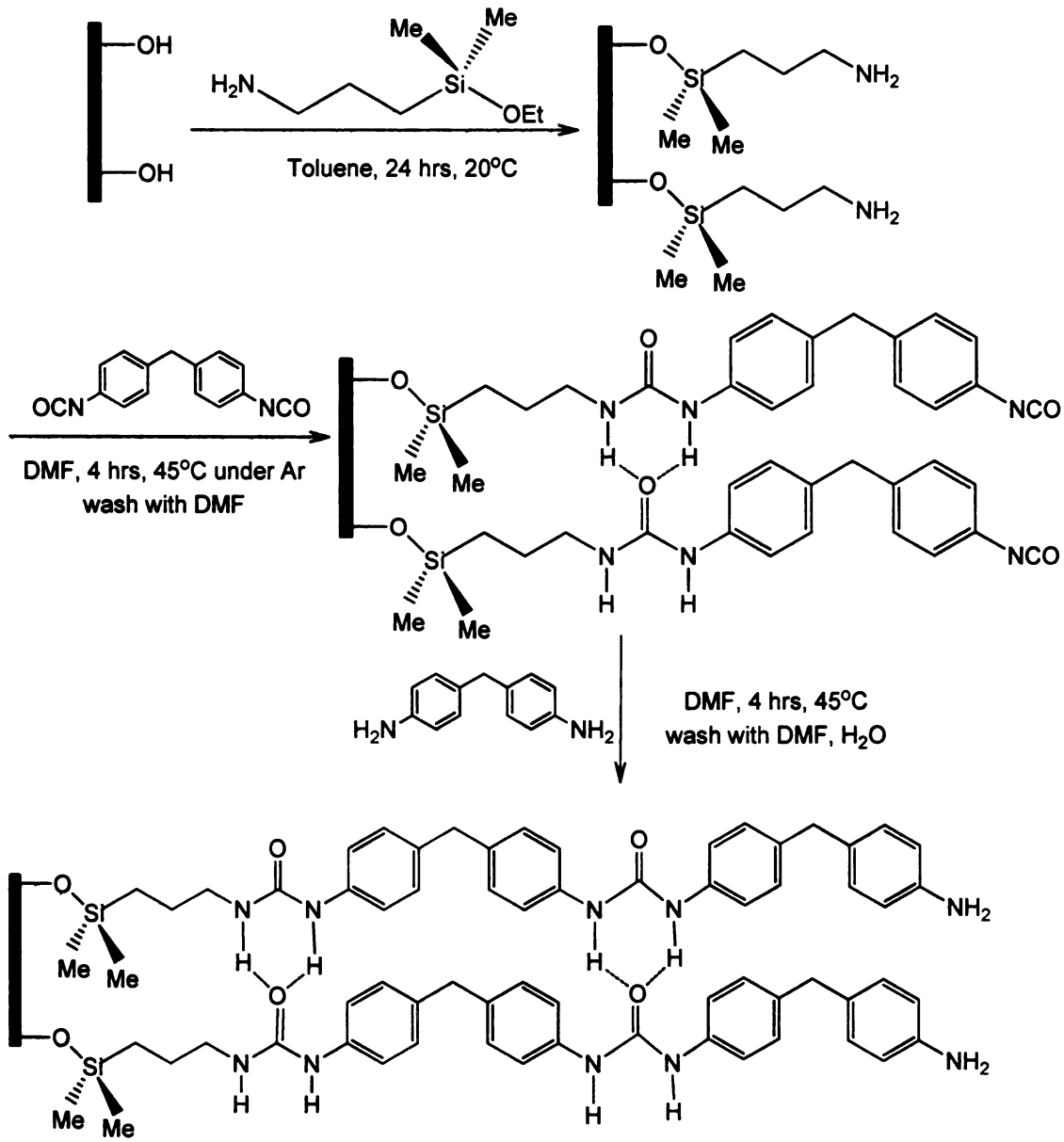

Scheme 1.4. Synthethis of multilayer films via stepwise reaction of diisocyanates and diamines. Further layers can be deposited similarly. (Redrawn from *Langmuir* **2000,** *16,* 4655-4661.)

Caruso and coworker recently described covalent LBL assembly through "click" chemistry.[102] "Click" chemistry refers to a set of high-yield reactions that can be

performed under simple conditions.[103] One of the most commonly used click reaction is the Cu(I)-catalyzed variant of the Huisgen 1,3-dipolar cycloaddition of azides and alkynes to form 1,2,3-triazoles.[103,104] Caruso and coworkers demonstrated covalent LBL assembly on quartz, silicon or gold through alternating immersion in Cu(I)-containing solutions of poly(acrylic acid) copolymerized with either azide or alkyne-containing monomers (Scheme 1.5).[102] Film thickness increased linearly with the number of layers when using alternating poly(acrylic acids) with ~16% azide and ~14% alkyne. This method yields stable films prepared from only one type of polyelectrolyte, which cannot be realized using conventional LBL assembly. A subsequent study applied this film-formation method on particle substrates. Dissolution of the particles gave polymer capsules with a pH-dependent size.[105]

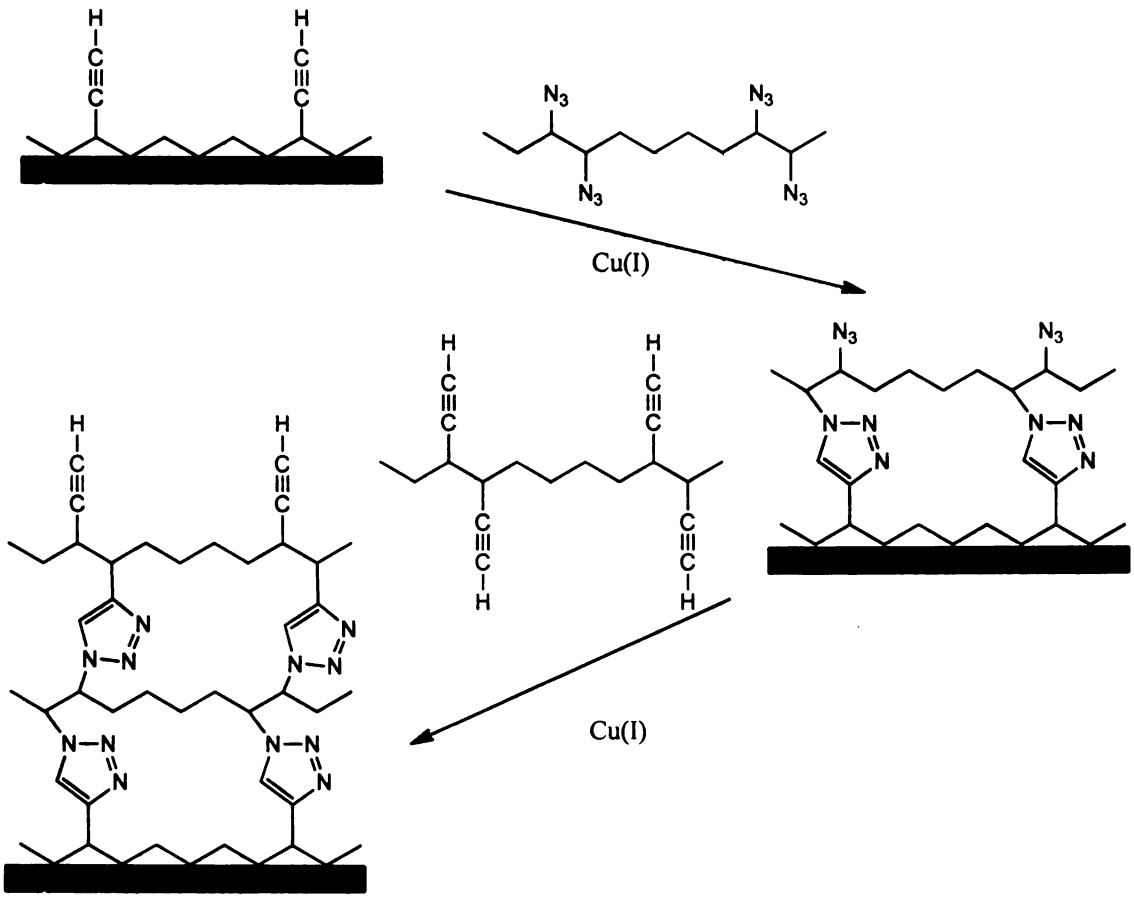

Scheme 1.5. LBL assembly of polymer films through "click" chemistry. (Redrawn from *J. Am. Chem. Soc.* **2006,** *128,* 9318-9319.)

1.2.3.1.4. Other Interactions Involved in LBL Assembly

Extensive recent research shows that the driving force for LBL assembly is not limited to electrostatic interactions and hydrogen or covalent bonding. Hydrophobic interactions,[106] bio-specific recognition,[107,108] charge transfer interactions,[109-111] supramolecular interactions,[43] and π-π interactions[112] can all facilitate LBL film formation. The versatility of the driving forces in LBL assembly enables the utilization of a wide range of molecules in film formation, and thus, expands the application of this technique.

1.2.3.2. LBL Assembly on Substrates of Various Geometries

One of the most attractive features of LBL assembly is its applicability to not only planar substrates, but also to porous membranes or even colloids and nanorods.[1,90,92,93,113,114] Our group demonstrated the deposition of metal nanoparticle/polyelectrolyte multilayer films on colloidal particles and in porous membranes.[115-120] Kidambi and Bhattacharjee deposited Pd nanoparticles in PEMs by alternating immersion of alumina particles in solutions of poly(acrylic acid) (PAA) and poly(ethylenimine) (PEI)-Pd(II) followed by reduction of Pd(II) with $NaBH_4$ (Scheme 1.6).[115-117] Dotzauer immobilized Au nanoparticles in alumina membranes by alternating adsorption of PAA, poly(allylamine hydrochloride) (PAH), and citrate-stabilized Au colloids (Figure 1.7). The high surface area of 0.2 μm-diameter pores of alumina membranes gave rise to a high catalyst loading.[119]

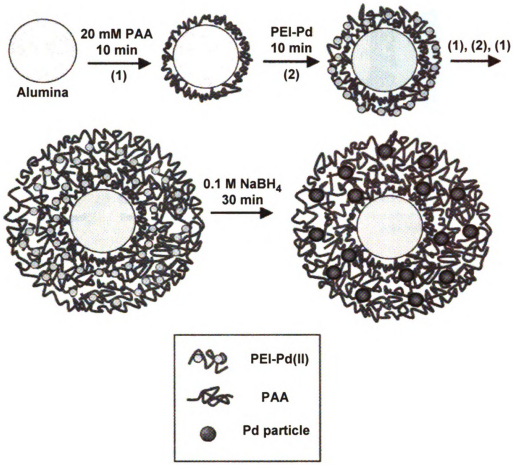

Scheme 1.6. Formation of Pd nanoparticles through reduction of Pd(II) in [PAA/PEI-Pd(II)]$_n$PAA films. (Reproduced with permission from *Chem. Mater.* **2005,** *17,* 301-307.)

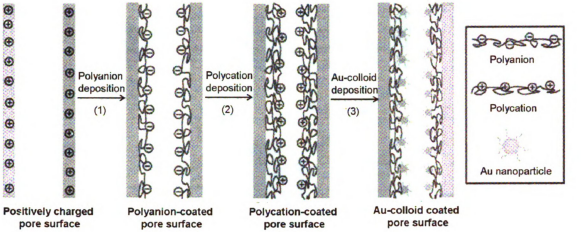

Figure 1.7. Modification of a pore of an alumina membrane by LBL adsorption of two oppositely charged polyelectrolytes and Au nanoparticles. (Reproduced with permission from *Nano Lett.* **2006,** *6,* 2268-2272.)

As shown in Figure 1.8, dissolution or calcination of the colloidal particles that sometimes serve as LBL substrates yields hollow materials.[121,122] In the case of calcination, the LBL method should include the deposition of inorganic materials that are stable under these conditions. Hollow capsules prepared by LBL methods can potentially be used in the fields of medicine, pharmaceutics, and material science for applications involving encapsulation or controlled release.[121,123,124-127]

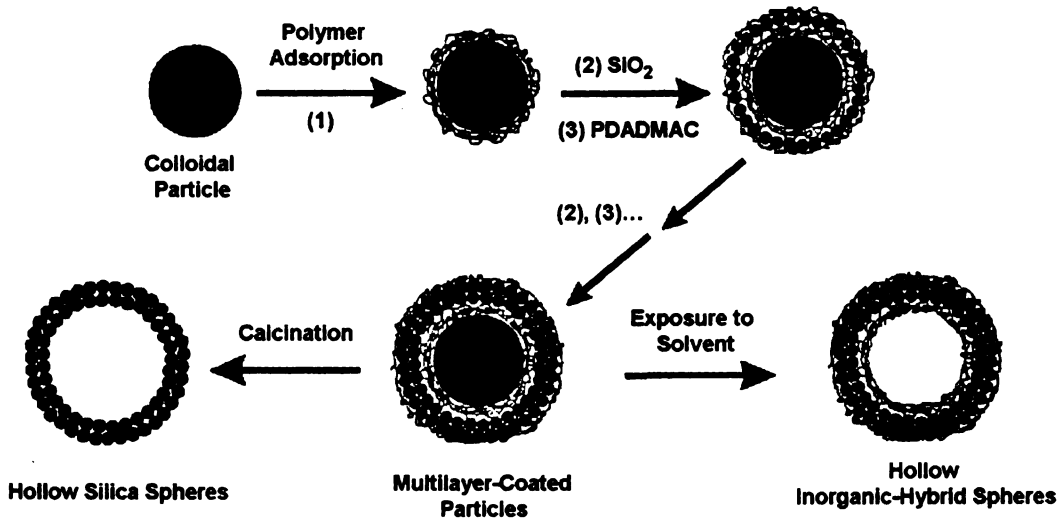

Figure 1.8. LBL assembly on particle templates for hollow-sphere formation. The substrates are polystyrene (PS) latex particles with a diameter of 640 nm. (Reproduced with permission from *Science* **1998,** *282,* 1111-1114.)

A similar synthetic approach with nanotube substrates yields hollow nanotubular structures that may be of interest in optical, electronic, and magnetic devices.[122,128,129] Polymer nanotubes were prepared by alternating adsorption of poly(diallyldimethylammonium chloride) (PDADMAC) and poly(styrene sulfonate) (PSS) on nickel nanorods followed by core dissolution (route A in Figure 1.9). Titania-based nanotubes were obtained with a similar approach (route B in Figure 1.9) where nickel nanorods were coated with PDADMAC and an inorganic precursor, titanium (IV) bis(ammonium lactate) dihydroxide (TALH). Hydrolysis of the titania precursor under reflux was followed by nickel core dissolution. This method is a water-based technique, and it allows for formation of nanotubes of various compositions, including protein nanotubes,[128,130] and control over the wall thickness of the nanotubes.[122]

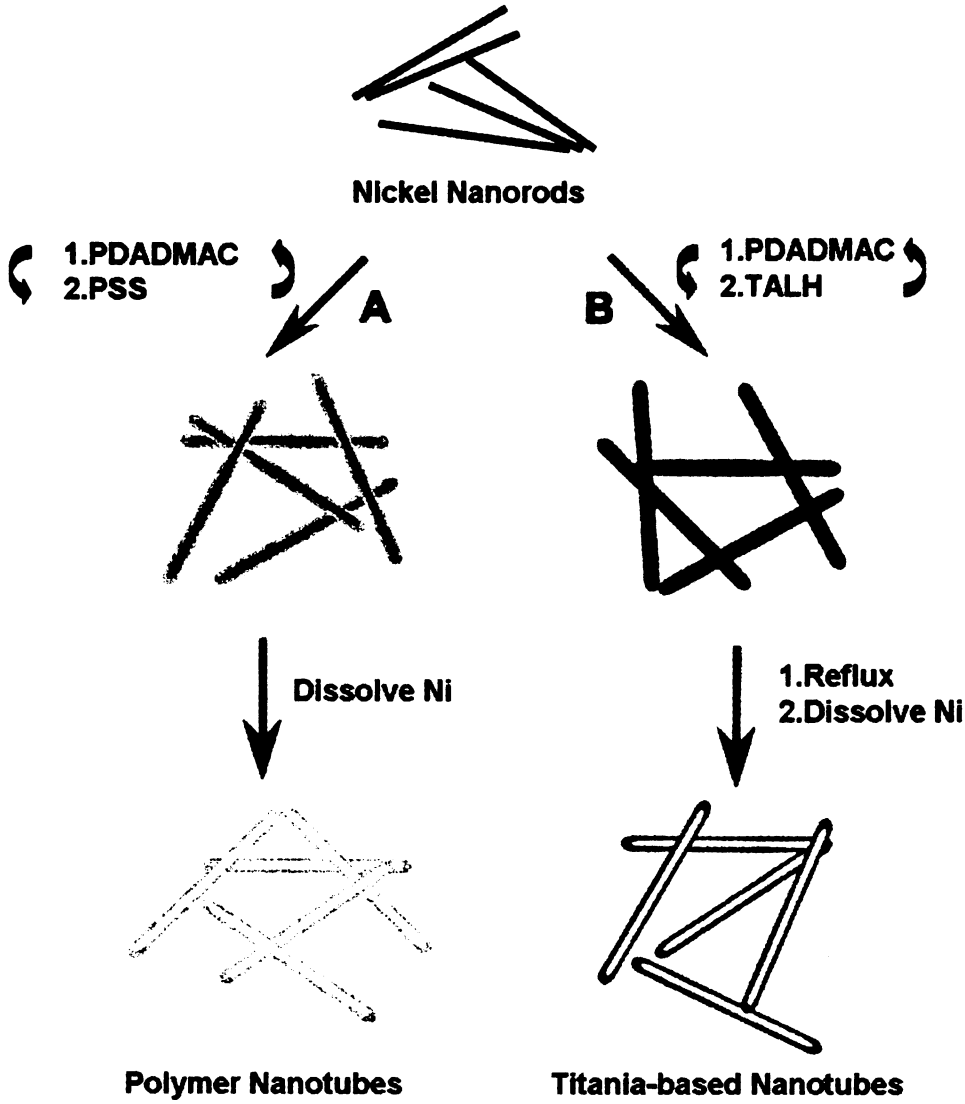

Figure 1.9. Preparation of polymer and inorganic-organic composite nanotubes by an LBL-colloid templating approach. (Reproduced with permission from *Nano Lett.* **2001**, *1*, 727-730.)

1.2.3.3. Optimization of the LBL Adsorption Process

Although LBL assembly is relatively simple, the tedious dipping and rinsing steps limit the potential application of this technique.[131] To overcome this challenge, Shiratori

and coworkers developed an automatic LBL film formation system with precise control over the mass of materials deposited.[132,133] In this case, a QCM with an integrated oscillation circuit was attached to the arm of a robot to monitor the frequency shift during the adsorption or rinsing process. Using the frequency change as feedback, the mass of materials deposited in each step was controlled precisely. Transmission electron microscopy and atomic force microscopy (AFM) showed that the surface roughness of the films formed by this method was much smaller than the roughness of films prepared by the conventional time-controlled dipping method. Not only polyelectrolytes, but also inorganic materials such as TiO_2 can form uniform structures with this method.[133]

However, automation of the LBL method does not reduce the time required for film formation, which usually ranges between several minutes and several hours, depending on the absorbing systems and the target number of bilayers.[134] This adsorption process is time consuming because the polyelectrolyte molecules must diffuse toward the substrate, interact with the surface, and then rearrange to pack densely.[134-136] The spin-coating method developed by Lee and coworkers (Figure 1.10) dramatically reduces the preparation time per layer from minutes to seconds.[134] This significant time reduction stems from several sources. First, the adsorption and rearrangement of adsorbed chains on the substrate and the elimination of weakly bound molecules are achieved almost simultaneously in a short time. Second, the polyelectrolyte concentration increases significantly due to the rapid elimination of water during the spinning process, and thus thick layers are formed. Finally, the electrostatic interactions between oppositely charged polymers are enhanced because the adsorbed water molecules, which generally screen the electrostatic attraction, may be partially forced out of the film during spinning.[135]

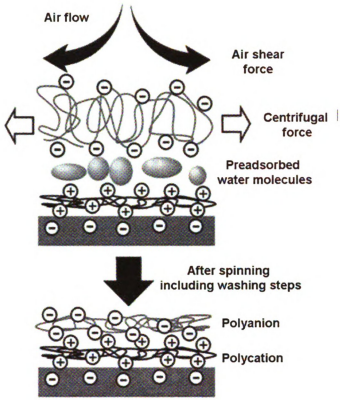

Figure 1.10. Buildup of LBL films by consecutive spinning of polycation and polyanion molecules. (Reproduced by permission of the PCCP Owner Societies from *Phys. Chem. Chem. Phys.* **2007,** *9,* 2319-2340.)

Another advantage associated with the spin-coating method is that it yields a highly ordered internal structure, which cannot be easily obtained with the conventional dipping method.[135] Figure 1.11 clearly shows this effect by comparing the structures of the $(PAH/CdS)_n$ films obtained with dipping and spin-coating methods. (The structures in the figure are based on X-ray reflectometry and AFM imaging.) This difference in film structures presumably occurs due to the mechanical effects of the air shear force during the spinning process.[3] Later research showed that the spin-coating method is

effective in LBL assembly of a wide variety of polyelectrolytes including polymers, dendrimers, and dye molecules.[137-139]

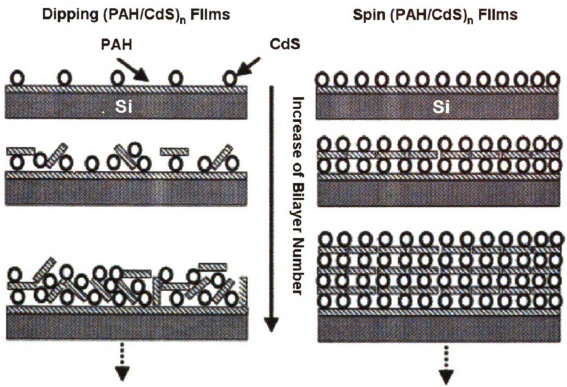

Figure 1.11. Schematic diagram of the internal structure of $(PAH/CdS)_n$ films prepared by dipping and spin methods. (Reproduced with permission from *Adv. Mater.* **2001,** *13,* 1076-1078.)

Although the spin-coating method may reduce the time required for LBL assembly, it requires special equipment and will likely not be applicable to large substrates. In 2000, Schlenoff and coworkers first reported the deposition of PEMs by alternating spraying of the polycation and polyanion solutions on the substrate (Figure 1.12), which is faster, more convenient, and generally more applicable for modification of large surfaces than the spin-coating method.[140] Specifically, Schenoff's group

prepared PEMs of PDADMAC/PSS on silica wafers by the spray-coating method. These films had a similar composition and thickness as films formed by the conventional dipping method.[140] In 2005, Decher and coworkers examined spray coating of PSS/PAH films to investigate the influence of various deposition parameters (spraying time, polyelectrolyte concentration, and the effect of drying during film formation) on film growth.[141] Film thickness increased linearly with the number of layer pairs, which is similar to the conventional dipping method, and AFM and X-ray reflectometry data showed that films with small surface roughnesses formed in spraying times as short as 6 s per layer. In dipping methods, homogeneous films cannot be formed in such short contact times. Moreover, because drainage constantly removes a certain quantity of the excess materials on the substrate, the rinsing step can be eliminated to further speed up the film formation process.[141]

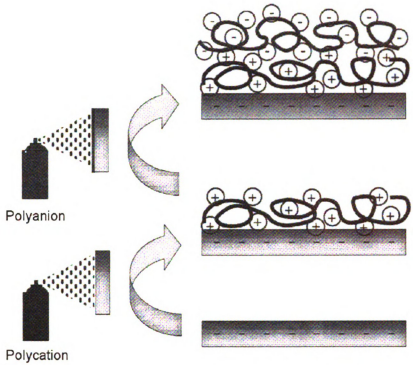

Figure 1.12. LBL deposition by alternating spray-coating of polycations and polyanions on a negatively charged substrate. (The rinsing between deposition steps is not shown.) (Reproduced with permission from *Nat. Mater.* **2009,** *8,* 449-450.)

Frey and coworkers later demonstrated the applicability of the spray-coating method to inorganic/organic nanocomposite films consisting of Au nanoparticles and the photosensitive polycation nitrodiazoresin.[142] Hammond and coworkers developed an automated spray system and extended the versatility of the spray-coating method to deposition of films of strong and weak polyelectrolytes, hydrogen-bonded films, and films containing colloidal nanoparticles. They also reported a 25-fold decrease in process time compared to the conventional dipping method and coating of colloidal nanoparticles.[143] In contrast to the fast spin-coating method, spray-coating is not restricted with respect to substrate size.

1.2.4. Comparison of LB Films, SAMs and LBL Films

The above discussions show that the LB method provides highly ordered monolayer or multilayer structures, but it is a relatively time-consuming process and requires use of expensive instruments and precise control over surface pressure during dipping and film transfer.[36] The LB method is also not generally applicable to many kinds of non-amphiphilic materials, and films suffer from instability.[3,40] SAMs are more robust than films prepared with the LB method,[40] but SAMs provide film with a very limited thickness.[3] Compared to LB and SAM methods, LBL adsorption technique is a more versatile technique with many advantages for multilayer film formation.

Among the advantages of LBL assembly, film fabrication is relatively simple and sophisticated instruments are not necessary for the assembly process.[40,92] Because LBL assembly can occur via different intermolecular interactions, it allows for controlled incorporation of a wide range of materials including polyelectrolytes,[71,73-76,132] biomaterials,[80,87,88,128,130] dye molecules, [88,89,138,144,145] and inorganic substances.[81-84,121] Another outstanding property of LBL adsorption is the ability to coat substrates of various geometries including flat surfaces, membranes, and colloidal particles that can sometimes be removed to give hollow capsule materials.[113,121,123,124,146] In addition, the film thickness can be controlled at the nm scale by varying the number of layers deposited and adsorption conditions such as the pH and ionic strength of the polyelectrolyte deposition solutions.[1,90,93,147] Due to these prominent assets, the LBL method has been explored for development of functional materials ranging from separation membranes to nano-sized reactors and drug delivery systems.[2,3] These applications will be discussed in more detail in the following section.

1.3. Selected Applications of LBL Films

1.3.1. Separation Membranes

Different from highly ordered LB films, LBL films tend to be amorphous structures with the polyelectrolytes penetrating into adjacent layers.[72] This kind of structure allows the transport of small molecules and ions through the films, making LBL films interesting barriers for selective passage of small molecules. Below I discuss nanofiltration and gas separation with membranes prepared by LBL deposition.

1.3.1.1. Nanofiltration Membranes

Nanofiltration is a pressure-driven, membrane-based filtration process that is widely used in water softening and pollutant removal.[148] Different from reverse osmosis, nanofiltration occurs at a lower pressure and provides lower rejection of monovalent ions.[149] These factors provide substantial energy savings compared to reverse osmosis in applications such as water softening that do not require the removal of monovalent ions.

Highly permeable membranes generally consist of a thin selective layer deposited on a thicker porous support that provides mechanical strength.[150-152] Tieke's group reported that PEMs comprised of 60 layer pairs of poly(vinylamine) and poly(vinylsulfate) (PVS) on a poly(acrylonitrile) (PAN)/poly(ethylene terephthalate) (PET) support exhibited a 95% rejection of $MgCl_2$ at an operating pressure of 10 bar with a feed concentration of 0.01 M $MgCl_2$.[153] However, the use of such a large number of layers makes fabrication impractical and yields very low flux. We showed that 5-bilayer PSS/PAH films on porous alumina supports exhibit a 95% rejection of $MgCl_2$ along with

a Na^+/Mg^{2+} selectivity of 22 under a pressure of 4.8 bar.[154] Chapter 2 presents the details of that work.

PEMs also proved useful in the selective removal of multivalent anions from solutions containing monovalent anions. El-Hashani and coworkers prepared 60-bilayer films of the dicopper complex of 18-azocrown-N_6 (hexacyclen, 1,4,7,10,13,16-hexaazaoctadecane, aza6) and PVS for separation of chloride and sulfate.[155] These films exhibited a chloride rejection of 45.7% and a sulfate rejection of 91.9% using an applied pressure of 25 bar.[155] Previous work in our group also investigated the separation of sulfate from chloride using different polyelectrolyte systems. Stanton and coworkers reported that 4.5-bilayer PSS/PAH films showed a Cl^-/SO_4^{2-} selectivity of about 30 when the top layer was deposited from a solution of high ionic strength.[152] By changing the top layer from PSS to PAA, the Cl^-/SO_4^{2-} selectivity was increased to as high as 80, albeit with a 50% drop in solution flux.[152] Alumina membranes coated with $(PSS/PDADMAC)_3PSS$ films are also proved to be useful in chloride/sulfate separation. The Cl^-/SO_4^{2-} selectivity of these membranes was comparable to that of PSS/PAH systems, but the flux was about 50% higher.[156]

Deng and coworkers developed a hybrid NF membrane using PSS, PAH and a copolymer polyelectrolyte poly(4-styrenesulfonic acid-co-maleic acid) sodium salt (PSSMA).[148] Films containing only two bilayers of (PAH/PSS/PAH/PSSMA) on PAN ultrafiltration substrates exhibited a Na_2SO_4 rejection as high as 91.4% at an applied pressure of 2 bar.[148] Other work reported that PEMs on porous supports are effective in NF removal of salt from reactive-dye solutions and selective removal of fluoride or phosphate from aqueous solutions.[157-159]

1.3.1.2. Membranes for Gas Separation

Fabrication of gas separation membranes using LBL adsorption is more difficult than formation of NF membranes, because gas separations are more susceptible to defects in the film. Nevertheless, McCarthy reported selective gas permeation through PAH/PSS films deposited on oxidized poly(4-methyl-1-pentene).[160] The poly(4-methyl-1-pentene) provides a continuous support that minimizes defects. Enhanced selectivities in the permeation of H_2, N_2 and O_2 occurred upon increasing the number of PSS/PAH layers from 20 to 200, and 200-layer films gave an O_2/N_2 selectivity as high as 15.[160] Tieke's group also tested the gas separation performance of PAH/PSS films on a PAN/PET support, but even 60-bilayer films showed essentially no selectivity in the permeation of N_2, O_2 and Ar.[161]

Sullivan created selective gas-selective membranes by LBL adsorption of poly(amic acid) and PAH followed by heat-induced imidization (Scheme 1.7).[162] Films containing 9.5 bilayers of this film on alumina exhibited O_2/N_2 selectivities of 6.9 and CO_2/CH_4 selectivities of 69.[162] These membranes are promising for gas separation because of their stability and the selectivity of polyimides, and their formation does not involve the tedious deposition of hundreds of layers.

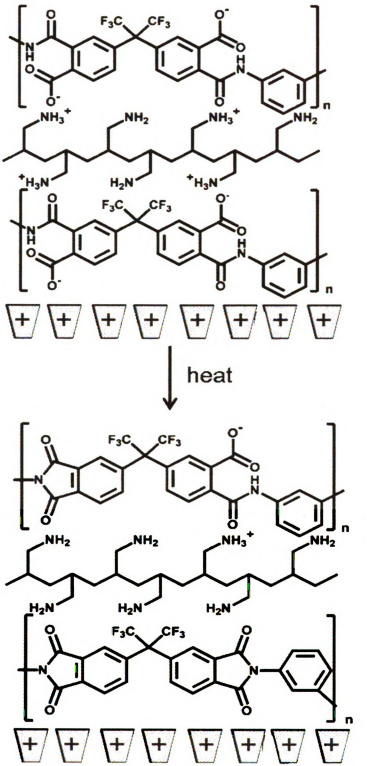

Scheme 1.7. Imidization of a poly(amic acid)/PAH film via heating to produce a gas-selective material. (Reproduced from *Langmuir,* **2008,** *24,* 7663-7673.)

1.3.2. Membranes for Protein Adsorption

As discussed in section 1.2.3.2, LBL adsorption is useful for modifying the interior of porous substrates to exploit the high internal surface area of these supports in applications such as catalysis and protein purification through adsorption.[2] Dai coated the interior surface of a porous alumina support (pore size of 0.2 μm) with $(PAA/PAH)_nPAA$ films and subsequently activated the free –COOH groups of the terminating PAA layer with N-(3-dimethylaminopropyl)-N'-ethylcarbodiimide (EDC) and N-hydroxysuccinimide to allow for covalent attachment of antibodies (Figure 1.13).[163] This method allowed development of a flow-through system for antigen analysis, with minimal nonspecific protein adsorption on the PAA terminated films.[164]

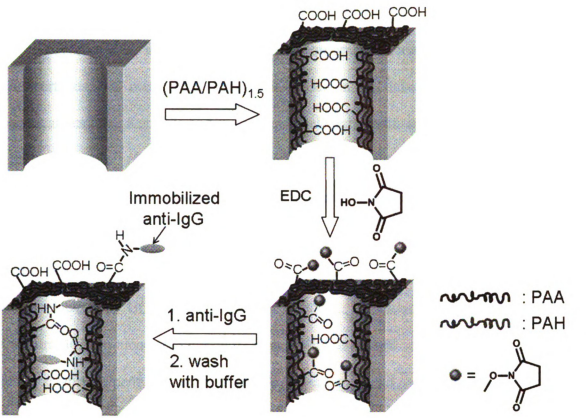

Figure 1.13. Schematic diagram of modification of the interior of membranes with PAA-terminated PAA/PAH films and activation of these films for covalent protein attachment. (Reproduced with permission from *Langmuir,* **2008,** *24,* 7663-7673.)

In 2006, Caruso and coworkers reported the use of PAA/PAH nanoporous polymer spheres (NPS) for protein immobilization.[165] After incubation in a lysozyme solution for 60 min, the cross-linked $(PAA/PAH)_2PAA$ NPS contained ~90 wt% lysozyme, which corresponds to a lysozyme loading of 470 mg/mL in the NPS. The loading can be reversed by changing the solution pH to mediate the electrostatic interactions between the proteins and the NPS. These materials are potentially useful in biosensing, enzyme catalysis and controlled drug delivery.[165]

1.3.3. Bio- and Chemical Reactors

Because LBL adsorption can easily incorporate materials such as enzymes and nanoparticles, this method has been widely used in the development of enzyme and chemical reactors. Kunitake and coworkers developed a multi-enzyme reactor containing glucose oxidase (GOD) and glucoamylase (GA) by alternating deposition of polyelectrolytes and these two enzymes on an ultrafiltration membrane (Figure 1.14).[166] Starch passing through these modified membranes was converted to glucose through the hydrolysis of the glycoside bond by GA, and the glucose was subsequently converted to gluconolactone by GOD with H_2O_2 as a byproduct. Unreacted starch was removed by the ultrafiltration membrane due to its high molecular weight. Optimization of flow rate and the arrangement and number of film layers can lead to development of highly specific enzyme reactors.[166]

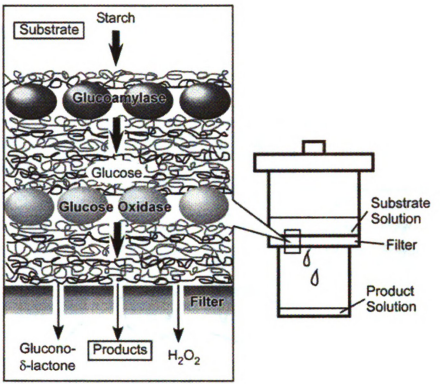

Figure 1.14. Multi-enzyme reactor prepared by LBL deposition on an ultrafiltration membrane. (Reproduced by permission of the PCCP Owner Societies from *Phys. Chem. Chem. Phys.* **2007,** *9,* 2319-2340.)

Dotzauer and coworkers prepared catalytic membranes through LBL adsorption of polyelectrolytes and Au nanoparticles in porous alumina (Figure 1.15).[119] These membranes catalyzed the reduction of 4-nitrophenol by $NaBH_4$ with remarkably high and stable conversions of 4-nitrophenol at a flow rate of 0.17 mL/(cm^2 s). These results indicate a turnover number > 1000 mol of 4-nitrophenol per mol of Au in the membrane. In addition to high stability and turnover numbers, the LBL method is also applicable to deposition of catalytic nanoparticles in polymeric membranes such as track-etched polycarbonate and porous nylon.[119,120]

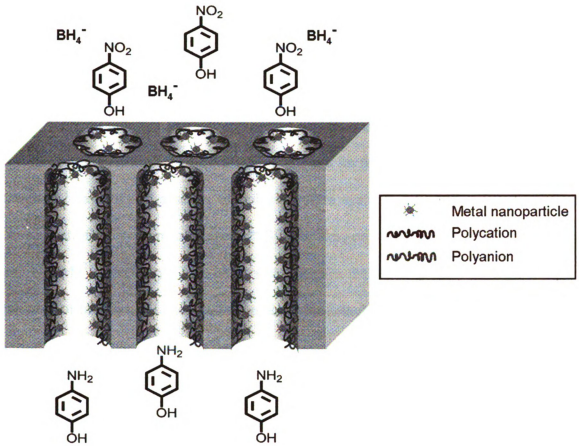

Figure 1.15. Schematic diagram of the reduction of 4-nitrophenol by $NaBH_4$ during flow through a membrane modified with nanoparticle/polyelectrolyte films. (Reproduced with permission from *Langmuir,* **2008,** *24,* 7663-7673.)

As discussed in section 1.2.3.2, the LBL method can be used to form PEM capsules. Shchukin and Möhwald prepared PSS/PAH capsules containing TiO_2 nanoparticles that catalyze the photosynthesis of urea from inorganic precursors (CO_2 and NO_3^-) in aqueous solution.[167] Poly(vinyl alcohol), which served as an electron donor to facilitate the reaction, was encapsulated inside the capsules together with TiO_2 nanoparticles. The effect of the capsule size was investigated and the highest yield in urea photosynthesis was achieved by Cu-modified TiO_2 nanoparticles encapsulated inside

2.2-μm PSS/PAH capsules.

1.4. Scope of This Work

This dissertation focuses on the use of LBL adsorption for preparation of NF membranes tailored for specific NF separations and for formation of catalytic membranes. Chapter 2 investigates a series of polyelectrolyte systems for cation separations and shows that of the systems examined, PSS/PAH films provide the highest Mg^{2+} rejection and Na^{+}/Mg^{2+} selectivity. This chapter also studies the effect of deposition parameters (number of bilayers, pH and ionic strength of the polyelectrolyte deposition solution) on selectivity and flux. Streaming potential measurements demonstrate that the magnitude of positive surface charge increases with increasing concentrations of Mg^{2+} in feed solutions or when the outer polycation layer is deposited from a solution of high ionic strength. These membranes are potentially useful in water softening and wastewater treatment in the pulp and paper industry.

Chapter 3 describes the use of $(PSS/PDADMAC)_nPSS$ films for removal of phosphate in the presence of chloride. The phosphate rejection depends on the pH of the feed solution, and the highest rejection occurs when the feed pH is 8.4, as opposed to pH 5.6 or 7.0, presumably due to the fact that a large fraction of phosphate is HPO_4^{2-} rather than $H_2PO_4^{-}$ at the higher pH. At a feed pH of 8.4, $(PSS/PDADMAC)_4PSS$ films on porous alumina supports exhibit a phosphate rejection of 98%, a chloride/phosphate selectivity of 48 and a solution flux of 2.4 $m^3/(m^2$ day) at 4.8 bar. The low chloride rejection and high solution flux make these membranes attractive for chloride/phosphate separations.

In chapters 4 and 5, I present the formation of catalytic membrane reactors by modifying the interior pores of porous hollow fiber or flat-sheet membranes through alternating adsorption of polyelectrolytes and metal nanoparticles, which serve as catalysts in chemical reactions. The LBL method affords control over the amount of catalyst deposited through varying the number of bilayers in the film. Moreover, the deposition yields a high density of metal nanoparticles in the film, and scanning electron microscopy (SEM) images show that the colloids are well separated with no visible aggregation.

Chapter 4 focuses primarily on catalytic hollow fiber membranes. Immobilization of metal nanoparticles in hollow fiber pores via LBL adsorption of polyelectrolytes and negatively charged Au nanoparticles yields catalytic reactors with high surface areas. Catalytic reduction of 4-nitrophenol with $NaBH_4$, which can be easily monitored by UV-Vis spectrophotometry, demonstrates that the Au nanoparticles in the hollow fiber membrane are highly catalytically active. In a single pass through the membrane, >99% of the 4-nitrophenol is reduced to 4-aminophenol, but this conversion decreases over time, perhaps because of catalyst fouling by byproducts of 4-aminophenol oxidation.

In chapter 5, I describe catalytic flat-sheet membrane reactors that contain Pd nanoparticles immobilized in the membrane pores. Films of PSS/PEI/PdNP have a higher Pd loading than PSS/PAH/PdNP coatings, presumably because of strong interactions between PEI and Pd. These membranes catalyze 4-nitrophenol reduction by HCOONa. High (>99%) 4-nitrophenol conversion occurs, but deposits appear on the membrane surface, perhaps again due to 4-aminophenol oxidation.

The last chapter presents conclusions and some proposed future work, particularly

with regard to stabilizing membranes and facilitating their manufacture.

1.5. References

(1) Davis, F.; Higson, S. P. J. *Biosens. Bioelectron.* **2005**, *21*, 1-20.

(2) Bruening, M. L.; Dotzauer, D. M.; Jain, P.; Ouyang, L.; Baker, G. L. *Langmuir* **2008**, *24*, 7663-7673.

(3) Ariga, K.; Hill, J. P.; Ji, Q. *Phys. Chem. Chem. Phys.* **2007**, *9*, 2319-2340.

(4) Seon, J.-B.; Lee, S.; Kim, J. M.; Jeong, H.-D. *Chem. Mater.* **2009**, *21*, 604-611.

(5) Yin, L.-T.; Hu, C.-Y.; Chang, C.-H. *Sens. Actuators, B* **2008**, *130*, 374-378.

(6) Darren, S.; Anthony, H.; Robert, S. *J. Appl. Polym. Sci.* **2007**, *103*, 1287-1294.

(7) Park, M. S.; Lee, Y.; Kim, J. K. *Chem. Mater.* **2005**, *17*, 3944-3950.

(8) Hoggan, E. N.; Flowers, D.; Wang, K.; DeSimone, J. M.; Carbonell, R. G. *Ind. Eng. Chem. Res.* **2004**, *43*, 2113-2122.

(9) Muller-Buschbaum, P.; Stamm, M. *Macromolecules* **1998**, *31*, 3686-3692.

(10) Kumar, N.; Yanguas-Gil, A.; Daly, S. R.; Girolami, G. S.; Abelson, J. R. *J. Am. Chem. Soc.* **2008**, *130*, 17660-17661.

(11) Binions, R.; Carmalt, C. J.; Parkin, I. P.; Pratt, K. F. E.; Shaw, G. A. *Chem. Mater.* **2004**, *16*, 2489-2493.

(12) Montero, L.; Baxamusa, S. H.; Borros, S.; Gleason, K. K. *Chem. Mater.* **2008**, *21*, 399-403.

(13) Manning, T. D.; Parkin, I. P.; Pemble, M. E.; Sheel, D.; Vernardou, D. *Chem. Mater.* **2004**, *16*, 744-749.

(14) Berry, A. D.; Holm, R. T.; Mowery, R. L.; Turner, N. H.; Fatemi, M. *Chem. Mater.* **2002**, *3*, 72-77.

(15) Shirman, T.; Freeman, D.; Posner, Y. D.; Feldman, I.; Facchetti, A.; van der Boom, M. E. *J. Am. Chem. Soc.* **2008**, *130*, 8162-8163.

(16) Li, L.; Yang, Y.; Yang, G.; Chen, X.; Hsiao, B. S.; Chu, B.; Spanier, J. E.; Li, C. Y. *Nano Lett.* **2006**, *6*, 1007-1012.

(17) Rietveld, I. B.; Kobayashi, K.; Yamada, H.; Matsushige, K. *J. Phys. Chem. B* **2006**, *110*, 23351-23364.

(18) NcNeal, C. J.; Macfarlane, R. D.; Thurston, E. L. *Anal. Chem.* **1979**, *51*, 2036-2039.

(19) Rajeshwar, K.; de Tacconi, N. R.; Chenthamarakshan, C. R. *Chem. Mater.* **2001**, *13*, 2765-2782.

(20) Bagheri-Tar, F.; Sahimi, M.; Tsotsis, T. T. *Ind. Eng. Chem. Res.* **2007**, *46*, 3348-3357.

(21) Tatoulian, M.; Arefi-Khonsari, F.; Tatoulian, L.; Amouroux, J.; Borra, J. P. *Chem. Mater.* **2006**, *18*, 5860-5863.

(22) Armelao, L.; Bottaro, G.; Bruno, G.; Losurdo, M.; Pascolini, M.; Soini, E.; Tondello, E. *J. Phys. Chem. C* **2008**, *112*, 14508-14512.

(23) Haruvy, Y.; Webber, S. E. *Chem. Mater.* **1992**, *4*, 89-94.

(24) Fireman-Shoresh, S.; Popov, I.; Avnir, D.; Marx, S. *J. Am. Chem. Soc.* **2005**, *127*, 2650-2655.

(25) Caruso, R. A.; Antonietti, M. *Chem. Mater.* **2001**, *13*, 3272-3282.

(26) Xiao, L.; Zhang, H.; Scanlon, E.; Ramanathan, L. S.; Choe, E.-W.; Rogers, D.; Apple, T.; Benicewicz, B. C. *Chem. Mater.* **2005**, *17*, 5328-5333.

(27) Sreenivas, G.; Ang, S. S.; Fritsch, I.; Brown, W. D.; Gerhardt, G. A.; Woodward, D. J. *Anal. Chem.* **1996**, *68*, 1858-1864.

(28) Yang, G. H.; Zhang, Y.; Kang, E. T.; Neoh, K. G. *J. Phys. Chem. B* **2003**, *107*, 2780-2787.

(29) Biederman, H.; Zeuner, M.; Zalman, J.; Bílková, P.; Slavínská, D.; Stelmasuk, V.; Boldyreva, A. *Thin Solid Films* **2001**, *392*, 208-213.

(30) Lu, Z. G.; Lo, M. F.; Chung, C. Y. *J. Phys. Chem. C* **2008**, *112*, 7069-7078.

(31) Patel, N.; Fernandes, R.; Guella, G.; Kale, A.; Miotello, A.; Patton, B.; Zanchetta, C. *J. Phys. Chem. C* **2008**, *112*, 6968-6976.

(32) Kim, I.-D.; Rothschild, A.; Hyodo, T.; Tuller, H. L. *Nano Lett.* **2006**, *6*, 193-198.

(33) Nam, H.-J.; Sasaki, T.; Koshizaki, N. *J. Phys. Chem. B* **2006**, *110*, 23081-23084.

(34) Tsai, P.-S.; Yang, Y.-M.; Lee, Y.-L. *Langmuir* **2006**, *22*, 5660-5665.

(35) Langmuir, I. *J. Am. Chem. Soc.* **1917**, *39*, 1848-1906.

(36) McCullough, D. H. I.; Regen, S. L. *Chem. Commun.* **2004**, 2787-2791.

(37) Blodgett, K. B. *J. Am. Chem. Soc.* **1935**, *57*, 1007-1022.

(38) Talham, D. R. *Chem. Rev.* **2004**, *104*, 5479-5501.

(39) Clemente-León, M.; Coronado, E.; Soriano-Portillo, A.; Mingotaud, C.; Dominguez-Vera, J. M. *Adv. Colloid Interface Sci.* **2005**, *116*, 193-203.

(40) Ariga, K.; Nakanishi, T.; Michinobu, T. *J. Nanosci. Nanotechnol.* **2006**, *6*, 2278-2301.

(41) Talham, D. R.; Yamamoto, T.; Meisel, M. W. *J. Phys.: Condens. Matter* **2008**, *20*, 184006 (13pp).

(42) Major, S. S.; Talwar, S. S.; Srinivasa, R. S. *Pramana* **2006**, *67*, 121-134.

(43) Crespo-Biel, O.; Dordi, B.; Reinhoudt, D. N.; Huskens, J. *J. Am. Chem. Soc.* **2005**, *127*, 7594-7600.

(44) Jaiswal, A.; Rajagopal, D.; Lakshmikantham, M. V.; Cava, M. P.; Metzger, R. M. *Phys. Chem. Chem. Phys.* **2007**, *9*, 4007-4017.

(45) Fendler, J. H. *Chem. Mater.* **2001**, *13*, 3196-3210.

(46) Arya, S. K.; Solanki, P. R.; Datta, M.; Malhotra, B. D. *Biosens. Bioelectron.* **2009**, *24*, 2810-2817.

(47) Kondo, T.; Uosaki, K. *J. Photochem. Photobiol., C* **2007**, *8*, 1-17.

(48) Bigelow, W. C.; Pickett, D. L.; Zisman, W. A. *J. Colloid Sci.* **1946**, *1*, 513-538.

(49) Shafrin, E. G.; Zisman, W. A. *J. Colloid Sci.* **1949**, *4*, 571-590.

(50) Allara, D. L.; Nuzzo, R. G. *Langmuir* **1985**, *1*, 45-52.

(51) Pomerantz, M.; Segmüller, A.; Netzer, L.; Sagiv, J. *Thin Solid Films* **1985**, *132*, 153-162.

(52) Sagiv, J. *J. Am. Chem. Soc.* **1980**, *102*, 92-98.

(53) Nuzzo, R. G.; Zegarski, B. R.; Dubois, L. H. *J. Am. Chem. Soc.* **1987**, *109*, 733-740.

(54) Bain, C. D.; Whitesides, G. M. *J. Am. Chem. Soc.* **1988**, *110*, 3665-3666.

(55) Bain, C. D.; Troughton, E. B.; Tao, Y. T.; Evall, J.; Whitesides, G. M.; Nuzzo, R. G. *J. Am. Chem. Soc.* **1989**, *111*, 321-335.

(56) Poirier, G. E.; Pylant, E. D. *Science* **1996**, *272*, 1145-1148.

(57) Kang, J. F.; Ulman, A.; Liao, S.; Jordan, R.; Yang, G.; Liu, G.-Y. *Langmuir* **2001**, *17*, 95-106.

(58) Laibinis, P. E.; Whitesides, G. M.; Allara, D. L.; Tao, Y.-T.; Parikh, A. N.; Nuzzo, R. G. *J. Am. Chem. Soc.* **1991**, *113*, 7152-7167.

(59) Walczak, M. M.; Chung, C.; Stole, S. M.; Widrig, C. A.; Porter, M. D. *J. Am. Chem. Soc.* **1991**, *113*, 2370-2378.

(60) Love, J. C.; Wolfe, D. B.; Haasch, R.; Chabinyc, M. L.; Paul, K. E.; Whitesides, G. M.; Nuzzo, R. G. *J. Am. Chem. Soc.* **2003**, *125*, 2597-2609.

(61) Carvalho, A.; Geissler, M.; Schmid, H.; Michel, B.; Delamarche, E. *Langmuir* **2002**, *18*, 2406-2412.

(62) Li, Z.; Chang, S.-C.; Williams, R. S. *Langmuir* **2003**, *19*, 6744-6749.

(63) Love, J. C.; Estroff, L. A.; Kriebel, J. K.; Nuzzo, R. G.; Whitesides, G. M. *Chem. Rev.* **2005**, *105*, 1103-1170.

(64) Ulman, A. *Chem. Rev.* **1996**, *96*, 1533-1554.

(65) Genzer, J.; Efimenko, K. *Science* **2000**, *290*, 2130-2133.

(66) Rangger, G. M.; Romaner, L.; Heimel, G.; Zojer, E. *Surf. Interface Anal.* **2008**, *40*, 371-378.

(67) Jennings, G. K.; Laibinis, P. E. *Colloids Surf., A* **1996**, *116*, 105-114.

(68) Ulman, A.; Evans, S. D.; Shnidman, Y.; Sharma, R.; Eilers, J. E.; Chang, J. C. *J. Am. Chem. Soc.* **1991**, *113*, 1499-1506.

(69) Schreiber, F. *Prog. Surf. Sci.* **2000**, *65*, 151-257.

(70) Bent, S. F. *ACS Nano* **2007**, *1*, 10-12.

(71) Decher, G.; Hong, J. D.; Schmitt, J. *Thin Solid Films* **1992**, *210-211*, 831-835.

(72) Decher, G. *Science* **1997**, *277*, 1232-1237.

(73) Lvov, Y.; Decher, G.; Moehwald, H. *Langmuir* **1993**, *9*, 481-486.

(74) Decher, G.; Lvov, Y.; Schmitt, J. *Thin Solid Films* **1994**, *244*, 772-777.

(75) Hoogeveen, N. G.; Cohen Stuart, M. A.; Fleer, G. J.; Böhmer, M. R. *Langmuir* **1996**, *12*, 3675-3681.

(76) Chen, W.; McCarthy, T. J. *Macromolecules* **1997**, *30*, 78-86.

(77) Lvov, Y.; Ariga, K.; Ichinose, I.; Kunitake, T. *J. Am. Chem. Soc.* **1995**, *117*, 6117-6123.

(78) Sultana, N.; Schenkman, J. B.; Rusling, J. F. *J. Am. Chem. Soc.* **2005**, *127*, 13460-13461.

(79) Beissenhirtz, M. K.; Scheller, F. W.; Lisdat, F. *Anal. Chem.* **2004**, *76*, 4665-4671.

(80) Caruso, F.; Furlong, D. N.; Ariga, K.; Ichinose, I.; Kunitake, T. *Langmuir* **1998**, *14*, 4559-4565.

(81) Lvov, Y.; Ariga, K.; Onda, M.; Ichinose, I.; Kunitake, T. *Langmuir* **1997**, *13*, 6195-6203.

(82) Cassagneau, T.; Mallouk, T. E.; Fendler, J. H. *J. Am. Chem. Soc.* **1998**, *120*, 7848-7859.

(83) Ostrander, J. W.; Mamedov, A. A.; Kotov, N. A. *J. Am. Chem. Soc.* **2001**, *123*, 1101-1110.

(84) Tian, S.; Liu, J.; Zhu, T.; Knoll, W. *Chem. Mater.* **2004**, *16*, 4103-4108.

(85) Johnston, A. P. R.; Mitomo, H.; Read, E. S.; Caruso, F. *Langmuir* **2006**, *22*, 3251-3258.

(86) Chen, X.; Lang, J.; Liu, M. *Thin Solid Films* **2002**, *409*, 227-232.

(87) Lvov, Y.; Decher, G.; Sukhorukov, G. *Macromolecules* **1993**, *26*, 5396-5399.

(88) Ariga, K.; Lvov, Y.; Kunitake, T. *J. Am. Chem. Soc.* **1997**, *119*, 2224-2231.

(89) Tedeschi, C.; Caruso, F.; Mohwald, H.; Kirstein, S. *J. Am. Chem. Soc.* **2000**, *122*, 5841-5848.

(90) Bergbreiter, D. E.; Liao, K.-S. *Soft Matter* **2009**, *5*, 23-28.

(91) Berndt, P.; Kurihara, K.; Kunitake, T. *Langmuir* **1992**, *8*, 2486-2490.

(92) Zhang, X.; Chen, H.; Zhang, H. *Chem. Commun.* **2007**, 1395-1405.

(93) Quinn, J. F.; Johnston, A. P. R.; Such, G. K.; Zelikin, A. N.; Caruso, F. *Chem. Soc. Rev.* **2007**, *36*, 707-718.

(94) Stockton, W. B.; Rubner, M. F. *Macromolecules* **1997**, *30*, 2717-2725.

(95) Wang, L.; Wang, Z.; Zhang, X.; Shen, J.; Chi, L.; Fuchs, H. *Macromol. Rapid Commun.* **1997**, *18*, 509-514.

(96) Sukhishvili, S. A.; Granick, S. *J. Am. Chem. Soc.* **2000**, *122*, 9550-9551.

(97) Sukhishvili, S. A.; Granick, S. *Macromolecules* **2002**, *35*, 301-310.

(98) Liu, Y.; Bruening, M. L.; Bergbreiter, D. E.; Crooks, R. M. *Angew. Chem. Int. Ed. Engl.* **1997**, *36*, 2114-2116.

(99) Liu, Y.; Zhao, M.; Bergbreiter, D. E.; Crooks, R. M. *J. Am. Chem. Soc.* **1997**, *119*, 8720-8721.

(100) Kohli, P.; Blanchard, G. J. *Langmuir* **2000**, *16*, 4655-4661.

(101) Kohli, P.; Blanchard, G. J. *Langmuir* **2000**, *16*, 8518-8524.

(102) Such, G. K.; Quinn, J. F.; Quinn, A.; Tjipto, E.; Caruso, F. *J. Am. Chem. Soc.* **2006**, *128*, 9318-9319.

(103) Kolb, H. C.; Finn, M. G.; Sharpless, K. B. *Angew. Chem. Int. Ed.* **2001**, *40*, 2004-2021.

(104) Bock, V. D.; Hiemstra, H.; van Maarseveen, J. H. *Eur. J. Org. Chem.* **2006**, 51-68.

(105) Such, G. K.; Tjipto, E.; Postma, A.; Johnston, A. P. R.; Caruso, F. *Nano Lett.* **2007**, *7*, 1706-1710.

(106) Kotov, N. A. *Nanostruct. Mater.* **1999**, *12*, 789-796.

(107) Anzai, J.-i.; Kobayashi, Y. *Langmuir* **2000**, *16*, 2851-2856.

(108) Inoue, H.; Anzai, J.-i. *Langmuir* **2005**, *21*, 8354-8359.

(109) Shimazaki, Y.; Mitsuishi, M.; Ito, S.; Yamamoto, M. *Langmuir* **1997**, *13*, 1385-1387.

(110) Wang, X.; Naka, K.; Itoh, H.; Uemura, T.; Chujo, Y. *Macromolecules* **2003**, *36*, 533-535.

(111) Shimazaki, Y.; Nakamura, R.; Ito, S.; Yamamoto, M. *Langmuir* **2001**, *17*, 953-956.

(112) Tang, T.; Qu, J.; Mullen, K.; Webber, S. E. *Langmuir* **2006**, *22*, 26-28.

(113) Sukhorukov, G. B.; Donath, E.; Lichtenfeld, H.; Knippel, E.; Knippel, M.; Budde, A.; Möhwald, H. *Colloids Surf., A* **1998**, *137*, 253-266.

(114) Caruso, F. *Adv. Mater.* **2001**, *13*, 11-22.

(115) Kidambi, S.; Dai, J.; Li, J.; Bruening, M. L. *J. Am. Chem. Soc.* **2004**, *126*, 2658-2659.

(116) Kidambi, S.; Bruening, M. L. *Chem. Mater.* **2005**, *17*, 301-307.

(117) Bhattacharjee, S.; Bruening, M. L. *Langmuir* **2008**, *24*, 2916-2920.

(118) Bhattacharjee, S.; Dotzauer, D. M.; Bruening, M. L. *J. Am. Chem. Soc.* **2009**, *131*, 3601-3610.

(119) Dotzauer, D. M.; Dai, J.; Sun, L.; Bruening, M. L. *Nano Lett.* **2006**, *6*, 2268-2272.

(120) Dotzauer, D. M.; Bhattacharjee, S.; Wen, Y.; Bruening, M. L. *Langmuir* **2009**, *25*, 1865-1871.

(121) Caruso, F.; Caruso, R. A.; Möhwald, H. *Science* **1998**, *282*, 1111-1114.

(122) Mayya, K. S.; Gittins, D. I.; Dibaj, A. M.; Caruso, F. *Nano Lett.* **2001**, *1*, 727-730.

(123) Caruso, R. A.; Susha, A.; Caruso, F. *Chem. Mater.* **2001**, *13*, 400-409.

(124) Caruso, F.; Caruso, R. A.; Möhwald, H. *Chem. Mater.* **1999**, *11*, 3309-3314.

(125) Lvov, Y.; Antipov, A. A.; Mamedov, A.; Mohwald, H.; Sukhorukov, G. B. *Nano Lett.* **2001**, *1*, 125-128.

(126) Schneider, G.; Decher, G. *Nano Lett.* **2004**, *4*, 1833-1839.

(127) Liang, Z.; Susha, A.; Caruso, F. *Chem. Mater.* **2003**, *15*, 3176-3183.

(128) Tian, Y.; He, Q.; Cui, Y.; Li, J. *Biomacromolecules* **2006**, *7*, 2539-2542.

(129) Liang, Z.; Susha, A. S.; Yu, A.; Caruso, F. *Adv. Mater.* **2003**, *15*, 1849-1853.

(130) Hou, S.; Wang, J.; Martin, C. R. *Nano Lett.* **2005**, *5*, 231-234.

(131) Bruening, M.; Dotzauer, D. *Nat. Mater.* **2009**, *8*, 449-450.

(132) Shiratori, S. S.; Yamada, M. *Polym. Adv. Technol.* **2000**, *11*, 810-814.

(133) Shiratori, S. S.; Ito, T.; Yamada, T. *Colloids Surf., A* **2002**, *198-200*, 415-423.

(134) Lee, S.-S.; Hong, J.-D.; Kim, C. H.; Kim, K.; Koo, J. P.; Lee, K.-B. *Macromolecules* **2001**, *34*, 5358-5360.

(135) Cho, J.; Char, K.; Hong, J. D.; Lee, K.-B. *Adv. Mater.* **2001**, *13*, 1076-1078.

(136) Ladam, G.; Schaad, P.; Voegel, J. C.; Schaaf, P.; Decher, G.; Cuisinier, F. *Langmuir* **1999**, *16*, 1249-1255.

(137) Chiarelli, P. A.; Johal, M. S.; Holmes, D. J.; Casson, J. L.; Robinson, J. M.; Wang, H.-L. *Langmuir* **2002**, *18*, 168-173.

(138) Campbell, V. E.; Chiarelli, P. A.; Kaur, S.; Johal, M. S. *Chem. Mater.* **2005**, *17*, 186-190.

(139) Lefaux, C. J.; Zimberlin, J. A.; Dobrynin, A. V.; Mather, P. T. *J. Polym. Sci., Part B: Polym. Phys.* **2004**, *42*, 3654-3666.

(140) Schlenoff, J. B.; Dubas, S. T.; Farhat, T. *Langmuir* **2000**, *16*, 9968-9969.

(141) Izquierdo, A.; Ono, S. S.; Voegel, J. C.; Schaaf, P.; Decher, G. *Langmuir* **2005**, *21*, 7558-7567.

(142) Lu, C.; Donch, I.; Nolte, M.; Fery, A. *Chem. Mater.* **2006**, *18*, 6204-6210.

(143) Krogman, K. C.; Zacharia, N. S.; Schroeder, S.; Hammond, P. T. *Langmuir* **2007**, *23*, 3137-3141.

(144) Jiang, S.; Liu, M. *Chem. Mater.* **2004**, *16*, 3985-3987.

(145) Cooper, T. M.; Campbell, A. L.; Crane, R. L. *Langmuir* **1995**, *11*, 2713-2718.

(146) Caruso, F.; Möhwald, H. *J. Am. Chem. Soc.* **1999**, *121*, 6039-6046.

(147) Dubas, S. T.; Schlenoff, J. B. *Macromolecules* **1999**, *32*, 8153-8160.

(148) Deng, H.-Y.; Xu, Y.-Y.; Zhu, B.-K.; Wei, X.-Z.; Liu, F.; Cui, Z.-Y. *J. Membr. Sci.* **2008**, *323*, 125-133.

(149) Hilal, N.; Al-Zoubi, H.; Darwish, N. A.; Mohamma, A. W.; Abu Arabi, M. *Desalination* **2004**, *170*, 281-308.

(150) Liu, X.; Bruening, M. L. *Chem. Mater.* **2004**, *16*, 351-357.

(151) Miller, M. D.; Bruening, M. L. *Langmuir* **2004**, *20*, 11545-11551.

(152) Stanton, B. W.; Harris, J. J.; Miller, M. D.; Bruening, M. L. *Langmuir* **2003**, *19*, 7038-7042.

(153) Jin, W.; Toutianoush, A.; Tieke, B. *Langmuir* **2003**, *19*, 2550-2553.

(154) Ouyang, L.; Malaisamy, R.; Bruening, M. L. *J. Membr. Sci.* **2008**, *310*, 76-84.

(155) El-Hashani, A.; Toutianoush, A.; Tieke, B. *J. Membr. Sci.* **2008**, *318*, 65-70.

(156) Hong, S. U.; Malaisamy, R.; Bruening, M. L. *J. Membr. Sci.* **2006**, *283*, 366-372.

(157) Hong, S. U.; Miller, M. D.; Bruening, M. L. *Ind. Eng. Chem. Res.* **2006**, *45*, 6284-6288.

(158) Hong, S. U.; Malaisamy, R.; Bruening, M. L. *Langmuir* **2007**, *23*, 1716-1722.

(159) Hong, S. U.; Ouyang, L.; Bruening, M. L. *J. Membr. Sci.* **2009**, *327*, 2-5.

(160) Leväsalmi, J.-M.; McCarthy, T. J. *Macromolecules* **1997**, *30*, 1752-1757.

(161) van Ackern, F.; Krasemann, L.; Tieke, B. *Thin Solid Films* **1998**, *327-329*, 762-766.

(162) Sullivan, D. M.; Bruening, M. L. *Chem. Mater.* **2003**, *15*, 281-287.

(163) Dai, J.; Baker, G. L.; Bruening, M. L. *Anal. Chem.* **2006**, *78*, 135-140.

(164) Salloum, D. S.; Schlenoff, J. B. *Biomacromolecules* **2004**, *5*, 1089-1096.

(165) Wang, Y.; Caruso, F. *Chem. Mater.* **2006**, *18*, 4089-4100.

(166) Onda, M.; Lvov, Y.; Ariga, K.; Kunitake, T. *J. Ferment. Bioeng.* **1996**, *82*, 502-506.

(167) Shchukin, D. G.; Möhwald, H. *Langmuir* **2005**, *21*, 5582-5587.

Chapter 2

Polyelectrolyte Multilayer Films as Nanofiltration Membranes for Cation Separations

This work was recently published in Journal of Membrane Science.[1]

2.1. Introduction

Hard water is common throughout the world, and the United States Geological Survey reports that 85% of US homes have hard water that usually contains high levels of Ca^{2+} or Mg^{2+}.[2] Such water is not harmful, but it causes undesirable effects such as clogging of water faucets and deterioration of equipment, which is a costly problem in both residential and industrial settings.[3] The conventional water softening method, which is still popular around the world, is ion exchange using cation exchange resins in their sodium form.[4] However, the resin must be regenerated periodically in a process that consumes time, salt, and energy. Membrane-based separations provide an alternative to conventional treatments of hard water, and nanofiltration (NF) is probably the most promising membrane-based technology for alleviating water hardness because of its relatively low energy costs.[4-7] Unlike reverse osmosis (RO), NF allows the passage of small monovalent ions such as Na^{+} whose rejection is not necessary for softening water.[4,8,9] Passage of these monovalent ions reduces the osmotic pressure that must be overcome for water softening, and the high permeability of NF membranes (relative to RO membranes) also leads to low-pressure separations.[7] Hence, NF is attractive for

removal of multivalent ions in water softening and other applications including purification of wastewater in the pulp and paper industry, where environmental legislation requires the removal of elements such as Ca, Fe or Mg.[10]

Several research groups performed fundamental studies to understand the mechanisms behind multivalent ion removal in NF and showed that separation of charged solutes is based on both size and Donnan exclusion.[4,5,11] Thus, cation separations require a positively charged membrane with a relatively small effective pore size. Unfortunately, most commercial NF membranes are negatively charged,[9,11-13] although several experimental studies show that positively charged membranes can be fabricated.[14-16]

This chapter examines the properties of a series of positively charged membranes prepared by layer-by-layer adsorption of polyanions and polycations. The layer-by-layer deposition method was developed in the 1990s,[17,18] and a number of studies examined its utility for creating pervaporation, NF, and gas-separation membranes.[19-23] This method is attractive for preparing the ultrathin skin of composite membranes because film thickness can be controlled at the nanometer scale to allow for high flux, and film properties can be optimized by varying polyelectrolytes or deposition conditions.[24-29] Additionally, the charge near the surface of the film can be either positive or negative depending on whether films are terminated with a polycation or a polyanion.

Although a number of papers examined the use of polyelectrolyte multilayers (PEMs) in anion separations,[20,30-34] very few studies investigated cation separations. Tieke's group reported that PEMs comprised of 60 layer pairs of poly(vinylamine) and poly(vinylsulfate) exhibit a 95% rejection of $MgCl_2$ at an operating pressure of 10 bar,[21] but the use of such a large number of layers makes membrane fabrication time consuming

and yields very low flux. We studied NF of $MgSO_4$ with much thinner PEMs that allow high flux,[35] but ultrathin, highly permeable PEMs have not been examined for the separation of monovalent and divalent cations, which is important in water softening.

This work focuses on NF of mixed-salt solutions containing Na^+ and Mg^{2+} or Na^+ and Ca^{2+}, the three typical components of hard water. Notably, four- or five-bilayer poly(styrenesulfonate)/poly(allylamine hydrochloride) (PSS/PAH) films deposited on ultrafiltration membranes or porous alumina substrates provide ~95% rejection of Mg^{2+} and a Na^+/Mg^{2+} selectivity of around 20. Ca^{2+} rejections are similar to those of Mg^{2+}. Variation of polyelectrolytes and deposition conditions allows optimization of cation rejections by controlling film properties such as ionic crosslink density,[33] zeta potential,[36] and swelling.[37] Streaming potential investigations demonstrate that the use of higher salt concentrations in polycation deposition solutions leads to higher charge near the film surface and, hence, higher Mg^{2+} rejections. Moreover, ζ potentials obtained using different concentrations of KCl and $MgCl_2$ suggest that adsorption of Mg^{2+} on the membrane surface leads to high Mg^{2+} rejections even at high $MgCl_2$ concentrations.[12,38,39]

2.2. Experimental Section

2.2.1. Materials

Poly(sodium 4-styrenesulfonate) (PSS, M_w = 70,000 Da), poly(allylamine hydrochloride) (PAH, M_w = 70,000 Da), and poly(diallyldimethylammonium chloride) (PDADMAC, M_w = 100,000-200,000 Da, 20 wt% in water) were obtained from Sigma-

Aldrich and used without further purification. NaCl and NaBr (Jade Scientific), $MnCl_2$ (Alfa Aesar), $MgCl_2 \cdot 6H_2O$ (Columbus Chemical), and $CaCl_2 \cdot 2H_2O$ (Sigma-Aldrich) were also used as received. Deionized water (Milli-Q purification system, 18.2 MΩ·cm) was employed for rinsing membranes and preparing polyelectrolyte and feed solutions. The pH of polyelectrolyte solutions was adjusted with dilute HCl or NaOH.

Two types of substrates were used in the experiments: porous alumina supports (0.02-μm Whatman Anodisk filters, average membrane thickness of 60 μm) and polyethersulfone (PES) ultrafiltration membranes (Millipore, cat. number PBQK 02510, molecular weight cutoff of 50 000 Da, effective pore size of 4-5 nm, membrane thickness of 100-150 μm). Prior to film deposition, the porous alumina supports were UV/O_3 cleaned with the feed side up (Boekel UV-Clean Model 135500) for 15 min. To remove the wetting agent on the surface of the PES ultrafiltration membranes, these materials were soaked in deionized water for about one hour, during which the water was replaced two or three times.

2.2.2. Film Deposition

The pretreated substrate was loaded in a home-made membrane holder that exposes only the feed side of the membrane to the polyelectrolyte solutions. Deposition started with immersion of the membrane surface in 0.02 M PSS. (Polyelectrolyte concentrations are always given with respect to the repeating unit.) PSS was deposited first due to potential electrostatic attractions with the positively charged alumina support or hydrophobic interactions with PES.[31,40] The substrate was then rinsed with deionized water for 1 min before immersion in a polycation solution (PAH or PDADMAC) followed by another 1-min rinse. Additional layers were deposited similarly to give the

desired number of bilayers. The time allowed for polyelectrolyte adsorption varied according to the type of multilayer deposited. For PSS/PAH, the substrate was dipped for 2 min in PSS solutions and 5 min in PAH solutions, while for PSS/PDADMAC, the deposition time was 3 min for both polyelectrolytes. Different deposition conditions (type and concentration of supporting electrolyte and pH value) were chosen based on prior work with anion separations.[35] Figure 2.1 shows the structures of the polyelectrolytes investigated in this study.

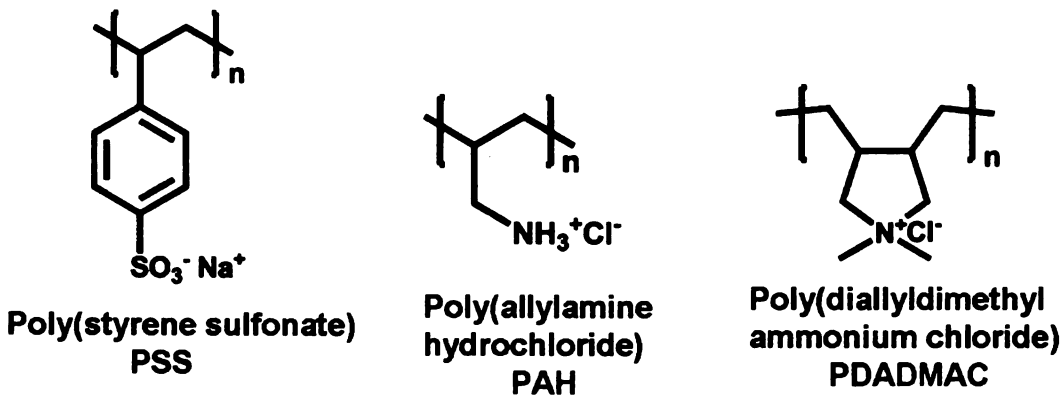

Figure 2.1. Structures of the polyelectrolytes used in this study.

2.2.3. Characterization of Membranes

2.2.3.1. Film Thickness Estimations with SEM

Cross-sectional images of porous alumina supports coated with PEMs were obtained with a Hitachi S-4700 II field-emission scanning electron microscope (FESEM). Membranes were fractured immediately after exposure to liquid nitrogen and the top, bottom, and cross-sectional surfaces of the membrane were subsequently sputter-coated (Pelco model SC-7 auto sputter coater) with 5 nm of gold before imaging.

2.2.3.2. Zeta Potential measurements

An asymmetric clamping cell (Anton Paar, Graz, Austria) attached to a streaming potential analyzer (BI-EKA, Brookhaven Instruments, Holtsville, NY) was employed to measure the ζ potentials of surfaces coated with PEMs. The test sample was placed against a grooved poly(methyl methacrylate) (PMMA) spacer, and the streaming potential was measured between two Ag/AgCl electrodes on opposite ends of the clamping cell. Solutions of KCl (1 mM, 5 mM, or 10 mM) or $MgCl_2$ (0.333 mM, 1.666 mM, and 3.33 mM) served as the electrolytes for the measurements. Polyelectrolyte multilayer films on PES membranes were prepared in the same way as for transport studies, but different PES substrates (50 kDa membranes from Pall, Port Washington, NY) were used due to the large surface area requirement of the clamping cell. The ζ potentials of the PEMs were calculated using equation 1, where ζ_{Test} is the ζ potential of the membrane, ζ_{Avg} is the effective ζ potential measured with the membrane pressed against the spacer, and ζ_{Spacer} is the ζ potential of the PMMA spacer surface.[41]

$$\zeta_{Test} = 2\zeta_{Avg} - \zeta_{Spacer} \qquad (1)$$

To find ζ_{Spacer}, or ζ_{PMMA}, the ζ potential of PMMA clamped to the PMMA spacer was determined prior to the streaming potential measurement of the membranes coated with PEM films. The reported values are the average of ζ potentials determined in two flow directions with at least two membranes.

2.2.4. Nanofiltration Studies

NF experiments were performed at room temperature (23 °C) using a customized cross-flow system described previously.[35] The system was pressurized with Ar to 4.8 bar,

and the feed tank was filled with a 2 L solution containing NaCl, $MgCl_2$, or $CaCl_2$, or a combination of these salts. Approximate osmotic pressures of 1g/L Na^+ (from NaCl), Mg^{2+} (from $MgCl_2$), and Ca^{2+} (from $CaCl_2$) solutions are 2.1 bar, 3.0 bar, and 1.8 bar, respectively, assuming 100% rejection. A stainless steel frit (Mott Corp., Farmington, CT) was used as a prefilter to remove rust or particulate matter from the feed solution. The flow meter, which was located between the pump and the membrane cells, was set to 18 mL/min, which is high enough to minimize concentration polarization.[35] The membrane was housed in an O-ring cell that exposes an active surface area of 1.7 cm^2. After an 18 h-stabilization period, permeate samples were collected every 30 min for 2 h, and the reported fluxes are the steady-state permeate fluxes after 18 h of filtration. The feed solution was sampled at the end of the filtration to take into account any concentration changes during the experiment. Cation concentrations were determined by atomic absorption spectroscopy (AAS) using a Varian Spectra Atomic Absorption-200 instrument, and the solute rejection, R, was calculated using equation (2), where C_p and C_f are solute concentrations in the permeate and feed, respectively. Rejection and flux values are averages from at least two membranes, and ± values represent standard deviations.

$$R = \left(1 - C_p / C_f\right) \times 100\% \quad (2)$$

Equation (3) defines the transport selectivity of solute A over solute B, α_B^A, which can be simply expressed in terms of rejections.

$$\alpha_B^A = \frac{C_{A,p}}{C_{A,f}} \cdot \frac{C_{B,f}}{C_{B,p}} = \frac{100 - R_A(\%)}{100 - R_B(\%)} \quad (3)$$

2.3. Results and Discussion

Table 2.1 lists the diffusion coefficients and Stokes' radii of hydrated Na^+, $Mg^{2+}$and Ca^{2+} ions. (Stokes' radii are determined from diffusion coefficients and are similar to hydrated radii.) The Stokes' radius of Mg^{2+} is almost twice that of Na^+, which is reflected by the smaller diffusivity for Mg^{2+}. Although the Stokes' radius of Ca^{2+} is smaller than that of Mg^{2+}, it is still 0.125 nm larger than that of Na^+. Given these radii, size-selective nanofiltration of hydrated Mg^{2+} or Ca^{2+} in the presence of Na^+ will require membranes with pore sizes on the sub-nm scale. Previous studies of neutral molecule transport suggest that the effective pore diameters of PSS/PAH[42] and PSS/PDADMAC[33] membranes are about 0.4-0.5 nm and 0.7-1.0 nm, respectively. Thus, we investigated these polyelectrolyte systems for selective removal of Mg^{2+} or Ca^{2+} in the presence of Na^+.

Table 2.1. Aqueous diffusion coefficients (D) and Stokes' radii (r_s) of several cations.[5,43]

Ions	D (m^2/s)	r_s (nm)
Na^+	1.333×10^{-9}	0.183
Mg^{2+}	0.706×10^{-9}	0.345
Ca^{2+}	0.792×10^{-9}	0.308

2.3.1. Estimation of the Thicknesses of PEMs

One of the major assets of PEMs is their minimal thickness, which should allow high fluxes in NF. However, quantifying the thicknesses of films on porous substrates is difficult. Under typical deposition conditions (0.5 M NaCl in PSS solutions and 1 M NaCl in PAH solutions), $[PSS/PAH]_5$ films deposited on aluminum-coated Si wafers have an ellipsometric thickness of 22±1 nm, and previous work suggests that the thicknesses of PEMs grown on flat surfaces are similar to those of films formed on porous alumina membranes.[20] Figure 2.2-(a) shows a cross-sectional SEM image of a porous alumina membrane coated with a $[PSS/PAH]_5$ film. Although it is difficult to tell exactly where the polyelectrolyte multilayer begins and ends, the image shows that the film is generally less than 50 nm thick. In Figure 2.2-(b) of alumina coated with $[PSS/PAH]_{10}$ films, the polyelectrolyte coating is somewhat easier to see and has a thickness of about 50 nm. Importantly, the interior of the alumina membrane is clearly open. The structure of porous alumina, which includes 20 nm surface pores and larger (0.2 μm-diameter) underlying pores in the bulk, facilitates complete coverage of these supports.

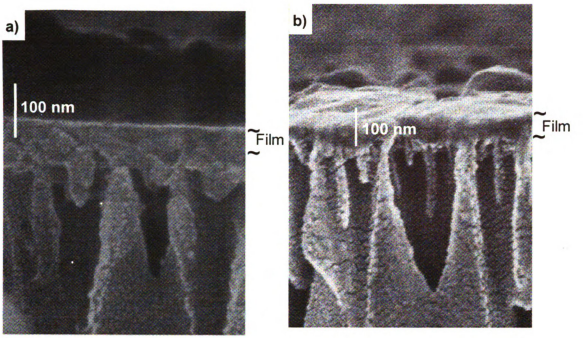

Figure 2.2 Cross-sectional SEM images of a porous alumina membrane coated with a $[PSS/PAH]_n$ film. (a) $[PSS/PAH]_5$ and (b) $[PSS/PAH]_{10}$.

2.3.2. Nanofiltration of Mixed-Salt Solutions with PSS/PAH on PES Supports

To examine the separation of cations, we perform NF of solutions containing 1 g/L Na^+ (added in the form of NaCl) and 1 g/L Mg^{2+} (added in the form of $MgCl_2$). Previous research showed that $[PSS/PAH]_4PSS$ and $[PSS/PAH]_5$ films on porous alumina exhibit a rejection of $MgSO_4$ as high as 96% in single salt experiments,[35] so we begin our studies with membranes containing PSS/PAH films.

Table 2.2 presents NF results obtained with PSS/PAH films deposited on 50 kDa PES supports and shows how deposition conditions affect NF performance. Membrane A is produced using the same solution compositions that previously yielded 96% $MgSO_4$ rejection,[35] but the rejection of Mg^{2+} from a solution containing $MgCl_2$ and NaCl is only

82%. This result suggests that the 96% $MgSO_4$ rejection observed previously in single salt experiments occurred in large part because of high exclusion of SO_4^{2-} ions. To enhance the rejection of Mg^{2+} from chloride solutions, we change the top layer of PSS/PAH membranes from PSS to PAH, which is positively charged. A 6% increase in Mg^{2+} rejection results from this change (compare membranes A and B, Table 2.2), suggesting that Donnan exclusion plays a role in the separation process. However, the flux decreass by about 25% on going from $[PSS/PAH]_4PSS$ to $[PSS/PAH]_4$ because membranes capped with PAH swell less than those capped with PSS, and less swelling should also lead to higher size-based Mg^{2+} rejection.[44,45]

Table 2.2. Solution fluxes and ion rejections from NF with PSS/PAH films deposited on 50 kDa PES supports. NF experiments were performed at 4.8 bar using mixed feed solutions containing 1 g/L Na^+ and 1 g/L Mg^{2+} (chloride salts).

Membrane (supporting salt concentration and pH value in deposition solutions)		Rejection of Cations (%)		Flux (m^3/m^2 day)	Selectivity (Na^+/Mg^{2+})
		Na^+	Mg^{2+}		
A	$[PSS/PAH]_4PSS$ PSS: 0.5 M $MnCl_2$, pH=2.1 PAH: 0.5 M NaBr, pH=2.3	-35±1	82.3±0.9	0.52±0.06	7.6±0.5
B	$[PSS/PAH]_4$ PSS: 0.5 M $MnCl_2$, pH=2.1 PAH: 0.5 M NaBr, pH=2.3	-27±3	88.6±0.7	0.38±0.02	11.1±0.4
C	$[PSS/PAH]_4$ PSS: 0.5 M NaCl, pH=2.1 PAH: 0.5 M NaCl, pH=2.3	-20±1	87.8±0.8	0.38±0.02	9.9±0.6
D*	$[PSS/PAH]_4$ PSS: 0.5 M NaCl, pH=2.1 PAH: 0.5 M NaCl, pH=2.3	-13±4	92.0±1.1	0.33±0.02	14.2±1.3
E	$[PSS/PAH]_4$ PSS: 0.5 M NaCl, pH=2.1 PAH: 1 M NaCl, pH=2.3	-9±1	92.0±0.2	0.56±0.02	13.6±0.3
F	$[PSS/PAH]_4$ PSS: 0.5 M NaCl, pH=2.3 PAH: 1 M NaCl, pH=2.3	-20±2	94.1±0.8	0.52±0.01	18.3±2.1
G	$[PSS/PAH]_4$ PSS: 0.5 M NaCl, pH=4.5 PAH: 1 M NaCl, pH=2.3	-13±3	92.4±0.4	0.50±0.09	14.8±0.6
H	$[PSS/PAH]_4$ PSS: 0.5 M NaCl, pH=2.3 PAH: 1 M NaCl, pH=4.5	-13±3	89.8±1.5	0.55±0.05	11.2±1.2
I	$[PSS/PAH]_3$ PSS: 0.5 M NaCl, pH=2.3 PAH: 1 M NaCl, pH=2.3	-17±2	83.5±1.1	0.72±0.03	7.1±0.4

* The top PAH layer was formed in a solution with 1 M NaCl at pH of 2.3.

Interestingly, negative Na^+ rejection appears in all the NF experiments with mixed NaCl and $MgCl_2$ solutions in this study. This phenomenon occurs due to the strong Mg^{2+} rejection and low Cl^- rejection of these membranes. Because the feed concentration of Cl^- is higher than that of Na^+ and little Mg^{2+} passes through the membrane, anions (Cl^-)

momentarily cross the membrane faster than cations to create a diffusion potential that enhances the transport of Na^+. (This diffusion potential also accelerates Mg^{2+} transport, but Mg^{2+} is highly excluded from the membrane.) In other words, with a high Mg^{2+} rejection, the co-transport of Na^+ with Cl^- results in a Na^+ concentration in the permeate that exceeds the Na^+ concentration in the feed, i.e., negative rejection.[46] (An equivalent explanation can be made using Donnan potentials.[47])

In early studies of polyelectrolyte films, we and others employed $MnCl_2$ and NaBr as supporting electrolytes during deposition of PSS and PAH, respectively.[17,48,49] However, NaCl is a more economical and environmentally friendly reagent, so we also examin membranes prepared with 0.5 M NaCl in PSS and PAH deposition solutions. Comparison of membranes B and C in Table 2.2 shows that flux and rejection are comparable for $[PSS/PAH]_4$ films deposited using either NaCl or $MnCl_2$/NaBr as supporting electrolytes. Thus, all the PEMs subsequently described here are produced using NaCl as supporting electrolyte.

In addition to changing the sign of the charge near the surface of PEMs by changing the top layer from a polyanion to a polycation, we can alter the magnitude of this charge by varying the ionic strength of polyelectrolyte deposition solutions. Previous work in our group showed that increasing the ionic strength employed during deposition of the top PSS layer in PSS/PAH membranes greatly enhances Cl^-/SO_4^{2-} selectivity in NF.[35] Thus, we increase the concentration of NaCl from 0.5 M to 1.0 M in the solutions used to deposit the top PAH layer of $[PSS/PAH]_4$ films in an attempt to increase Na^+/Mg^{2+} selectivity. Due to this change, rejection of Mg^{2+} increase from 88% to 92% while flux decrease slightly from 0.38 to 0.33 $m^3/(m^2\ day)$ (compare membranes C and D

in Table 2.2). In an effort to further improve the rejection of multivalent cations, all the PAH layers are deposited from solutions containing 1 M NaCl, while 0.5 M NaCl is employed during deposition of PSS layers (membrane E). Rejection remains the same as for membrane D, presumably because the composition of the outer layer is most critical in determining the charge near the surface of PEMs. At the same time, flux increases by 70% when using 1 M NaCl during deposition of all PAH layers rather than just the top layer. This suggests that the films are more highly swollen when all PAH layers are deposited from solutions of high ionic strength.[50,51] Higher swelling could occur because when high ionic strengths are employed during deposition, some of the charged groups in the polyelectrolyte films will have Na^+ or Cl^- counterions.[51,52] This should decrease the electrostatic interactions between polymer chains and enhance swelling.

The charge densities of weak polyelectrolytes vary with solution pH, so the pH of weak polyelectrolyte deposition solutions plays an important role in the formation of PEMs.[28,53] Krasemann and Tieke suggested that the density of ionic cross-links in PEMs reaches a maximum value when the deposition pH corresponds to the average of the pK_a values of the polycation and polyanion.[19] PSS is a strong polyelectrolyte and thus, changes in pH should not significantly alter its charge density. However, the pH of PSS deposition solution could affect the degree of PAH protonation in the film to which PSS is adsorbing. Comparison of membranes E and F (Table 2.2) shows that Mg^{2+} rejection increases slightly from 92 to 94% when changing the PSS deposition pH from 2.1 to 2.3. Additionally, Na^+ rejection decreases from -9% to -20% to give an overall Na^+/Mg^{2+} selectivity of 18. Increasing pH of the PSS deposition solution further to 4.5 slightly decreases Mg^{2+} rejection and Na^+/Mg^{2+} selectivity (membrane G).

PAH is a weak polyelectrolyte whose charge density varies greatly with deposition pH.[28,54] When pH of the PAH deposition solution is 4.5 (membrane H) rather than 2.3 (membrane F), rejection of Mg^{2+} decreases. This presumably occurs because of a lower charge density in the PEMs, which results from PAH being less protonated at pH 4.5.

Although the best PEM membranes exhibit a 94% Mg^{2+} rejection (membrane F in Table 2.2), flux is 30% less than the value of ~0.75 $m^3/(m^2$ day) at 4.8 bar, that is representative of pure water flux through commercial NF membranes. Therefore, we investigate the possibility of increasing flux by decreasing the number of PSS/PAH bilayers. On going from $[PSS/PAH]_4$ to $[PSS/PAH]_3$ films (compare membranes F and I in Table 2.2), flux increases by 40%, but Mg^{2+} rejection drops to 84%, suggesting that three bilayers of PSS/PAH may not be thick enough to fully cover the 50 kDa support. Unfortunately, decreasing the number of deposited layers is not an effective means for increasing flux without reducing Mg^{2+} rejection.

2.3.3. Nanofiltration of Mixed-Salt Solutions with Commercial NF Membranes and PSS/PAH on Porous Alumina Supports

In addition to the polyelectrolyte film, the underlying support can provide significant resistance to water flow if it is not highly permeable. Indeed, the flux through unmodified 50 kDa membranes at 4.8 bar after 18 h of equilibration was only 5.3 $m^3/(m^2$ day),[31] so the resistance of the support could be significant. To enhance flux, we deposite PSS/PAH films on porous alumina supports that have a surface pore diameter of 0.02 μm and an internal pore diameter of 0.2 μm. Pure water flux measurements show that the resistance of bare porous alumina membranes is approximately half of the resistance of

uncoated 50 kDa PES substrates after 18 h of filtration. Table 2.3 demonstrates that both $[PSS/PAH]_4$ and $[PSS/PAH]_5$ films on porous alumina give rejections of Mg^{2+} that are greater than 92%, and that the flux through these composite membranes exceeds 0.8 $m^3/(m^2\ day)$ at a pressure of 4.8 bar. In the case of porous alumina, the resistance of the support to water flow is likely negligible compared to the resistance of the PSS/PAH films. Optimization of polymer supports could potentially enhance flux to the levels found with alumina substrates.

Table 2.3. Solution fluxes and ion rejections from NF with PSS/PAH films deposited on porous alumina (0.02 μm-diameter surface pores) supports. Results with a commercial NF270 membrane are provided for comparison. NF experiments were performed at 4.8 bar using mixed feed solutions containing 1 g/L Na^+ and 1 g/L Mg^{2+} (chloride salts).

	Membrane (supporting salt concentration and pH value in deposition solutions)	Rejection of Cations (%)		Flux (m^3/m^2 day)	Selectivity (Na^+/Mg^{2+})
		Na^+	Mg^{2+}		
J	$[PSS/PAH]_4$ PSS: 0.5 M NaCl, pH=2.3 PAH: 1 M NaCl, pH=2.3	-3±2	92.5±0.5	1.05±0.03	13.9±1.0
K	$[PSS/PAH]_5$ PSS: 0.5 M NaCl, pH=2.3 PAH: 1 M NaCl, pH=2.3	-11±2	95.0±0.5	0.85±0.02	22.5±2.3
L	NF 270	-15±2	68.1±1.1	0.85±0.07	3.6±0.1

We also investigate the separation performance of a commercial NF membrane, NF270, provided by Dow-FILMTEC. NF 270 is a polyamide thin-film composite membrane with a negative surface charge, which is not beneficial for cation rejection. As Table 2.3 shows, NF 270 exhibits a Mg^{2+} rejection less than 70% along with a Na^+/Mg^{2+}

selectivity of only 3.6. In contrast, as mentioned above, composite membranes consisting of $[PSS/PAH]_4$ and $[PSS/PAH]_5$ on porous alumina allow fluxes comparable to that through NF 270, while exhibiting >92% rejection of Mg^{2+} and a Na^+/Mg^{2+} selectivity as high as 22 (Table 2.3).

2.3.4. Nanofiltration of Single-Salt Solutions at Two Salt Concentrations

To better understand the factors affecting salt rejection, we perform single-salt NF with both NF270 membranes and PSS/PAH films deposited on porous alumina or 50 kDa PES substrates (Table 2.4). Consistent with the mixed solution results, $MgCl_2$ rejections are remarkably higher with PSS/PAH membranes than with NF270. As expected, the fluxes through all membranes decline at higher salt concentrations due to an increased osmotic pressure, and this effect is less severe in the case of NaCl because of lower rejections. For reasons that we do not understand, however, the flux through NF270 membranes is a much stronger function of feed ionic strength than would be expected based on osmotic pressure arguments.

Table 2.4. Cation rejections (%) and flux values (listed in parentheses in $m^3\ m^{-2}\ day^{-1}$) for single-salt NF with PSS/PAH films deposited on different substrates. Results with a commercial NF270 membrane are provided for comparison. NF experiments were performed at 4.8 bar.

Membrane (supporting salt concentration and pH value in deposition solutions)	Rejection of Na^+ ($NaCl$)[a]		Rejection of Mg^{2+} ($MgCl_2$)[a]	
	0.1 g/L	1 g/L	0.1 g/L	1 g/L
F $[PSS/PAH]_4$ on a 50 kDa PES membrane PSS: 0.5 M NaCl,pH=2.3 PAH: 1 M NaCl, pH=2.3	74±3 (0.98±0.07)	40±2 (0.80±0.12)	93.5±0.9 (1.13±0.12)	93.6±1.6 (0.47±0.07)
K $[PSS/PAH]_5$ on 0.02 μm porous alumina PSS: 0.5 M NaCl,pH=2.3 PAH: 1 M NaCl, pH=2.3	62±5 (1.51±0.15)	48±7 (1.37±0.10)	97.3±1.1 (1.84±0.03)	96.3±0.4 (0.82±0.02)
L NF 270	59±1 (1.53±0.09)	41±2 (0.81±0.14)	47.4±1.0 (1.79±0.10)	52.4±1.9 (0.47±0.07)

[a]As elsewhere in this paper, concentrations of feed solutions refer to the cation, not the salt.

The drop in NaCl rejection with increasing NaCl concentrations (Table 2.4) is consistent with a Donnan exclusion mechanism for cation rejection, but the absence of such an effect with $MgCl_2$ is not. At high salt concentrations, Donnan exclusion should decrease considerably because the concentration of fixed charge in the membrane is closer to the concentration of ions in solution. The insensitivity of $MgCl_2$ rejection to $MgCl_2$ concentration could result from greater adsorption of Mg^{2+} on membranes at high $MgCl_2$ concentrations, which would give a more highly charged surface layer.[5,39,55] Greater charge near the surface may overcome the effects of increased charge screening

due to a higher ionic strength. However, if $MgCl_2$ rejection were primarily due to the large size of hydrated Mg^{2+}, rejection might also be a weak function of concentration. Streaming potential measurements described in section 2.3.7 suggest that Mg^{2+} adsorbs to the membrane to increase positive charge near the surface.

2.3.5. Nanofiltration of Mixed-Salt Solutions with PSS/PDADMAC or Hybrid Membranes

To enhance the permeability of the PEMs, we employ PSS/PDADMAC films because this polyelectrolyte system swells more in water than PSS/PAH due to the relatively low charge density of PDADMAC and the accompanying lower density of ionic cross links.[33,37] Table 2.5 shows the results of NF of mixed solutions containing 1 g/L Na^+ and 1 g/L Mg^{2+} (chloride salts) using membranes composed of PSS/PDADMAC films on alumina supports.

Table 2.5. Solution fluxes and ion rejections from NF with PSS/PDADMAC and hybrid $(PSS/PDADMAC)_4$+(PSS/PAH) films deposited on porous alumina (0.02 μm-diameter surface pores) supports. NF experiments were performed at 4.8 bar using mixed feed solutions containing 1 g/L Na^+ and 1 g/L Mg^{2+} (chloride salts).

Membrane (supporting salt concentration and pH value in deposition solutions)	Rejection of Cations (%)		Flux (m^3/m^2 day)	Selectivity (Na^+/Mg^{2+})
	Na^+	Mg^{2+}		
M* $[PSS/PDADMAC]_4PSS$ PSS: 0.5 M NaCl PDADMAC: 0.5 M NaCl	1±5	38.3±0.8	1.74±0.03	1.6±0.1
N $[PSS/PDADMAC]_5$ PSS: 0.5 M NaCl PDADMAC: 0.5 M NaCl	-5±1	42.0±0.4	1.95±0.05	1.8±0.1
O $[PSS/PDADMAC]_7$ PSS: 0.1 M NaCl PDADMAC: 0.1 M NaCl	6±5	24.4±1.3	3.58±0.11	1.2±0.1
P $[PSS/PDADMAC]_4PSS/PAH$ PSS: 0.5 M NaCl PDADMAC: 0.5 M NaCl PSS: 0.5 M NaCl, pH=2.3 PAH: 0.5 M NaCl, pH=2.3	-29±1	76.1±0.5	1.40±0.13	5.4±0.1
Q $[PSS/PDADMAC]_4PSS/PAH$ PSS: 0.5 M NaCl PDADMAC: 0.5 M NaCl PSS: 0.5 M NaCl, pH=2.3 PAH: 1 M NaCl, pH=2.3	-28±2	87.5±1.6	1.14±0.13	11.1±0.7
R $[PSS/PDADMAC]_4PSS/PAH$ PSS: 0.5 M NaCl PDADMAC: 0.5 M NaCl PSS: 0.5 M NaCl, pH=2.3 PAH: 2.5 M NaCl, pH=2.3	-19±2	92.6±0.8	1.04±0.15	16.2±1.7

* The top PSS layer was formed in a solution with 1 M NaCl.

Because both PSS and PDADMAC are strong polyelectrolytes, varying the pH value of the deposition solutions should not change the structure of the PEMs significantly. Thus, PSS/PDADMAC membranes were prepared without adjusting the

pH of the polyelectrolyte solutions, and unadjusted pH values is 6.2 for PSS solutions containing 0.1 or 0.5 M NaCl, 4.5 for PDADMAC solutions containing 0.1 M NaCl, and 5.0 for PDADMAC containing 0.5 M NaCl. NF with $[PSS/PDADMAC]_4PSS$ membranes deposited from 0.5 M NaCl solutions (membrane M, Table 2.5) shows a solution flux of 1.7 $m^3/(m^2\ day)$, but a Mg^{2+} rejection of only 40%. Termination of these membranes with a layer of polycation, PDADMAC, does not greatly enhance Mg^{2+} rejection (membrane N, Table 2.5).

Our previous research showed that PSS/PDADMAC films prepared from 0.1 M NaCl solutions swell 65% less than films prepared from 0.5 M NaCl.[37] Therefore, we also examine NF with PSS/PDADMAC membranes prepared using solutions containing 0.1 M NaCl. Even though we use 7 PSS/PDADMAC bilayers in membranes prepared using 0.1 M NaCl deposition solutions, flux through these systems is still almost twice that through $[PSS/PDADMAC]_5$ films prepared using solutions containing 0.5 M NaCl (compare membranes O and N in Table 2.5). The high flux through membrane O presumably occurs because films prepared in the presence of 0.1 M NaCl are very thin. (Such films typically have bilayers thicknesses that are about 50% of those for films prepared in 0.5 M NaCl.[37]) Consistent with a thin film that does not fully cover the support, Mg^{2+} rejection is only 24% for membrane O.

One could try to fully cover the support by depositing more PSS/PDADMAC bilayers, but this would result in an impractically long deposition process. Rather than coating the substrate with many bilayers of PSS/PDADMAC, we deposite one capping bilayer of PSS/PAH on four bilayers of PSS/PDADMAC deposited from 0.5 M NaCl. Three different membranes were prepared with the outer PAH layer deposited from

solutions containing 0.5 M, 1 M, or 2.5 M NaCl (membranes P, Q, and R in Table 2.5). In all cases, flux decreases and rejection of Mg^{2+} increases compared to $[PSS/PDADMAC]_5$ membranes, presumably because deposition of the PSS/PAH bilayers yields a more dense surface.[37] However, only deposition of the outer PAH layer from 2.5 M NaCl gives a Mg^{2+} rejection greater than 90%. In this case, the membrane performance is essentially equivalent to that of a $[PSS/PAH]_4$ film deposited on porous alumina (membrane J, Table 2.3), so there is no major advantage to formation of hybrid membranes.

2.3.6. Calcium Rejection by PSS/PAH Films on Porous Alumina

Because Ca^{2+} is also an important component in hard water, we examine the ability of membrane K (Table 2.4, $[PSS/PAH]_5$ on porous alumina) to reject Ca^{2+}. We choose this membrane because it gives the highest Mg^{2+} rejections and Na^+/Mg^{2+} selectivities. When the feed solution contains 1 g/L of Na^+ and 1 g/L of Ca^{2+} (chloride salts), rejection of Ca^{2+} is 98% and the Na^+/Ca^{2+} selectivity is as high as 50 (Table 2.6). Higher rejection of Ca^{2+} than Mg^{2+} is probably due to more extensive adsorption of Ca^{2+} on the film, which results in a more positively charged membrane.[56] The higher positive charge may also be responsible for the relatively high rejection of Na^+ in the $NaCl/CaCl_2$ solution. With feed solutions containing Ca^{2+}, Mg^{2+}, and Na^+, rejections are greater than 95% for both Ca^{2+} and Mg^{2+}, and the rejection of Na^+ decreases substantially compared to NF of solutions with only Na^+ and Ca^{2+}.

Table 2.6. Solution fluxes and ion rejections from NF with Membrane K (five bilayers of PSS/PAH deposited on porous alumina supports). NF experiments were performed at 4.8 bar using mixed feed solutions containing either Na^+ and Ca^{2+} or Na^+, Ca^{2+} and Mg^{2+} (chloride salts).

Feed Concentration (g/L)			Rejection of Cations (%)			Flux (m^3/m^2 day)	Selectivity	
Na^+	Ca^{2+}	Mg^{2+}	Na^+	Ca^{2+}	Mg^{2+}		(Na^+/Ca^{2+})	(Na^+/Mg^{2+})
1	1	0	28±5	98.5±0.4	-	0.94±0.14	50±10	-
1	0.62[a]	0.38[a]	-5±2	96.0±0.2	95.2±0.4	0.79±0.09	25±2	21±3

[a] Ca^{2+} and Mg^{2+} concentrations were chosen to achieve 1 g/L of divalent cation with an equimolar solution.

2.3.7. Streaming Potential Measurements

The above results suggest that the charge near the surface of the PEMs plays an important role in ion separations, so we perform streaming potential measurements to better correlate ion transport with surface charge. Figure 2.3 presents the ζ potentials derived from streaming potential measurements in 1 mM KCl with both PSS/PAH and PSS/PDADMAC films deposited on 50 kDa PES membranes. As expected, the ζ potential is negative after deposition of a polyanion and positive after deposition of a polycation.[36,57,58] The ζ potential of the first PSS layer is always more negative than the others because the bare PES substrate has a ζ potential of approximately -18 mV. (Adsorption of PSS to the PES membrane likely occurs via hydrophobic interactions.) The positive ζ potential induced by PDADMAC was 5-10 mV larger than that due to PAH, presumably because of a greater overcompensation of the negative charge by

PDADMAC.[59] Nevertheless, PEMs capped with PDADMAC show lower Mg^{2+} rejections than PEMs capped with PAH, presumably because of higher swelling, as noted earlier.[37]

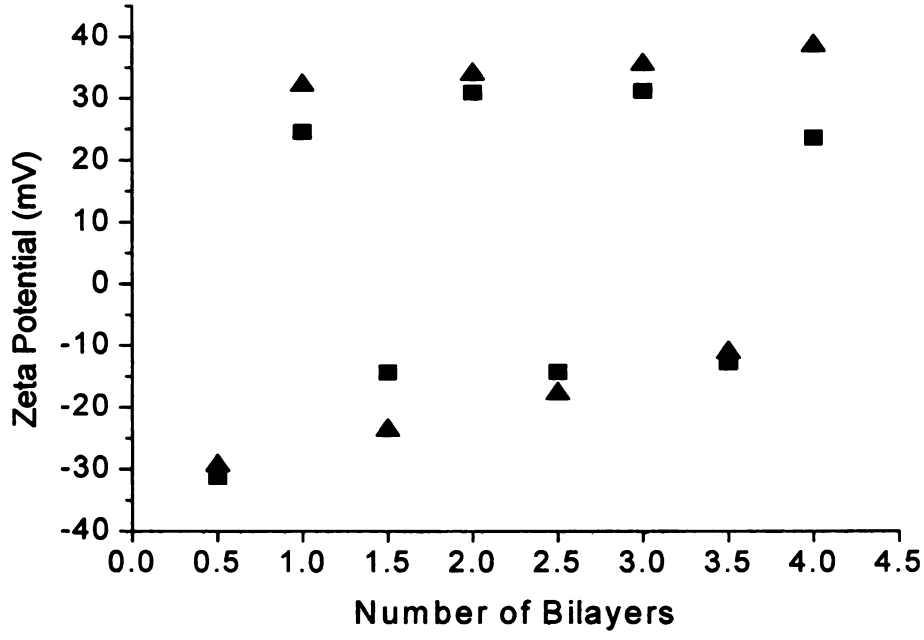

Figure 2.3. ζ potentials of $[PSS/PAH]_n$ (squares) and $[PSS/PDADMAC]_n$ (triangles) films on PES substrates. Non-integer numbers of bilayers represent films terminated with PSS, whereas integer numbers of bilayers denote polycation-terminated films. Streaming potential measurements were performed in 1 mM KCl, and the standard deviation of the measurements was about 1 mV.

Figure 2.4 demonstrates that ζ potentials depend on both the ionic strength at which the outer layer was deposited and the ionic strength of the probe solution. For streaming potential measurements obtained with 1 mM KCl and membranes coated with $[PSS/PDADMAC]_4$+PSS/PAH films, deposition of the outer PAH layer from 2.5 M NaCl

yields an 8 mV higher ζ potential than deposition of PAH from a solution containing 0.5 M NaCl. The film with the top PAH layer deposited from 1.0 M NaCl shows an intermediate ζ potential. This is consistent with the supposition that deposition of the terminal polycation layer from solutions of high ionic strength induces more charge near the surface to increase Mg^{2+} rejection. Similar trends appear in the streaming potential measurements with 5 and 10 mM KCl solutions, but for a given membrane the ζ potential becomes less positive as KCl concentration increases.[60] This is expected because the diffuse double layer becomes more compact at higher ionic strengths, and more of the surface-solution potential drop occurs between the film surface and the plane of shear. The ζ potential represents only the potential drop between the plane of shear and the bulk solution.

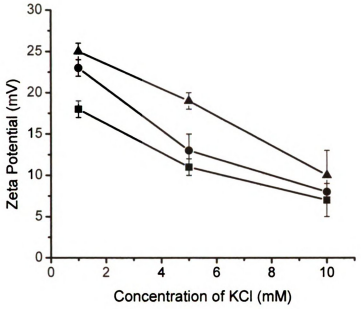

Figure 2.4. ζ potentials of $[PSS/PDADMAC]_4$+[PSS/PAH] films as a function of the concentration of KCl employed in the streaming potential measurements. Polyelectrolyte films were deposited on PES substrates using three different concentrations of NaCl during deposition of the terminal PAH layer: 0.5 M NaCl, squares; 1.0 M NaCl, circles; 2.5 M NaCl, triangles.

To examine whether adsorption of Mg^{2+} may be responsible for the fact that Mg^{2+} rejections do not decrease with increasing $MgCl_2$ concentrations, we perform streaming potential measurements using solutions containing three different concentrations of $MgCl_2$ (Figure 2.5). In contrast to measurements in KCl, ζ potentials determined in $MgCl_2$ solutions increase with increasing concentrations of $MgCl_2$. (The $MgCl_2$ concentrations in Figure 2.5 were chosen to duplicate the ionic strengths used for the measurements in KCl in Figure 2.4.) Although the diffuse layer should still become

thinner at higher ionic strengths in $MgCl_2$ solutions, adsorption of divalent Mg^{2+} on the film surface[38] probably increases the amount of positive charge near the surface to make the ζ potential more positive. This more positive ζ potential likely overcomes any decreases in rejection due to reduced Donnan exclusion at higher ionic strength, so rejection is essentially independent of concentration. (The high standard deviations of ζ potentials determined at 1.66 and 3.33 mM $MgCl_2$ are typical for streaming potential measurements in these more concentrated solutions.)

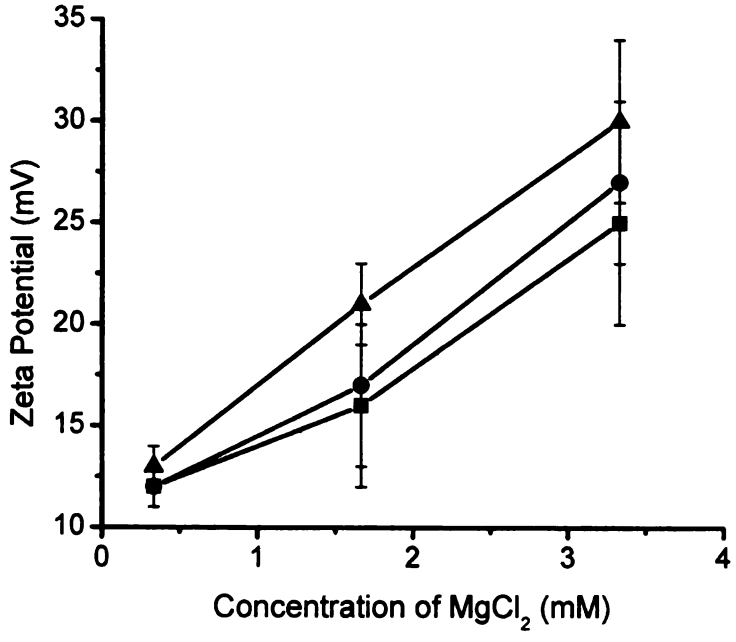

Figure 2.5. ζ potentials of $[PSS/PDADMAC]_4$+[PSS/PAH] films as a function of the concentration of $MgCl_2$ employed in the streaming potential measurements. Polyelectrolyte films were deposited on PES substrates using three different concentrations of NaCl during deposition of the terminal PAH layer: 0.5 M NaCl, squares; 1.0 M NaCl, circles; 2.5 M NaCl, triangles.

2.4. Conclusions

PEMs composed of PSS/PAH or hybrid PSS/PDADMAC + PSS/PAH films are effective in selectively removing Mg^{2+} from solutions containing NaCl and $MgCl_2$, but pure PSS/PDADMAC films and commercial NF270 membranes show only relatively low rejections of Mg^{2+}. For PAH-terminated films, Mg^{2+} rejection and Na^+/Mg^{2+} selectivity increase with the magnitude of the charge near the surface of the PEMs, and this can be enhanced by increasing the ionic strength of the terminating PAH deposition solutions. In single-salt experiments, $MgCl_2$ rejection did not vary significantly with the $MgCl_2$ concentration in the feed solution. Streaming potential measurements suggest that as $MgCl_2$ concentration increases, more Mg^{2+} adsorbs to the membrane to enhance charge near the surface and overcome decreases in Donnan exclusion due to higher salt concentrations. High rejections of both Ca^{2+} and Mg^{2+} in the presence of Na^+ make these membranes potentially useful for water softening.

2.5. References

(1) Ouyang, L.; Malaisamy, R.; Bruening, M. L. *J. Membr. Sci.* **2008**, *310*, 76-84.

(2) Das, G. *J. Clin. Pharmacol.* **1988**, *28*, 683-690.

(3) Ghizellaoui, S.; Taha, S.; Dorange, G.; Chibani, A.; Gabon, J. *Desalination* **2004**, *171*, 133-138.

(4) Nanda, D.; Tung, K.-L.; Hsiung, C.-C.; Chuang, C.-J.; Ruaan, R.-C.; Chiang, Y.-C.; Chen, C.-S.; Wu, T.-H. *Desalination* **2008**, *234*, 344-353.

(5) Wang, D.-X.; Su, M.; Yu, Z.-Y.; Wang, X.-L.; Ando, M.; Shintani, T. *Desalination* **2005**, *175*, 219-225.

(6) Lu, X.; Bian, X.; Shi, L. *J. Membr. Sci.* **2002**, *210*, 3-11.

(7) Bruening, M. L.; Dotzauer, D. M.; Jain, P.; Ouyang, L.; Baker, G. L. *Langmuir* **2008**, *24*, 7663-7673.

(8) Eriksson, P.; Kyburz, M.; Pergande, W. *Desalination* **2005**, *184*, 281-294.

(9) Anim-Mensah, A. R.; Krantz, W. B.; Govind, R. *Eur. Polym. J.* **2008**, *44*.

(10) Tavares, C. R.; Vieira, M.; Petrus, J. C. C.; Bortoletto, E. C.; Ceravollo, F. *Desalination* **2002**, *144*, 261-265.

(11) Wang, X.-L.; Tsuru, T.; Nakao, S.; Kimura, S. *J. Membr. Sci.* **1997**, *135*, 19-32.

(12) Wang, D.; Wu, L.; Liao, Z.; Wang, X.; Tomi, Y.; Ando, M.; Shintani, T. *J. Membr. Sci.* **2006**, *284*, 384-392.

(13) Petersen, R. J. *J. Membr. Sci.* **1993**, *83*, 81-150.

(14) Du, R.; Zhao, J. *J. Membr. Sci.* **2004**, *239*, 183-188.

(15) Huang, R.; Chen, G.; Sun, M.; Gao, C. *Carbohydr. Res.* **2006**, *341*, 2777-2784.

(16) Li, L.; Wang, B.; Tan, H.; Chen, T.; Xu, J. *J. Membr. Sci.* **2006**, *269*, 84-93.

(17) Decher, G.; Hong, J. D.; Schmitt, J. *Thin Solid Films* **1992**, *210-211*, 831-835.

(18) Decher, G. *Science* **1997**, *277*, 1232-1237.

(19) Krasemann, L.; Toutianoush, A.; Tieke, B. *J. Membr. Sci.* **2001**, *181*, 221-228.

(20) Harris, J. J.; Stair, J. L.; Bruening, M. L. *Chem. Mater.* **2000**, *12*, 1941-1946.

(21) Jin, W.; Toutianoush, A.; Tieke, B. *Langmuir* **2003**, *19*, 2550-2553.

(22) Chen, H.; Zeng, G.; Wang, Z.; Zhang, X. *Macromolecules* **2007**, *40*, 653-660.

(23) Zhang, G.; Yan, H.; Ji, S.; Liu, Z. *J. Membr. Sci.* **2007**, *292*, 1-8.

(24) Lösche, M.; Schmitt, J.; Decher, G.; Bouwman, W. G.; Kjaer, K. *Macromolecules* **1998**, *31*, 8893-8906.

(25) Ladam, G.; Schaad, P.; Voegel, J. C.; Schaaf, P.; Decher, G.; Cuisinier, F. *Langmuir* **2000**, *16*, 1249-1255.

(26) Steitz, R.; Leiner, V.; Siebrecht, R.; Klitzing, R. v. *Colloids Surf., A* **2000**, *163*, 63-70.

(27) Yoo, D.; Shiratori, S. S.; Rubner, M. F. *Macromolecules* **1998**, *31*, 4309-4318.

(28) Shiratori, S. S.; Rubner, M. F. *Macromolecules* **2000**, *33*, 4213-4219.

(29) Mendelsohn, J. D.; Barrett, C. J.; Chan, V. V.; Pal, A. J.; Mayes, A. M.; Rubner, M. F. *Langmuir* **2000**, *16*, 5017-5023.

(30) Krasemann, L.; Tieke, B. *Langmuir* **2000**, *16*, 287-290.

(31) Malaisamy, R.; Bruening, M. L. *Langmuir* **2005**, *21*, 10587-10592.

(32) Hong, S. U.; Malaisamy, R.; Bruening, M. L. *Langmuir* **2007**, *23*, 1716-1722.

(33) Tieke, B.; Toutianoush, A.; Jin, W. *Adv. Colloid Interface Sci.* **2005**, *116*, 121-131.

(34) Farhat, T. R.; Schlenoff, J. B. *J. Am. Chem. Soc.* **2003**, *125*, 4627-4636.

(35) Stanton, B. W.; Harris, J. J.; Miller, M. D.; Bruening, M. L. *Langmuir* **2003**, *19*, 7038-7042.

(36) Adamczyk, Z.; Zembala, M.; Warszynski, P.; Jachimska, B. *Langmuir* **2004**, *20*, 10517-10525.

(37) Miller, M. D.; Bruening, M. L. *Chem. Mater.* **2005**, *17*, 5375-5381.

(38) Childress, A. E.; Elimelech, M. *J. Membr. Sci.* **1996**, *119*, 253-268.

(39) Chung, C. V.; Buu, N. Q.; Chau, N. H. *Sci. Tech. Adv. Mater.* **2005**, *6*, 246-250.

(40) Kotov, N. A. *Nanostruct. Mater.* **1999**, *12*, 789-796.

(41) Walker, S. L.; Bhattacharjee, S.; Hoek, E. M. V.; Elimelech, M. *Langmuir* **2002**, *18*, 2193-2198.

(42) Liu, X.; Bruening, M. L. *Chem. Mater.* **2004**, *16*, 351-357.

(43) Jin, W.; Toutianoush, A.; Pyrasch, M.; Schnepf, J.; Gottschalk, H.; Rammensee, W.; Tieke, B. *J. Phys. Chem. B* **2003**, *107*, 12062-12070.

(44) Carrière, D.; Krastev, R.; Schönhoff, M. *Langmuir* **2004**, *20*, 11465-11472.

(45) Wong, J. E.; Rehfeldt, F.; Hänni, P.; Tanaka, M.; Klitzing, R. v. *Macromolecules* **2004**, *37*, 7285-7289.

(46) Gilron, J.; Gara, N.; Kedem, O. *J. Membr.Sci.* **2001**, *185*, 223-236.

(47) Levenstein, R.; Hasson, D.; Semiat, R. *J. Membr. Sci.* **1996**, *116*, 77-92.

(48) Harris, J. J.; Bruening, M. L. *Langmuir* **2000**, *16*, 2006-2013.

(49) Phuvanartnuruks, V.; McCarthy, T. J. *Macromolecules* **1998**, *31*, 1906-1914.

(50) Antipov, A. A.; Sukhorukov, G. B.; Möhwald, H. *Langmuir* **2003**, *19*, 2444-2448.

(51) Dubas, S. T.; Schlenoff, J. B. *Macromolecules* **2001**, *34*, 3736-3740.

(52) Lowack, K.; Helm, C. A. *Macromolecules* **1998**, *31*, 823-833.

(53) Schönhoff, M. *J. Phys. Condens. Matter* **2003**, *15*, R1781-R1808.

(54) Choi, J.; Rubner, M. F. *Macromolecules* **2005**, *38*, 116-124.

(55) Peeters, J. M. M.; Boom, J. P.; Mulder, M. H. V.; Strathmann, H. *J. Membr. Sci.* **1998**, *145*, 199-209.

(56) Furusawa, K.; Iwamoto, M.; Matsumura, H. *Bull. Chem. Soc. Jpn* **1987**, *60*, 845-849.

(57) Schwarz, B.; Schönhoff, M. *Langmuir* **2002**, *18*, 2964-2966.

(58) Schwarz, S.; Eichhorn, K.-J.; Wischerhoff, E.; Laschewesky, A. *Colloids Surf., A* **1999**, *159*, 491-501.

(59) Adusumilli, M.; Bruening, M. L. *Langmuir* **2009**, *25*, 7478-7485.

(60) Sterthaus, R.; Wegner, G. *Langmuir* **2002,** *18*, 5414-5421.

Chapter 3

Multilayer Polyelectrolyte Nanofiltration Membranes for Selective Phosphate Removal

This work was done in collaboration with Professor Seong Uk Hong of the Department of Chemical Engineering at Hanbat National University, Daejeon, South Korea, and the data were recently published in Journal of Membrane Science.[1]

3.1. Introduction

Chapter 2 discussed the use of polyelectrolyte multilayer films (PEMs) on porous alumina and polymeric supports as nanofiltration (NF) membranes for separation of multivalent and monovalent cations. This chapter explores the formation of selective PEM membrane skins for selective phosphate removal from chloride-containing solutions. Variation of PEM composition, and especially whether the terminating layer is a polycation or a polyanion, allows tailoring of membranes for specific separations.

The concentration of phosphorus in natural waters is critically important in a variety of biological and chemical processes,[2] and the discharge of excess phosphorus into water bodies may cause eutrophication and subsequent deterioration of water quality.[3,4] Therefore, it is important to remove phosphate from wastewater before discharge into natural water.[5] (In this chapter, we refer to phosphate as PO_4^{3-} and all of its protonated forms.) The US EPA recommends a regulatory limit of 0.05 mg

phosphorus/L for direct discharge into lakes and 0.1 mg phosphorus/L for indirect discharge into lakes..[6,7]

Common phosphate removal techniques include chemical precipitation,[8,9] biological removal,[10-12] adsorption,[3-5,13] and two membrane-based processes, reverse osmosis (RO) and NF.[7,14] Of these two membrane separation techniques, NF is preferable for selective phosphate removal because it allows the passage of monovalent ions to lower osmotic pressure. Hence, when compared with RO, NF allows selective phosphate removal at relatively low pressures.[15,16]

The goal of this project is to develop a highly permeable NF membrane that rejects phosphate while passing common monovalent anions such as chloride. To achieve high permeability, the membrane will most likely consist of a thin selective layer deposited on a thicker porous support that provides the mechanical strength.[17-19] This study examines phosphate/chloride separations using membranes formed by layer-by-layer adsorption of PEMs on porous alumina supports. PEMs are especially attractive for these separations because the layer-by-layer method affords control over the film thickness, and the film composition can be tuned for a wide range of permeation properties.[17,18,20-23] In general, ion transport through NF membranes is a function of both the charge and effective pore size of the skin layer.[24,25] Layer-by-layer deposition of polyelectrolytes naturally affords a charged surface, and the pore size can be controlled through variation of the constituent polyelectrolytes and deposition conditions.[26-30]

A recent study in our group reports the use of PEMs composed of poly(styrenesulfonate) (PSS) and poly(diallyldimethylammonium chloride) (PDADMAC) in selective removal of fluoride from solutions containing chloride or bromide.[31]

Remarkably, $(PSS/PDADMAC)_4PSS$ films on porous alumina supports exhibit chloride/fluoride or bromide/fluoride selectivities >3 with minimum chloride or bromide rejections, even though the Stokes' radii of hydrated F^- and Cl^- differ by only 0.045 nm. Table 3.1 lists the diffusion coefficients and Stokes' radii of some hydrated anions.

Table 3.1. Molecular weights (M_w), Stokes' radii (r_s) and aqueous diffusion coefficients (D) of several anions.[32]

Anions	M_w (g mol^{-1})	r_s (nm)	D (m^2/s)
HPO_4^{2-}	96.0	0.560	0.44×10^{-9}
$H_2PO_4^-$	97.0	0.279	0.88×10^{-9}
F^-	19.0	0.166	1.48×10^{-9}
Cl^-	35.5	0.121	2.03×10^{-9}
Br^-	79.9	0.118	2.08×10^{-9}

Given the fact that the Stokes' radius of $H_2PO_4^-$ or HPO_4^{2-} in water is at least 0.15 nm larger than that of Cl^-, size-based selective removal of $H_2PO_4^-$ or HPO_4^{2-} in the presence of Cl^- should be possible. In addition, the form of phosphate ions varies with pH, so phosphate rejections and chloride/phosphate selectivities can be tailored by varying the pH of the feed solution. As Figure 3.1 shows, the fraction of phosphate that is HPO_4^{2-}, which has both a larger size and a higher charge than $H_2PO_4^-$, increases with solution pH for pH values between 5 and 10. Hence, the overall phosphate rejection should increase with feed pH. This work explores the use of PSS/PDADMAC

membranes for selective phosphate removal as a function of both the feed pH and the number of PSS/PDADMAC bilayers in the membrane. Studies of the separation of phosphate and chloride with commercial NF membranes are included for comparison.

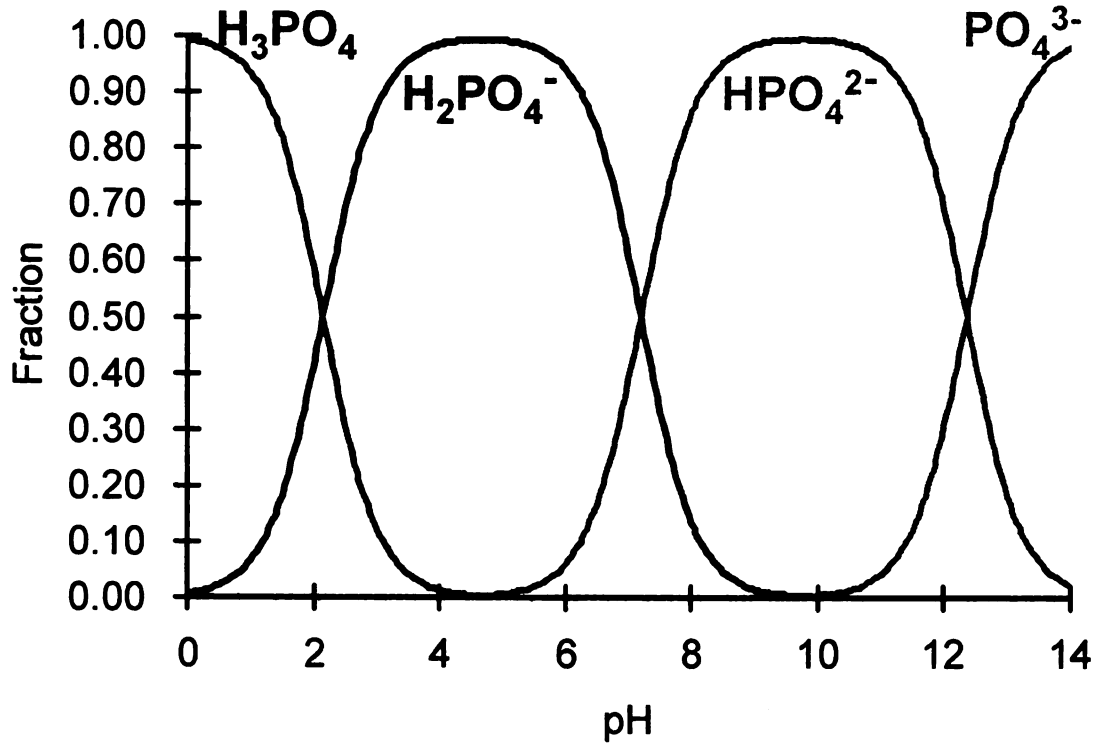

Figure 3.1. Fractional speciation of phosphate as a function of pH. (pKa values are 12.35, 7.20, and 2.15.[33])

3.2. Experimental Section

3.2.1. Materials

Poly(sodium 4-styrenesulfonate) (PSS, M_w = 70,000 Da) and poly(diallyldimethylammonium chloride) (PDADMAC, M_w = 100,000 – 200,000 Da, 20 wt% in water) were purchased from Sigma-Aldrich and used without further purification.

NaCl and NaH_2PO_4 were obtained from CCI and also used as received. Porous alumina supports (0.02 μm Whatman Anodisk filters, average membrane thickness of 60 μm) were UV/O_3 cleaned (Boekel UV-Clean Model 135500) with the feed side up for 15 min before film deposition. Deionized water (Milli-Q purification system, 18.2 MΩ·cm) was used for membrane rinsing and preparation of the polyelectrolyte and feed solutions. The two commercial NF membranes used in this study, NF 90 and NF 270, were kindly provided by Dow-FILMTEC.

3.2.2. Film Formation on Porous Alumina

The pretreated alumina membrane was sandwiched in a home-made membrane holder that exposes only the feed side of the membrane to the polyelectrolyte solutions. Deposition started with immersion of the membrane surface in a 0.02 M PSS solution (polyelectrolyte concentrations are always given with respect to the repeating unit) for 3 min. PSS was deposited first due to the potential for electrostatic interactions with the positively charged alumina support. Following a 1-min rinse with deionized water, the support was exposed to a 0.02 M PDADMAC solution for 3 min and rinsed with deionized water for 1 min. Additional layers were deposited similarly to give the desired number of bilayers. Both polyelectrolyte deposition solutions contained 0.5 M NaCl as supporting salt. After film deposition, membranes were stored in deionized water until use. Polyelectrolyte deposition time and salt concentrations were chosen based on previous ion separation studies.[18,31,34]

3.2.3. Transport Studies

NF experiments were performed at room temperature (23 °C) using a cross-flow system described previously.[19] The system was pressurized with Ar to 4.8 bar, and a

centrifugal pump circulated the feed solution through the system and across the membrane surfaces. The flow meter located between the pump and membrane cells was set at 18 mL/min to minimize concentration polarization.[19] The feed tank was filled with a 2 L solution containing 1 mM NaH_2PO_4 and 1 mM NaCl, and the pH of the feed solution was adjusted with 1 M NaOH. After an initial 18 h of filtration to condition the membrane, permeate samples were collected every 15 min for 1 h. The feed solution was sampled at the end of the experiment to take into account small concentration changes during the filtration. The reported fluxes are usually the steady-state permeate fluxes after 18 h of filtration, but in some cases, NF experiments at pH 5.6 were followed by experiments at either pH 7 or 8.4, so only a ~6 h-filtration was employed for conditioning at pH 7 or 8.4. Ion chromatography (Dionex 600 Ion Chromatograph with an Ionpac AS16A column) with conductivity detection was used to determine the anion concentrations in the feed and permeate samples.

3.3. Results and Discussion

Previous anion separations with PSS/PDADMAC-modified ultrafiltration membranes showed high Cl^-/SO_4^{2-} and Cl^-/F^- selectivities along with a high solution flux,[30,31,35] so we chose to examine this polyelectrolyte system for phosphate/chloride separations. Additionally, PSS and PDADMAC are both strong polyelectrolytes whose charge density should not vary significantly at pH values >2. Thus, variations in phosphate rejections with feed pH will stem primarily from the speciation of phosphate but not changes in membrane properties. All the membranes in this study contain a PSS

terminating layer because the negative charge of the predominantly polyanionic surface increases selectivities among monovalent and multivalent anions.[19,31]

In this section, we first describe NF results with PSS/PDADMAC membranes and then compare these results with the performance of commercial NF 90 and NF 270 membranes. Two parameters, solute rejection, *R*, and selectivity, *S*, of solute A over solute B, characterize the selective removal of phosphate from chloride-containing solutions. Equation (1) defines *R*, where C_p and C_f are the solute concentrations in the permeate and feed, respectively, whereas equation (2) defines *S*, which can also be expressed in terms of the rejections of the two solutes.

$$R = \left(1 - C_p / C_f\right) \times 100\% \qquad (1)$$

$$S = \frac{C_{A,p}}{C_{A,f}} \cdot \frac{C_{B,f}}{C_{B,p}} = \frac{100 - R_A(\%)}{100 - R_B(\%)} \qquad (2)$$

3.3.1. Membrane Formation

To simultaneously achieve high permeability and selectivity, composite membranes often contain a thin selective layer on a thicker porous support that provides mechanical stability. In this work, the selective layer is a PEM film prepared using layer-by-layer deposition, and the film thickness is in the range of 20-30 nm.[36] An alumina membrane with 0.02 μm surface pores and an approximate thickness of 60 μm serves as the porous support. Previous ion-transport studies showed that after deposition of 4-5 bilayers, the PEMs forms a defect-free film on alumina supports,[19,28] and SEM images such as Figure 2.2 confirm that complete surface coverage occurs without filling of the underlying pores.[28,37]

3.3.2. NF Experiments with PSS/PDADMAC Membranes

Table 3.2 shows solution fluxes, solute rejections and chloride/phosphate selectivities from NF with PSS/PDADMAC membranes. Without addition of NaOH, the pH of the feed solution (1 mM NaH_2PO_4 and 1 mM NaCl) is 5.6, and under these conditions most phosphate ions are present as $H_2PO_4^-$ (Figure 3.1). In this case, $(PSS/PDADMAC)_4PSS$-coated alumina membranes exhibit 86% phosphate rejection, a chloride/phosphate selectivity of 5.8, and a solution flux of 2.2 $m^3/(m^2\ day)$. This result is consistent with the size-based selectivity in a previous NF study with 1 mM NaF and 1 mM NaCl, in which fluoride rejection was 73% and chloride rejection was 10% with the same membrane composition.[31] The higher rejection of $H_2PO_4^-$ than F^- most likely stems from the larger Stokes' radius of $H_2PO_4^-$ (Table 3.1).

Table 3.2. Solution fluxes, rejections and selectivities from NF with $(PSS/PDADMAC)_xPSS$-coated alumina membranes and feed solutions containing NaH_2PO_4 (1 mM) and NaCl (1 mM). The transmembrane pressure was 4.8 bar.

[a] The extra 0.5 bilayer indicates that films were terminated with a layer of PSS.

[b] Experiments were performed after NF experiments using a feed solution at pH 5.6

pH of feed solution = 5.6				
Number of bilayers[a]	Flux (m^3/m^2 day)	Chloride Rejection (%)	Phosphate Rejection (%)	Chloride/Phosphate Selectivity (-)
4.5	2.2±0.1	16.2±0.1	85.6±1.6	5.8±0.6
5.5	2.1±0.1	-2.1±4.7	74.8±4.2	4.1±1.0
pH of feed solution = 7.0				
Number of bilayers[a]	Flux (m^3/m^2 day)	Chloride Rejection (%)	Phosphate Rejection (%)	Chloride/Phosphate Selectivity (-)
4.5[b]	2.2±0.1	33.1±1.3	91.8±0.7	8.2±0.5
5.5[b]	2.1±0.0	9.3±1.7	81.5±0.5	4.9±0.0
pH of feed solution = 8.4				
Number of bilayers[a]	Flux (m^3/m^2 day)	Chloride Rejection (%)	Phosphate Rejection (%)	Chloride/Phosphate Selectivity (-)
3.5	2.9±0.1	1.0±0.6	76.9±0.4	4.3±0.1
4.5[b]	2.4±0.1	20.9±6.7	98.3±0.2	48.3±5.8
5.5	2.4±0.0	12.4±1.0	97.7±0.1	37.4±1.4

The thicknesses of PEM films usually increase with the number of bilayers,[38-40] and thicker films are less likely to contain defects. Hence, we increased the number of PSS/PDADMAC bilayers from 4.5 to 5.5 in an effort to improve chloride/phosphate selectivity. However, the presence of the extra bilayer results in decreased phosphate rejection (from 86% to 75%) and a drop in chloride/phosphate selectivity from 5.8 to 4.1. Previous studies of chloride/fluoride[31] and chloride/sulfate separations[38] also showed that both rejections and selectivities decrease when the number of bilayers of PSS/PDADMAC films on alumina supports increases from 4.5 to 5.5. Streaming potential measurements with PSS-terminated PSS/PDADMAC films indicate that the surface charge gradually changes from negative to positive as the number of adsorbed bilayers increases, and this decrease in negative charge should result in less electrostatic exclusion of the anions and lower rejections.[38] However, because both Cl^- and $H_2PO_4^-$ are singly charged anions, their separation is mainly based on sieving of $H_2PO_4^-$, which has a larger Stokes' radius than Cl^-. Recent studies suggest that the degree of hydration of PEMs increases after deposition of the first few layers.[41-43] Because the films become more swollen, the effective pore size of the PEMs might increase and causes a decline in the selectivity.

After adjustment of the feed pH from 5.6 to 7.0, the phosphate ions should consist of roughly 50% $H_2PO_4^-$ and 50% HPO_4^{2-} (Figure 3.1). Due to the presence of highly rejected divalent anions on increasing the feed pH from 5.6 to 7.0, the overall phosphate rejection increases from 86% to 92%, and the chloride/phosphate selectivity improves from 5.8 to 8.2. Similar to what we observe in NF with a feed pH of 5.6, phosphate

rejection and chloride/phosphate selectivity decrease when the number of PSS/PDADMAC bilayers increases from 4.5 to 5.5 at a feed pH of 7.0. The change in pH does not affect the solution fluxes, presumably because the membrane structure does not vary significantly with pH.

With a further increase in feed pH to 8.4, most phosphate ions exist as HPO_4^{2-}, which has both a larger size and a higher charge than $H_2PO_4^-$ (Table 3.1). As expected, on increasing the feed pH from 7.0 to 8.4, phosphate rejection increases from 92% to 98%, and the chloride/phosphate selectivity reaches a value of 48 with $(PSS/PDADMAC)_4PSS$ films. For $(PSS/PDADMAC)_3PSS$ films, the chloride/phosphate selectivity is 4.3, and the phosphate rejection is only 77%. This result indicates that films of $(PSS/PDADMAC)_3PSS$ might not fully cover the support. Different from the results obtained at lower feed pH values, phosphate rejection remains almost the same when the number of PSS/PDADMAC bilayers increases from 4.5 to 5.5. This result suggests that HPO_4^{2-} has enough charge and size to be rejected by $(PSS/PDADMAC)_5PSS$ films on alumina supports.

3.3.3. NF Experiments with Commercial NF Membranes

For comparison, we investigated the separation performance of two commercially available NF membranes, NF90 and NF 270 from Dow-FILMTEC. These are both polyamide thin-film composite membranes with a negative surface charge, but NF 90 is a denser membrane that typically gives higher salt rejection and lower fluxes than NF 270. Table 3.3 shows the solution fluxes, solute rejections and chloride/phosphate selectivities from NF experiments with these two membranes.

Table 3.3. Solution fluxes, rejections, and selectivities from NF with commercially available membranes and feed solutions containing NaH_2PO_4 (1 mM) and NaCl (1 mM). The transmembrane pressure was 4.8 bar.

pH of feed solution = 5.6				
Membrane	Flux (m^3/m^2 day)	Chloride Rejection (%)	Phosphate Rejection (%)	Chloride/Phosphate Selectivity (-)
NF 90	1.4±0.1	79.3±3.7	98.7±0.7	22.0±12.5
NF 270	1.1±0.2	55.5±11.7	87.6±0.5	3.6±0.8
pH of feed solution = 7.0				
Membrane	Flux (m^3/m^2 day)	Chloride Rejection (%)	Phosphate Rejection (%)	Chloride/Phosphate Selectivity (-)
NF 90	1.3±0.3	97.4±0.4	99.3±0.5	5.4±2.8
NF 270	1.5±0.1	61.8±9.8	91.2±4.3	4.9±1.3
pH of feed solution = 8.4				
Membrane	Flux (m^3/m^2 day)	Chloride Rejection (%)	Phosphate Rejection (%)	Chloride/Phosphate Selectivity (-)
NF 90	1.2±0.1	97.9±0.6	99.7±0.1	7.4±1.1
NF 270	2.0±0.1	71.2±7.1	94.8±1.2	5.5±0.2

At a feed pH of 5.6 where most of the phosphate ions are present as $H_2PO_4^-$, NF 90 shows 99% phosphate rejection, 79% chloride rejection and a chloride/phosphate selectivity of 22. In the case of NF 270, phosphate and chloride rejections are 88% and 56%, respectively, and the selectivity is only 4. Although phosphate rejections are higher with both of these membranes than with the PSS/PDAMAC-modified alumina membranes, NF90 and NF270 membranes are less permeable than porous alumina coated with PSS/PDADMAC films, perhaps because the polyamide skin layers of the commercial membranes are denser than PSS/PDADMAC films. (At the relatively low 1 mM solute concentrations in the present study, osmotic pressure is less than 0.1 bar at 100% rejection. This value is negligible compared to the transmembrane pressure of 4.8 bar.)

On going from a feed pH of 5.6 to 7.0, phosphate rejection increases with both NF 90 and NF 270 membranes (Table 3.3) due to the fact that half of the phosphate ions exist as HPO_4^{2-} (Figure 3.1). Chloride rejection also increases in both cases, probably because the membrane surface became more negatively charged at the higher pH. Although more than 99% of phosphate is rejected by NF 90 membranes, the selectivity is only 5 because the chloride rejection is 97%. A similar selectivity occurs with NF 270.

After increasing the feed pH to 8.4, phosphate rejection with NF 90 and NF 270 increases even more because most of the phosphate ions are present as HPO_4^{2-}. Specifically, NF 90 membranes reject more than 99.5% of phosphate with a relatively low flux of 1.2 $m^3/(m^2$ day), and NF 270 exhibits a phosphate rejection of 95% with a flux of 2 $m^3/(m^2$ day). However, chloride/phosphate selectivity is less than 8 in both cases due to high chloride rejection. In summary, these two commercial NF membranes

present high rejections for both phosphate and chloride, which makes them attractive in complete salt removal applications. In contrast, the combination of high phosphate rejection, low chloride rejection, and high flux make PSS/PDADMAC films particularly promising in selective phosphate removal in the presence of monovalent anions.

3.4. Conclusions

Layer-by-layer adsorption of PSS/PDADMAC films on porous alumina supports provides a simple way to fabricate high-flux NF membranes for selective removal of phosphate in the presence of chloride. Because a higher fraction of the phosphate ions are present as HPO_4^{2-} when the pH of the feed solution increases from 5.6 to 7.0 or 8.4, phosphate rejections and chloride/phosphate selectivities of PSS/PDADMAC membranes increase with the feed pH. Although the two commercial NF membranes we examined (NF 90 and NF 270) exhibit high phosphate and chloride rejections, the higher fluxes and chloride/phosphate selectivities of PSS/PDADMAC membranes make them potentially attractive in selective phosphate removal applications.

3.5. References

(1) Hong, S. U.; Ouyang, L.; Bruening, M. L. *J. Membr. Sci.* **2009**, *327*, 2-5.

(2) Chitrakar, R.; Tezuka, S.; Sonoda, A.; Sakane, K.; Ooi, K.; Hirotsu, T. *J. Colloid Interface Sci.* **2006**, *297*, 426-433.

(3) Zhang, G.; Liu, H.; Liu, R.; Qu, J. *J. Colloid Interface Sci.* **2009**, *335*, 168-174.

(4) Rodrigues, L. A.; da Silva, M. L. C. P. *Colloids Surf., A* **2009**, *334*, 191-196.

(5) Saha, B.; Chakraborty, S.; Das, G. *J. Colloid Interface Sci.* **2009**, *331*, 21-26.

(6) Mueller, D. K.; Helsel, D. R. In *U.S. Geological Survey Circular, 1136,* **1999**.

(7) Kumar, M.; Badruzzaman, M.; Adham, S.; Oppenheimer, J. *Water Res.* **2007**, *41*, 2211-2219.

(8) Hosni, K.; Ben Moussa, S.; Chachi, A.; Ben Amor, M. *Desalination* **2008**, *223*, 337-343.

(9) Katz, I.; Dosoretz, C. G. *Desalination* **2008**, *222*, 230-242.

(10) Clark, T.; Stephenson, T.; Pearce, P. A. *Water Res.* **1997**, *31*, 2557-2563.

(11) de-Bashan, L. E.; Bashan, Y. *Water Res.* **2004**, *38*, 4222-4246.

(12) Barat, R.; van Loosdrecht, M. C. M. *Water Res.* **2006**, *40*, 3507-3516.

(13) Xu, X.; Gao, B.; Wang, W.; Yue, Q.; Wang, Y.; Ni, S. *Colloids Surf., B* **2009**, *70*, 46-52.

(14) Balannec, B.; Vourch, M.; Rabiller-Baudry, M.; Chaufer, B. *Sep. Purif. Technol.* **2005**, *42*, 195-200.

(15) Petersen, R. J. *J. Membr. Sci.* **1993**, *83*, 81-150.

(16) Eriksson, P.; Kyburz, M.; Pergande, W. *Desalination* **2005**, *184*, 281-294.

(17) Liu, X.; Bruening, M. L. *Chem. Mater.* **2004**, *16*, 351-357.

(18) Miller, M. D.; Bruening, M. L. *Langmuir* **2004**, *20*, 11545-11551.

(19) Stanton, B. W.; Harris, J. J.; Miller, M. D.; Bruening, M. L. *Langmuir* **2003**, *19*, 7038-7042.

(20) Leväsalmi, J.-M.; McCarthy, T. J. *Macromolecules* **1997**, *30*, 1752-1757.

(21) Krasemann, L.; Tieke, B. *Langmuir* **2000**, *16*, 287-290.

(22) Hong, S. U.; Bruening, M. L. *J. Membr. Sci.* **2006**, *280*, 1-5.

(23) Tieke, B.; Toutianoush, A.; Jin, W. *Adv. Colloid Interface Sci.* **2005**, *116*, 121-131.

(24) Wang, D.-X.; Su, M.; Yu, Z.-Y.; Wang, X.-L.; Ando, M.; Shintani, T. *Desalination* **2005**, *175*, 219-225.

(25) Wang, X.-L.; Tsuru, T.; Nakao, S.; Kimura, S. *J. Membr. Sci.* **1997**, *135*, 19-32.

(26) Dubas, S. T.; Schlenoff, J. B. *Macromolecules* **1999**, *32*, 8153-8160.

(27) Antipov, A. A.; Sukhorukov, G. B.; Möhwald, H. *Langmuir* **2003**, *19*, 2444-2448.

(28) Harris, J. J.; Stair, J. L.; Bruening, M. L. *Chem. Mater.* **2000**, *12*, 1941-1946.

(29) Choi, J.; Rubner, M. F. *Macromolecules* **2004**, *38*, 116-124.

(30) Hong, S. U.; Malaisamy, R.; Bruening, M. L. *J. Membr. Sci.* **2006**, *283*, 366-372.

(31) Hong, S. U.; Malaisamy, R.; Bruening, M. L. *Langmuir* **2007**, *23*, 1716-1722.

(32) *Handbook of Chemistry and Physics*, CRC Press, Boca Raton, **2000-2001**.

(33) Smith, R. M.; Martell, A. E. *Critical stability constants*; Plenum Press: New York, 1976; Vol. 4.

(34) Ouyang, L.; Malaisamy, R.; Bruening, M. L. *J. Membr. Sci.* **2008**, *310*, 76-84.

(35) Malaisamy, R.; Bruening, M. L. *Langmuir* **2005**, *21*, 10587-10592.

(36) Miller, M. D.; Bruening, M. L. *Chem. Mater.* **2005**, *17*, 5375-5381.

(37) Hong, S. U.; Miller, M. D.; Bruening, M. L. *Ind. Eng. Chem. Res.* **2006**, *45*, 6284-6288.

(38) Adusumilli, M.; Bruening, M. L. *Langmuir* **2009**, *25*, 7478-7485.

(39) Hubsch, E.; Fleith, G.; Fatisson, J.; Labbe, P.; Voegel, J. C.; Schaaf, P.; Ball, V. *Langmuir* **2005**, *21*, 3664-3669.

(40) Kujawa, P.; Moraille, P.; Sanchez, J.; Badia, A.; Winnik, F. M. *J. Am. Chem. Soc.* **2005**, *127*, 9224-9234.

(41) Sälomaki, M.; Laiho, T.; Kankare, J. *Macromolecules* **2004**, *37*, 9585-9590.

(42) Ladam, G.; Schaad, P.; Voegel, J. C.; Schaaf, P.; Decher, G.; Cuisinier, F. *Langmuir* **2000**, *16*, 1249-1255.

(43) Tanchak, O. M.; Yager, K. G.; Fritzsche, H.; Harroun, T.; Katsaras, J.; Barrett, C. J. *Langmuir* **2006**, *22*, 5137-5143.

Chapter 4

Catalytic Hollow-Fiber Membranes Prepared Using Layer-by-Layer Adsorption of Polyelectrolytes and Metal Nanoparticles

This work has recently been submitted for publication in Catalysis Today.

4.1. Introduction

In the 1990's, Decher and coworkers developed layer-by-layer (LBL) adsorption of polyelectrolytes for the formation of functional thin films. This technique allows incorporation of a wide range of materials including polymers, lipids, nanoparticles, proteins and dye molecules, into thin films.[1-4] Chapters 2 and 3 described the use of LBL adsorption to create nanofiltration membranes for selective ion removal. In a further demonstration of the versatility of the LBL technique, Chapters 4 and 5 explore layer-by-layer adsorption of polyelectrolytes and metal nanoparticles to create catalytic membranes.

Hollow fiber membrane reactors, which initially appeared in the 1980s,[5] are attractive because their geometry provides a high surface area to volume ratio[6-8] and should facilitate gas-liquid reactions.[9-11] Moreover, the hollow fiber module is the membrane configuration with the highest packing density. Remarkably, the ratio of membrane surface area to module volume can reach values as high as 30 000 m^2/m^3.[12]

Thus, a number of recent studies examine hollow fibers as catalyst supports in membrane reactors.[9,13-15]

Metal nanoparticles are especially effective catalysts because of their relatively large percentage of surface atoms.[16,17] Additionally, these materials often possess unusual electronic properties due to their unique size, which is between the bulk and molecular regimes.[16-18] For most practical catalytic applications, however, the nanoparticles must be immobilized on solid supports to prevent aggregation and facilitate catalyst recovery.[16,19-25] Common methods for making supported noble metal catalysts include impregnation, coprecipitation (CP), and deposition-precipitation (DP).[26] In the case of impregnation, the support is typically immersed in a metal salt solution, heated in air, and the absorbed metal species are finally reduced in hydrogen.[27-29] For the CP [30,31] or DP methods,[30,32] the noble metal precursor is either coprecipitated with the support precursor or directly deposited on the support surface prior to precipitation with another reagent. These methods usually yield metal particles of nonuniform size and shape, and the degree of catalyst dispersion depends on various factors such as the type of support, the deposition pH, and the concentration of precursors in the solutions.[26,27,33] To make heterogeneous catalysts with more control over particle size and shape, metal nanoparticles can be synthesized in solution and then loaded on the support .[20,34]

LBL deposition of polycations and polyanions provides a particularly simple way to deposit a high density of well-defined metal nanoparticles on a wide range of substrates.[35-39] Alternating adsorption of charged nanoparticles and an oppositely charged polyelectrolyte affords control over the amount of nanoparticles deposited through variation of the number of adsorbed layers, and a wide range of particle sizes and

compositions are available through tuning of the nanoparticle synthesis.[40-44] The LBL technique is effective for membrane modification because it can occur on a wide variety of substrate geometries,[45] including flat surfaces, cylindrical particles, and the pores of flat sheet membranes.[35,40,41,44]

This chapter describes modification of hollow fiber microfiltration (MF) membranes through LBL adsorption of polyelectrolytes and citrate-stabilized metal nanoparticles to create catalytic reactors (Figure 4.1). The use of MF substrates with sufficiently large pores allows film formation without pore blockage. SEM images show that adsorption of poly(styrenesulfonate)/poly(allylamine hydrochloride)/Au-nanoparticle (PSS/PAH/AuNP) films results in uniformly distributed nanoparticles on the exterior and pore walls of both polyethersulfone (PES) and polysulfone (PS) MF hollow fiber membranes. These nanoparticles are highly active in catalyzing the reduction of 4-nitrophenol with $NaBH_4$ to give 4-aminophenol, but conversion decreases gradually with time probably because of catalyst fouling.

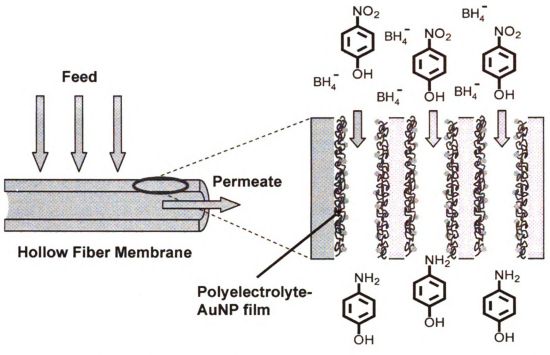

Figure 4.1. Schematic diagram of the cross section of a porous hollow fiber membrane modified with a polyelectrolyte/AuNP film. In this study, the fibers serve as catalytic reactors for the reduction of 4-nitrophenol by $NaBH_4$.

4.2. Experimental Section

4.2.1. Materials

Poly(sodium 4-styrenesulfonate) (PSS, M_w = 70,000 Da), poly(allylamine hydrochloride) (PAH, M_w = 56,000 Da), $HAuCl_4 \cdot 3H_2O$, sodium citrate, $NaBH_4$ and 4-nitrophenol were used as received from Sigma-Aldrich. Deionized water (Milli-Q purification system, 18.2 MΩ·cm) was employed for membrane rinsing and preparation of polyelectrolyte and reaction solutions.

PES MF hollow fiber membranes (MicroPES Capillary membrane Type TF10) were manufactured by MEMBRANA (Wuppertal, Germany). These membranes have a specified maximum pore size in the membrane skin of 0.5 ± 0.1 μm, an inner diameter of

300±40 μm, and a wall thickness of 100±25 μm. Figure 4.2 shows the SEM images of the fiber cross section, the shell and lumen surfaces, and the interior of the fiber.

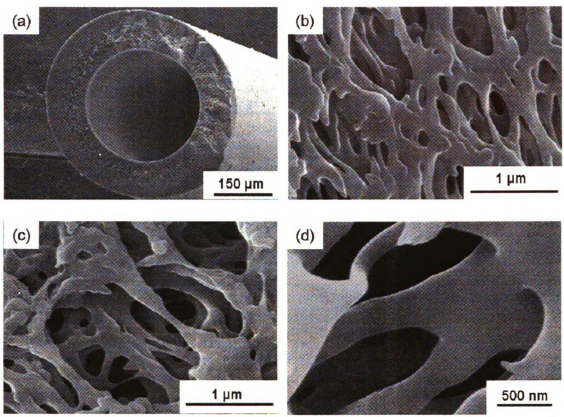

Figure 4.2. SEM images of PES hollow fiber membranes: (a) cross-sectional surface, (b) shell surface, (c) lumen surface, and (d) the interior of the membrane wall.

A module containing PS MF hollow fiber membranes was purchased from GE Healthcare (Model #: CFP-6-D-6A), and individual fibers were removed from the module and repotted. These fibers have an average skin pore size of 0.65 μm, an inner diameter of 750 μm, and a wall thickness of 225 μm. Figure 4.3 contains SEM images of these fibers.

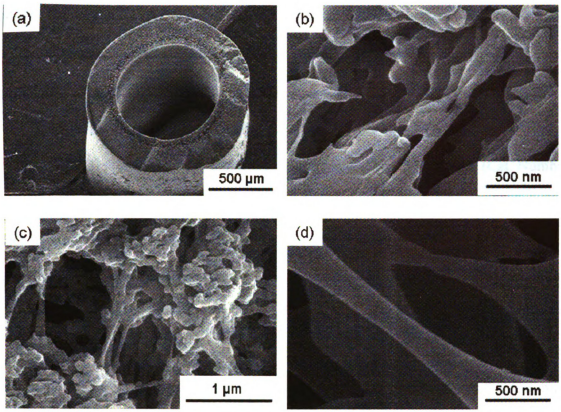

Figure 4.3. SEM images of PS hollow fiber membranes: (a) cross-sectional surface, (b) shell surface, (c) lumen surface, and (d) the interior of the membrane wall.

4.2.2. Preparation of Citrate-Stabilized Au Nanoparticles

Au nanoparticles were prepared by the citrate reduction method,[18,46,47] where citrate serves as both the reducing agent and the nanoparticle stabilizer. In a 250 mL round-bottom flask equipped with a condenser, 100 mL of 1 mM $HAuCl_4$ was heated to a rolling boil while stirring. Ten mL of 38.8 mM sodium citrate solution was also heated to a rolling boil and then rapidly added to the Au solution. After about 15 s, the solution changed from colorless to blue and then burgundy. The mixture was subsequently stirred with heating for another 10 min, and then without heating for 15 min. The nanoparticle solution was kept in an amber glass bottle and stored in a refrigerator until use. Prior to

particle deposition, the nanoparticle solution was diluted 9:1 with deionized water. TEM images show that the particle diameter is 12 ± 1 nm.[41]

4.2.3. Modification of the Hollow Fiber Membranes

Following a literature procedure, the hollow fibers were potted in a poly(vinyl chloride) (PVC) tube with epoxy glue purchased from Axson Technologies (Cat. Number: Adekit A 130).[48] All the modules in this study contained one fiber, with an effective fiber length (distance between the potting glue on the two ends) of about 22 cm for PES fibers and 15 cm for PS fibers. Prior to modification, the potted PES fiber was rinsed with water at 0.7 bar for 30 min. In the modification steps, all the solutions were passed through the membrane in the lumen to shell flow configuration with cross flow (see Figure 4.4) using a pressure of 0.7 bar. Cross flow was used during modification in an effort to minimize any pore blockage caused by the polyelectrolytes and nanoparticles.

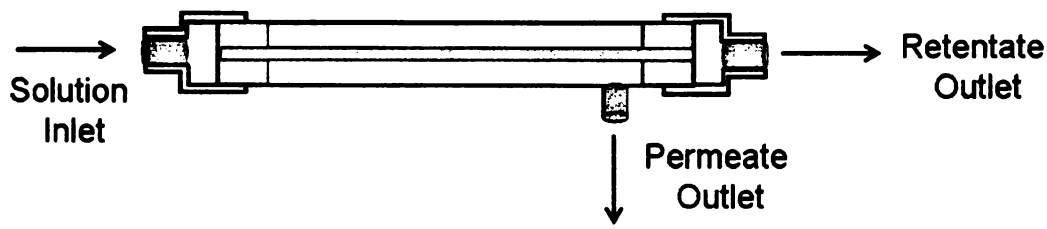

Figure 4.4. Schematic diagram of the flow configuration for modifying a hollow fiber membrane with a PSS/PAH/AuNP film. Flow occurs both axially along the membrane and from the inside to the outside of the fiber.

A prefilter (2.5 μm Ahlstrom qualitative filter paper) was used to remove particles that can potentially block the fiber, and this filter paper was replaced after deposition of each layer. Polyelectrolyte adsorption solutions contained 2 mM PSS or

PAH and 50 mM NaCl (polyelectrolyte concentrations are always given with respect to the repeating unit). The modification started with passage of 100 mL of PSS solution through the fiber (volume includes both transmembrane and cross flow). This initial adsorption of PSS is likely driven by hydrophobic interactions between PSS and the PES fiber.[49,50] The fiber was then rinsed with 300 mL of water to remove any extra polyelectrolytes. Subsequently, 100 mL of PAH solution was passed through the hollow fiber membrane followed by another 300-mL water rinse. Nanoparticles were loaded by passing 100 mL of citrate-stabilized Au colloid solution (~0.1 mM in Au atoms) through the membrane prior to rinsing with 300 mL of water. The permeate of the nanoparticle solution was initially colorless and then became light pink when the fiber was nearly saturated with Au nanoparticles.

Modification of the PS fibers occurred similarly with slight modifications due to the relatively high fiber permeabilities. Prior to polyelectrolyte deposition, the potted PS fiber was rinsed with water at 0.34 bar for 5-10 min. All the solutions were passed through the membrane in the same flow configuration (Figure 4.4) as for the PES fiber, but at a lower pressure of 0.34 bar, and a back pressure regulator (valve) was installed in the lumen flow after the membrane to maintain comparable permeate and retentate flow rates. The polyelectrolyte adsorption solutions contained 0.8 mM PSS or PAH and 20 mM NaCl. The volumes of polyelectrolyte solutions (250 mL) were higher for modification of PS fibers than for modification of PES fibers because of a higher flow rate through the PS fibers. Due to this higher volume, we also decreased the concentration of PSS and PAH for PS modification. 500 mL of water was used for rinsing between each layer deposition, and 400 mL of citrate-stabilized Au colloid

solution (~0.1 mM in Au atoms) was passed through the PS fiber to load Au nanoparticles.

4.2.4. Characterization of the Hollow Fiber Membranes

SEM images of bare and coated hollow fiber membranes were taken using a Hitachi S-4700 II field-emission scanning electron microscope (FESEM). For shell and lumen surface characterization, 5 nm of Au was sputter-coated (Pelco SC-7 auto sputter coater) on the surface before imaging. For cross-sectional images, the fiber was dipped in ethanol for 2 min, fractured in liquid nitrogen, and the cross section was sputter coated with 5 nm of Au.

To determine the amount of Au loaded in the fiber, the membrane was immersed in aqua regia (3 parts HCl and 1 part HNO_3) for 5 min, and this solution was then diluted and analyzed for Au by atomic absorption spectroscopy (AAS) (Varian Spectra Atomic Absorption-200 Spectrophotometer).

The water permeability of the PES fiber was tested in a shell to lumen flow configuration (no cross flow in the shell) at room temperature with pressures ranging from 0.7 to 2.1 bars. All reported fluxes are calculated with respect to the surface area of the outside of the fiber. Hydraulic permeability values, which were obtained from the slopes of plots of flux versus pressure, were determined before and after each modification step. For the PS fiber, water permeability was determined only at 0.7 bar because the membrane manufacturer does not recommend using the fibers under pressures higher than 1 bar.

4.2.5. Catalytic Reactions and Leaching Studies

Reduction of aqueous 4-nitrophenol with sodium borohydride served as a model reaction for examining the catalytic activity of the modified membranes. A feed tank was filled with 0.5 or 1 L of a freshly prepared solution containing 0.5 mM 4-nitrophenol and 25 mM $NaBH_4$, and this solution was forced through the hollow fiber membrane under pressure. Permeate samples were collected every 5 or 10 min, and the concentration of 4-nitrophenol in the feed and permeate was determined from the solution absorbance at 400 nm.[41,51] (UV-Vis spectra were acquired with a Perkin-Elmer Lambda 40 spectrophotomer.) To investigate the extent of catalyst leaching during the reaction, the amount of Au in the feed and permeate samples was determined using inductively coupled plasma optical emission spectroscopy (ICP-OES) (Varian 710-ES ICP Optical Emission Spectrometer).

4.3. Results and Discussion

4.3.1. Membrane Characterization

The first sign of successful modification of the hollow fiber membranes with Au nanoparticles is a change in the fiber color from white to red. SEM images, elemental analysis by AAS, and water permeability measurements afford a more quantitative picture of the fiber modification.

4.3.1.1. SEM Characterization of Immobilized Nanoparticles

Figure 4.2 shows SEM images of bare PES hollow fiber membranes. These fibers have a layered, porous structure on both lumen and shell sides, but pore sizes are smallest at the shell surface and become larger in the interior of the fiber wall, and small again at the lumen surface. The extensive internal surface area of the membrane pores should

allow a high loading of Au nanoparticles, and the relatively large pores (maximum pore size around 2 μm) facilitates film adsorption without pore blockage. However, pore blockage sometimes occurs during film adsorption, especially in fiber sections that contain somewhat smaller pores (see below). Figure 4.5 shows SEM images of the shell, lumen, and interior surfaces of PES hollow fiber membranes modified with PSS/PAH/AuNP films.

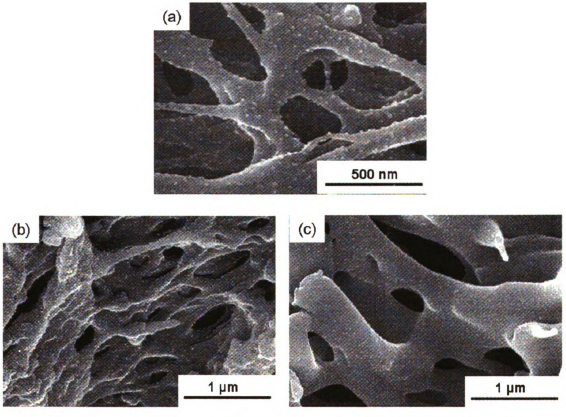

Figure 4.5. SEM images of PES hollow fiber membranes coated with PSS/PAH/AuNP films: (a) shell surface, (b) lumen surface, and (c) the interior of the membrane wall.

Adsorption of the PSS/PAH/AuNP films occurs while flowing solution along the lumen side of the fiber and also through the fiber wall (Figure 4.4). Consequently,

nanoparticles appear on all surfaces of the membranes. The nanoparticles are well separated with no visible aggregation, and the particle size is consistent with TEM images of the as-prepared particles.[40,41] Figure 4.6 shows that modification of PS fibers with PSS/PAH/AuNP films also results in a uniform Au nanoparticle distribution.

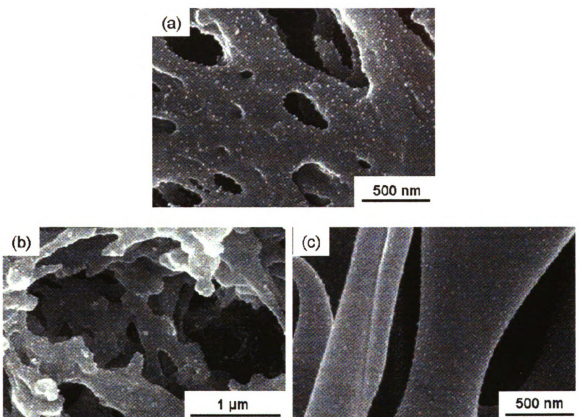

Figure 4.6. SEM images of PS hollow fiber membranes coated with PSS/PAH/AuNP films: (a) shell surface, (b) lumen surface, and (c) the interior of the membrane wall.

4.3.1.2. Catalyst Loading

SEM provides information on nanoparticle deposition in small spots with surface areas of 10's of μm^2, but these images may not give a good indication of Au loading on a macroscopic scale. To determine the overall Au content in a membrane and whether the

nanoparticles are evenly distributed along the length of the fiber, we cut coated PES fibers into several pieces and dissolved the nanoparticles in each piece in aqua regia for subsequent Au analysis by AAS. Table 4.1 summarizes these analyses and shows that the Au deposition in the PES fiber is very uniform.

Table 4.1. Au loading along PES fibers coated with PSS/PAH/AuNP films. The length of each segment is approximately 5 cm.

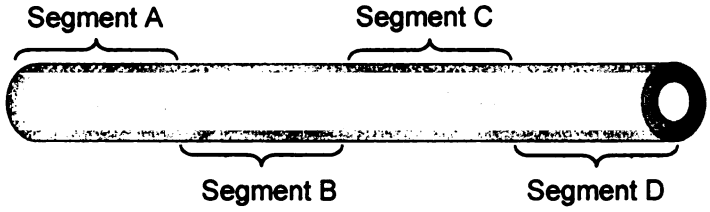

	Segment A (nmol)	Segment B (nmol)	Segment C (nmol)	Segment D (nmol)	Average (nmol)
*Fiber 1	357	371	347	375	363±13
*Fiber 2	345	339	326	370	345±18

* The reported values are normalized to a fiber length of 5 cm.

Remarkably, the amount of Au in each piece of the fiber differs by less than 8% from the average loading. The average amount of Au in a 5 cm-long PES fiber is 350 nmol, which corresponds to 0.3 mg of Au in a fiber with a length of 22 cm. Gold loading in a PS fiber (determined with the same method) is 1.2 μmol in a 5 cm segment or about 1 mg in a fiber with a length of 22 cm. The higher loading in the PS membranes likely occurs because the cross-sectional area of the walls of these fibers is 5.5 times that of PES fibers. The loading in both types of membranes is comparable to that in a chitosan fiber that was modified by the in-situ reduction method.[14] In that case, palladium

chloride was absorbed on the chitosan and subsequently reduced by hydrogen gas to give a Pd loading of 0.25 to 2.5 mg in a 50 cm long fiber.[14]

Adsorption of additional PAH/Au nanoparticle bilayers should further increase the Au loading in the film.[41] However, due to challenges with blocking of some membranes by the polyelectrolyte films (see below), the catalytic studies described here focus on modification with only one PAH/AuNP layer.

4.3.1.3. Water Permeability

Although a previous study showed no detectable plugging of pores during deposition of poly(acrylic acid)/PAH/AuNP films in flat-sheet porous alumina membranes (pore size of 0.2 μm),[41] the hollow fiber flow configuration and the spongy membrane structure in the present case may lead to pore blockage. Figure 4.7 shows the water permeabilities of PES fibers after each step in the deposition of PSS/PAH/AuNP films. (Permeabilities are determined by measuring the pressure dependence of pure water flux in the shell to lumen flow mode.)

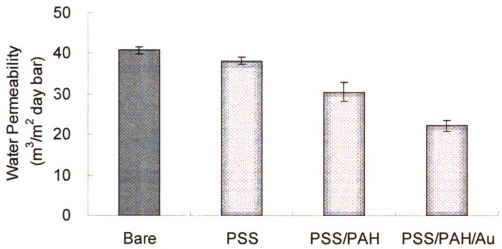

Figure 4.7. Water permeabilities of PES hollow fiber membranes before (bare) and after adsorption of different polyelectrolyte/AuNP films.

The bare PES fiber exhibits a water permeability of 41 $m^3/(m^2$ day bar), which is in the high range of fluxes through MF membranes.[12] After PSS deposition, water permeability decreases by less than 10%, but adsorption of one bilayer of PSS/PAH reduces permeability by 30% compared to a bare fiber. Moreover, adsorption of Au nanoparticles on the PSS/PAH film results in a water permeability of only 22 $m^3/(m^2$ day bar), about half of the value for the bare fiber. This decrease in water permeability is somewhat surprising because typical PSS/PAH films are only 1 nm thick,[52,53] and the pores sizes in these membranes are in the range of several hundred nanometers. Comparison of Figure 4.2-(c) and Figure 4.5-(b) (SEM images of lumen surfaces of the PES fibers before and after modification) suggests that film deposition partially occludes the lumen surface, which may account for the 50% drop in permeability after deposition of the PSS/PAH/AuNP film.

We should note that in some cases adsorption of PSS/PAH/AuNP films in PES fibers decreases flow to around 7% of that before modification. SEM images of different bare fibers indicate that the pore size varies greatly from roll to roll or perhaps changes with time (Figure 4.8). As expected, smaller pores are more prone to plugging during film adsorption. To overcome this problem, we employ PS fibers as substrates because these fibers have a permeability of 360 $m^3/(m^2$ day bar), which is about 9 times the permeability of the PES fibers. Adsorption of PSS/PAH/AuNP films in the PS fibers decreases permeability by less than 10%.

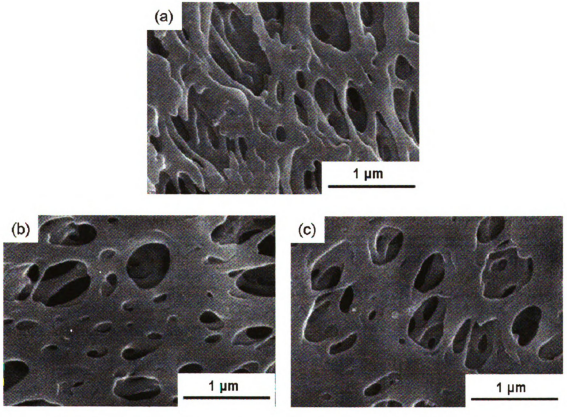

Figure 4.8. SEM images of the shell surfaces of bare PES hollow fiber membranes taken from different rolls.

4.3.2. Catalysis with Nanoparticle-Coated Fibers

We employed reduction of 4-nitrophenol with $NaBH_4$ (Scheme 4.1) as a test reaction for examining the catalytic activity of hollow fibers loaded with Au nanoparticles. This reaction is attractive because it does not proceed in the absence of catalyst, and yet it rapidly occurs in the presence of Au nanoparticles and can be easily monitored by UV-Vis spectrophotometry.[51,54,55] In a typical reaction, the feed solution contains 0.5 mM 4-nitrophenol and 25 mM $NaBH_4$ so the reducing agent is in large excess throughout the reaction.

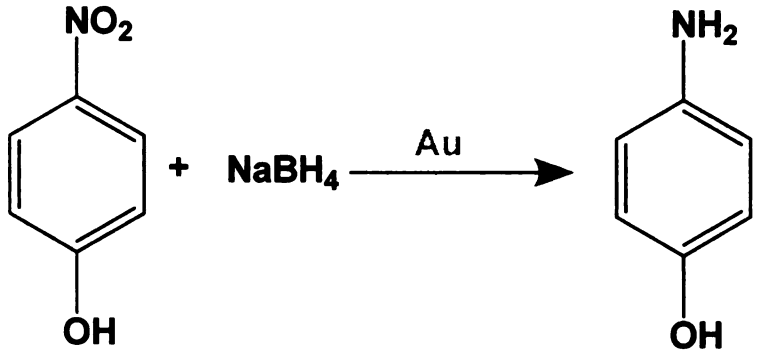

Scheme 4.1. Au-catalyzed reduction of 4-nitrophenol with $NaBH_4$.

4.3.2.1. Catalytic Reduction Using PES Fibers Coated With PSS/PAH/Au NP Films

We initially performed reduction of 4-nitrophenol in the lumen-shell flow configuration with the lumen outlet plugged (Figure 4.9). Because most of the catalyst is in the fiber wall, the reaction should primarily occur in the interior of the PES fiber. Figure 4.9 shows the 4-nitrophenol conversion over a 2-h period. Initially, more than 99% of the 4-nitrophenol passing through the membrane is converted to 4-aminophenol at a permeate flux of 0.24 ± 0.07 mL/(cm^2 min), which corresponds to a residence time of 600 ± 175 ms in the membrane (assuming 30% porosity). Thus, the nanoparticles are

highly catalytically active. After 1 h, more than 98% of the 4-nitrophenol passing through the membrane is still reduced, but the conversion slowly decreases to 80% after two hours of permeation through the membrane. One possible reason for the decline in conversion is that the amount of reducing agent in the feed tank decreases with time due to continuous $NaBH_4$ degradation. A previous study reports that $NaBH_4$ decomposes completely to $NaBO_2$ and hydrogen gas in 20 min at 75°C.[56] Although the membrane reactions occur at room temperature in our studies, an equation developed by Kreevoy suggests that 50% of the $NaBH_4$ should decompose in approximately one hour.[57] Additionally, hydrogen is produced continuously during the reaction, and this gas might be trapped in the limited space in the fiber to induce a drop in the effective membrane surface area. The permeate flux fluctuated by 40% during the experiment, perhaps because of entrapment and release of hydrogen bubbles.

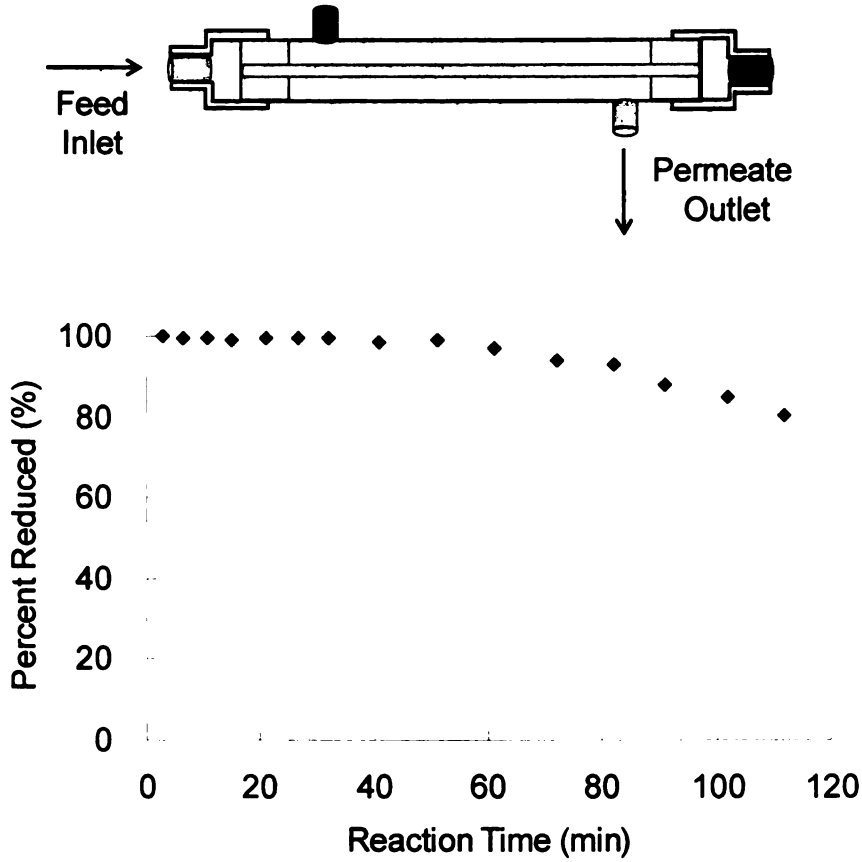

Figure 4.9. Percent reduction of 4-nitrophenol during passage of a 0.5 mM 4-nitrophenol, 25 mM $NaBH_4$ aqueous solution through a PES hollow fiber membrane coated with a PSS/PAH/AuNP film. The reaction occurs in the lumen-shell flow configuration without cross flow as shown in the diagram above the graph. (The two red cylinders represent outlet plugs.) The effective fiber length is 22 cm, and the applied pressure is 1.4 bar.

To prevent trapping of hydrogen gas in the lumen of the fiber, the reduction reaction was carried out in the shell to lumen configuration without cross flow as shown in Figure 4.10. In this case the fiber is perpendicular to the ground, and any trapped hydrogen should pass through the lumen outlet along with the permeate. The red plug on the shell (Figure 4.10) can be removed periodically to release H_2 that accumulates in the

shell. With this flow mode, the permeate flux is 0.7 ± 0.1 mL/(cm^2 min) with the same applied pressure of 1.4 bar as in the lumen-shell flow where the flux is only 0.24 ± 0.07 mL/(cm^2 min). The residence time in the membrane is only 210 ± 30 ms in the shell to lumen flow mode. Additionally, to minimize the effect of $NaBH_4$ degradation on conversion, we replaced feed solution every 60 min.

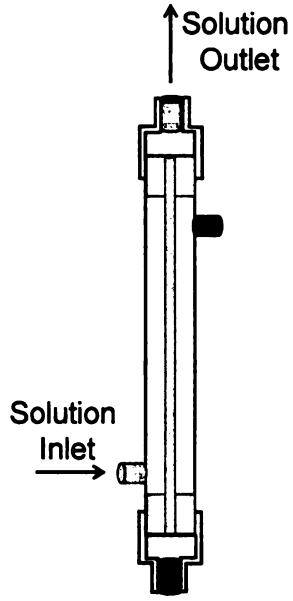

Figure 4.10. Schematic diagram of the shell to lumen solution flow configuration used in most catalytic reactions in this study. (The two red cylinders represent outlet plugs.)

As Figure 4.11 shows, in the shell to lumen flow configuration, 4-nitrophenol reduction is more than 99% for 30 min and then decreases to 83% in an hour. After replacing the feed solution, the 4-nitrophenol conversion recovers to values as high as 96%, but then begins decreasing again, so conversion is only 70% after two hours. When the feed is replaced for a second time after 2h, the conversion only recovers to 77% and finally drops to 60% after three hours. The incomplete recovery of conversion after

replacing the feed shows that degradation of $NaBH_4$ is not the sole cause for the conversion decline.

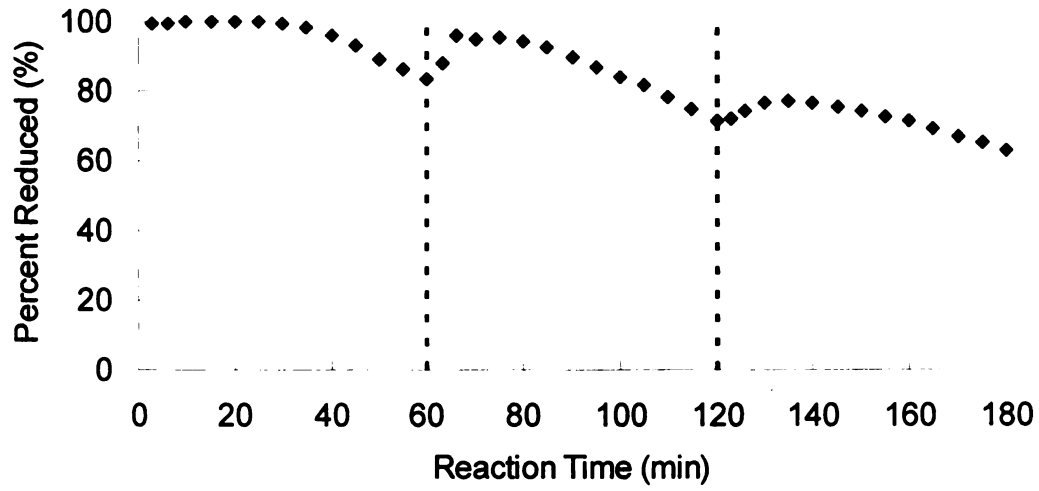

Figure 4.11. Percent reduction of 4-nitrophenol during passage of a 0.5 mM 4-nitrophenol, 25 mM $NaBH_4$ aqueous solution through a PES hollow fiber membrane coated with a PSS/PAH/AuNP film. Flow through the membrane occurs in the shell to lumen configuration without cross flow (Figure 4.10). The effective fiber length is 22 cm, and the applied pressure is 1.4 bar. The dashed, vertical lines represent the addition of a fresh 4-nitrophenol/$NaBH_4$ solution.

A second possible reason for the conversion decline is that reaction byproducts block the catalytic sites of the nanoparticles.[58] Comparison of SEM images of the lumen surfaces of modified PES fibers before (Figure 4.5-(b)) and after the $NaBH_4$/4-nitrophenol reaction (Figure 4.12) indicates that deposits form during the reaction. Interestingly, no deposits appear in the fiber wall where most of the catalyst is located.

Another possible cause of the conversion decline, catalyst leaching, is discussed in more detail below.

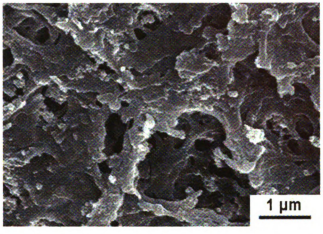

Figure 4.12. SEM image of the lumen surface of the catalytic hollow fiber after use in 4-nitrophenol reduction.

4.3.2.2. Catalytic Reduction Using PS Fibers Coated With PSS/PAH/Au NP Films

Reduction of 4-nitrophenol also occurs rapidly when using PSS/PAH/AuNP-modified PS hollow fiber membranes. Figure 4.13 shows 4-nitrophenol conversion over a 4-h period in which the feed is replaced after 80 and 180 min. Because of the high permeability of modified PS membranes, the permeate flux is 1.4 ± 0.2 mL/(cm^2 min) under a pressure <0.2 bar. (This flux corresponds to a membrane residence time of 240 ± 30 ms). Conversion is more than 99.9% for the first 30 min and decreases to 92% after 80 min. Once the feed solution is replaced, however, conversion recovers to around 99.9% and remains more than 99% for another 40 min. Conversion drops to 90% after 180 min, and replacing the feed solution a second time does not result in recovery of the catalytic activity.

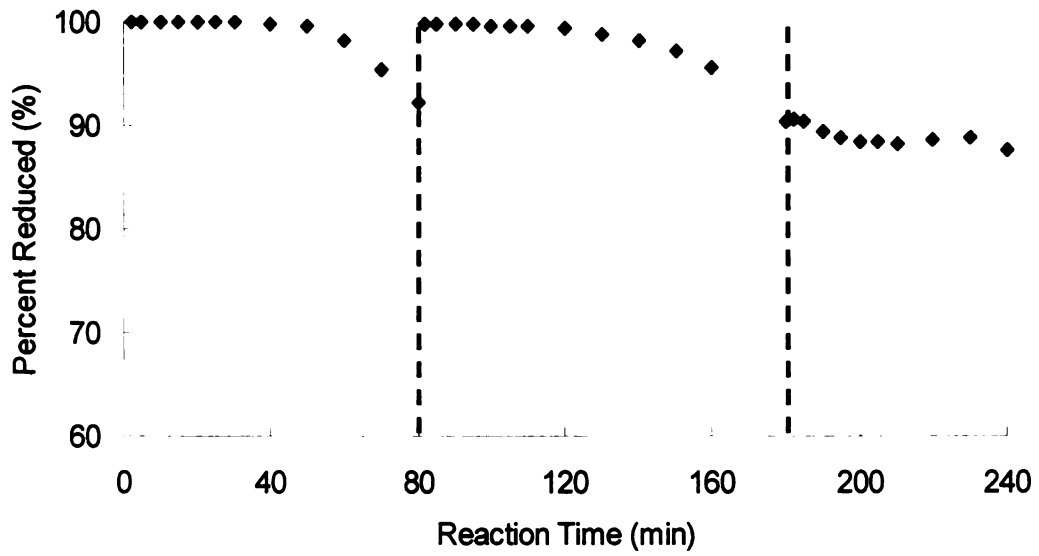

Figure 4.13. Percent reduction of 4-nitrophenol during passage of a 0.5 mM 4-nitrophenol, 25 mM $NaBH_4$ aqueous solution through a PS hollow fiber membrane coated with a PSS/PAH/AuNP film. The reaction takes place in the shell to lumen flow configuration without cross flow using an effective fiber length of 15.5 cm, and the flux through the membrane is 1.4 mL/(cm^2 min). The dashed, vertical lines represent the addition of a fresh 4-nitrophenol/$NaBH_4$ solution.

To determine whether the conversion decline stems from catalyst leaching, the Au concentration in the permeate samples was analyzed by ICP-OES. The permeate contains less than 5 ppb Au throughout the reaction period, which corresponds to less than 3% leaching of the Au in the membrane. Hence, Au leaching is not a likely cause for conversion decline in this experiment.

To minimize the effect of $NaBH_4$ degradation on conversion decline, a 4-h 4-nitrophenol reduction was performed where the feed solution (500 mL of 0.5 mM 4-

nitrophenol and 25 mM $NaBH_4$) was replaced every 30 min. Figure 4.14 shows the plot of conversion vs. reaction time at a flux of 1.4 mL/(cm^2 min). 4-Nitrophenol conversion is at least 99.9% for 90 min, and >99.7% for another 65 min. Even after 3 h, more than 99% of the 4-nitrophenol is reduced. However, during the 4th hour of reaction, conversion drops to between 95 and 98%. The Au concentration in the permeate samples is again < 5 ppb, showing that conversion declines are not due to leaching of Au. The maximum 5% conversion decline is significantly less than the conversion drop of 12% in the experiment where the feed solution was only replaced after 80 and 180 min (Figure 4.13). Conversion declines are less severe when the feed is replaced more often, and when the feed is not replaced, the $NaBH_4$ solution becomes less reducing. Thus, the fouling mechanism may include oxidation of aminophenol in the less reducing solution and formation of polymer products that foul the catalyst.

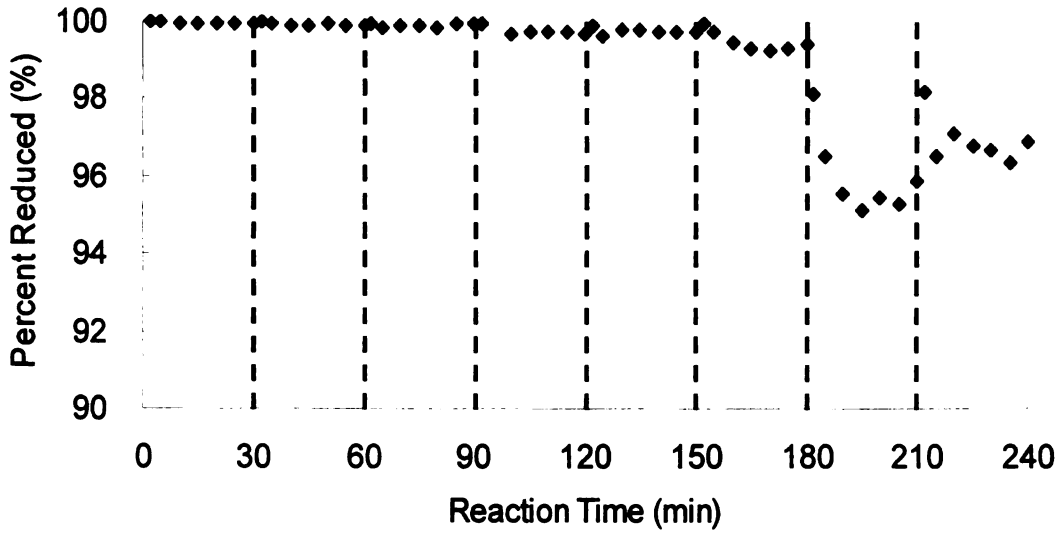

Figure 4.14. Percent reduction of 4-nitrophenol during passage of a 0.5 mM 4-nitrophenol, 25 mM $NaBH_4$ aqueous solution through a PS hollow fiber membrane coated with a PSS/PAH/AuNP film. The reaction takes place in the shell to lumen flow configuration without cross flow. The effective fiber length is 15.5 cm, and the flux through the membrane is 1.4 mL/(cm^2 min). The dashed, vertical lines represent the addition of a fresh 4-nitrophenol/$NaBH_4$ solution.

4.4. Conclusions

LBL adsorption of polyelectrolytes and Au nanoparticles provides a simple and effective way to modify the pores of hollow fibers and prepare catalytic membrane reactors. This procedure results in a dense layer of unaggregated nanoparticles in the membrane pores, although as pore size decreases, plugging of membranes can be a problem. Catalytic reduction of 4-nitrophenol with $NaBH_4$ shows that the immobilized nanoparticles are highly active, but their activity declines over time, possibly because of membrane fouling from oxidation products of aminophenol. The shell to lumen flow

configuration is probably better suited for this type of reaction than lumen to shell flow because in the former case, gas is less likely to build up in the fiber.

4.5. References

(1) Wang, Y.; Angelatos, A. S.; Caruso, F. *Chem. Mater.* **2008**, *20*, 848-858.

(2) Peyratout, C. S.; Dähne, L. *Angew. Chem. Int. Ed.* **2004**, *43*, 3762-3783.

(3) Quinn, J. F.; Johnston, A. P. R.; Such, G. K.; Zelikin, A. N.; Caruso, F. *Chem. Soc. Rev.* **2007**, *36*, 707-718.

(4) Ariga, K.; Hill, J. P.; Ji, Q. *Phys. Chem. Chem. Phys.* **2007**, *9*, 2319-2340.

(5) Butler, J. S.; Gordon, B.; Harrison, I. R. *J. Appl. Polym. Sci.* **1988**, *35*, 1183-1190.

(6) Kleinert, A.; Feldhoff, A.; Schiestel, T.; Caro, J. *Catal. Today* **2006**, *118*, 44-51.

(7) Peters, T. A.; Fontalvo, J.; Vorstman, M. A. G.; Keurentjes, J. T. F. *Chem. Eng. Res. Des.* **2004**, *82*, 220-228.

(8) Wang, H.; Tablet, C.; Schiestel, T.; Werth, S.; Caro, J. *Catal. Commun.* **2006**, *7*, 907-912.

(9) van der Vaart, R.; Lebedeva, V. I.; Petrova, I. V.; Plyasova, L. M.; Rudina, N. A.; Kochubey, D. I.; Tereshchenko, G. F.; Volkov, V. V.; van Erkel, J. *J. Membr. Sci.* **2007**, *299*, 38-44.

(10) Jiang, H.; Wang, H.; Werth, S.; Schiestel, T.; Caro, J. *Angew. Chem. Int. Ed.* **2008**, *37*, 9341-9344.

(11) Lebedeva, V. I.; Gryaznov, V. M.; Petrova, I. V.; Volkov, V. V.; Tereshchenko, G. F.; Shkol'nikov, E. I.; Plyasova, L. M.; Kochubey, D. I.; van der Vaart, R.; van Soest-Verecammen, E. L. J. *Kinet. Catal.* **2006**, *47*, 867-872.

(12) Mulder, M. *Basic Principles of Membrane technology*; Kluwer Academic Publishers: Dordrecht, 1996.

(13) Israni, S. H.; Nair, B. K. R.; Harold, M. P. *Catal. Today* **2009**, *139*, 299-311.

(14) Peirano, F.; Vincent, T.; Quignard, F.; Robitzer, M.; Guibal, E. *J. Membr. Sci.* **2009**, *329*, 30-45.

(15) Caro, J.; Caspary, K. J.; Hamel, C.; Hoting, B.; Kolsch, P.; Langanke, B.; Nassauer, K.; Schiestel, T.; Schmidt, A.; Schomacker, R.; Seidel-Morgenstern, A.; Tsotsas, E.; Voigt, I.; Wang, H.; Warsitz, R.; Werth, S.; Wolf, A. *Ind. Eng. Chem. Res* **2007**, *46*, 2286-2294.

(16) Astruc, D.; Lu, F.; Aranzaes, J. R. *Angew. Chem. Int. Ed.* **2005**, *44*, 7852-7872.

(17) Pool, R. *Science* **1990**, *248*, 1186-1188.

(18) Pachón, L. D.; Rothenberg, G. *Appl. Organomet. Chem.* **2008**, *22*, 288-299.

(19) Mei, Y.; Sharma, G.; Lu, Y.; Ballauff, M.; Drechsler, M.; Irrgang, T.; Kempe, R. *Langmuir* **2005**, *21*, 12229-12234.

(20) Comotti, M.; Li, W.-C.; Spliethoff, B.; Schüth, F. *J. Am. Chem. Soc.* **2006**, *128*, 917-924.

(21) Park, K. H.; Jang, K.; Kim, H. J.; Son, S. U. *Angew. Chem. Int. Ed.* **2007**, *46*, 1152-1155.

(22) Valden, M.; Lai, X.; Goodman, D. W. *Science* **1998**, *281*, 1647-1650.

(23) Jiang, Y.; Gao, Q. *J. Am. Chem. Soc.* **2006**, *128*, 716-717.

(24) Bengtson, G.; Fritsch, D. *Desalination* **2006**, *200*, 666-667.

(25) Xu, J.; Bhattacharyya, D. *J. Phys. Chem. C* **2008**, *112*, 9133-9144.

(26) Zhong, L.-S.; Hu, J.-S.; Cui, Z.-M.; Wan, L.-J.; Song, W.-G. *Chem. Mater.* **2007**, *19*, 4557-4562.

(27) Gates, B. C. *Chem. Rev.* **1995**, *95*, 511-522.

(28) Sarkar, J.; John, V. T.; He, J.; Brooks, C.; Gandhi, D.; Nunes, A.; Ramanath, G.; Bose, A. *Chem. Mater.* **2008**, *20*, 5301-5306.

(29) Nikolla, E.; Schwank, J.; Linic, S. *J. Am. Chem. Soc.* **2009**, *131*, 2747-2754.

(30) Akande, A. J.; Idem, R. O.; Dalai, A. K. *Appl. Catal., A* **2005**, *287*, 159-175.

(31) Kozlov, A. I.; Kozlova, A. P.; Asakura, K.; Matsui, Y.; Kogure, T.; Shido, T.; Iwasawa, Y. *J. Catal.* **2000**, *196*, 56-65.

(32) Claus, P.; Brückner, A.; Mohr, C.; Hofmeister, H. *J. Am. Chem. Soc.* **2000**, *122*, 11430-11439.

(33) Wolf, A.; Schüth, F. *Appl. Catal., A* **2002**, *226*, 1-13.

(34) Zheng, N.; Stucky, G. D. *J. Am. Chem. Soc.* **2006**, *128*, 14278-14280.

(35) Cho, J.; Caruso, F. *Chem. Mater.* **2005**, *17*, 4547-4553.

(36) Ostrander, J. W.; Mamedov, A. A.; Kotov, N. A. *J. Am. Chem. Soc.* **2001**, *123*, 1101-1110.

(37) Caruso, F.; Caruso, R. A.; Möhwald, H. *Science* **1998**, *282*, 1111-1114.

(38) Jiang, C.; Markutsya, S.; Tsukruk, V. V. *Langmuir* **2004**, *20*, 882-890.

(39) Kidambi, S.; Dai, J.; Li, J.; Bruening, M. L. *J. Am. Chem. Soc.* **2004**, *126*, 2658-2659.

(40) Dotzauer, D. M.; Bhattacharjee, S.; Wen, Y.; Bruening, M. L. *Langmuir* **2009**, *25*, 1865-1871.

(41) Dotzauer, D. M.; Dai, J.; Sun, L.; Bruening, M. L. *Nano Lett.* **2006**, *6*, 2268-2272.

(42) Bhattacharjee, S.; Bruening, M. L. *Langmuir* **2008**, *24*, 2916-2920.

(43) Bhattacharjee, S.; Dotzauer, D. M.; Bruening, M. L. *J. Am. Chem. Soc.* **2009**, *131*, 3601-3610.

(44) Kidambi, S.; Bruening, M. L. *Chem. Mater.* **2004**, *17*, 301-307.

(45) Schönhoff, M. *J. Phys.: Condens. Matter* **2003**, *15*.

(46) Enüstün, B. V.; Turkevich, J. *J. Am. Chem. Soc.* **1963**, *85*, 3317-3328.

(47) Kumar, S.; Gandhi, K. S.; Kumar, R. *Ind. Eng. Chem. Res* **2007**, *46*, 3128-3136.

(48) Rouaix, S.; Causserand, C.; Aimar, P. *J. Membr. Sci.* **2006**, *277*, 137-147.

(49) Malaisamy, R.; Bruening, M. L. *Langmuir* **2005**, *21*, 10587-10592.

(50) Kotov, N. A. *Nanostruct. Mater.* **1999**, *12*, 789-796.

(51) Pradhan, N.; Pal, A.; Pal, T. *Colloids Surf., A* **2002**, *196*, 247-257.

(52) Ouyang, L.; Malaisamy, R.; Bruening, M. L. *J. Membr. Sci.* **2008**, *310*, 76-84.

(53) Miller, M. D.; Bruening, M. L. *Chem. Mater.* **2005**, *17*, 5375-5381.

(54) Esumi, K.; Miyamoto, K.; Yoshimura, T. *J. Colloid Interface Sci.* **2002**, *254*, 402-405.

(55) Ghosh, S. K.; Mandal, M.; Kundu, S.; Nath, S.; Pal, T. *Appl. Catal., A* **2004**, *268*, 61-66.

(56) Soler, L.; Macanás, J.; Muñoz, M.; Casado, J. *Int. J. Hydrogen Energy* **2007**, *32*, 4702-4710.

(57) Kreevoy, M. M.; Jacobson, R. W. *Ventron Alembic* **1979**, *15*, 2-3.

(58) Vincent, T.; Guibal, E. *Langmuir* **2003**, *19*, 8475-8483.

Chapter 5

Reduction of 4-Nitrophenol with Sodium Formate Using Catalytic Flat-Sheet Membranes Containing Pd Nanoparticles

5.1. Introduction

Alternating adsorption of polyelectrolyte/metal nanoparticle films in porous supports is a convenient method to prepare membrane reactors with high catalytic activity, and this technique also affords control over the amount of catalyst deposited. Another prominent advantage of this membrane-modification method is its applicability to deposition of various catalysts including Au, Pd, Pt, and Ag nanoparticles.[1-7] The previous chapter demonstrated both the preparation of hollow fiber membrane reactors by alternating adsorption of polyelectrolytes and Au nanoparticles and the high catalytic activity of these nanoparticles in the reduction of 4-nitrophenol by $NaBH_4$. Although $NaBH_4$ is a very effective reducing agent, it is highly corrosive and not safe for use in closed systems due to the continuous release of hydrogen gas. A previous study reported that aqueous $NaBH_4$ decomposes completely to $NaBO_2$ and hydrogen gas in 20 min at 75°C,[8] hence, it is necessary to add fresh $NaBH_4$ periodically for reductions that take place over extended periods (>30 min in some cases).

Catalytic transfer hydrogenation with the aid of hydrogen donors is a useful alternative to $NaBH_4$ reduction or classical hydrogenation by H_2.[9,10] The use of a hydrogen donor rather than H_2 avoids the risks and constraints associated with hydrogen gas.[11] Among various hydrogen donors, formic acid and its salts are uniquely reactive,

due to the CO_2 release and subsequent bicarbonate formation that accompany hydrogen donation.[12] Alkali metal formate salts are of particular interest because they are mild in nature and readily available.[13] In addition, formate salts are recyclable hydrogen donors because their dehydrogenated product, bicarbonate salts, can be separated from the reaction mixture and subsequently rehydrogenated to formate under mild reaction conditions.[14] Equation (1) shows the typical catalytic transfer hydrogenation process for reaction of nitroarene and formate, whereas equation (2) represents the regeneration of formate by hydrogenation of the bicarbonate product from equation (1).[15]

$$ArNO_2 + 3HCO_2^- + H_2O \xrightarrow{\text{catalyst}} ArNH_2 + 3HCO_3^- \quad (1)$$

$$HCO_3^- + H_2 \rightleftharpoons HCO_2^- + H_2O \quad (2)$$

In this chapter we use HCOONa, a safer, more cost-effective, and more environmental friendly compound than $NaBH_4$, for reduction of 4-nitrophenol catalyzed by Pd nanoparticles in membranes. Flat-sheet membranes serve as the nanoparticle supports in these preliminary studies.

5.2. Experimental Section

5.2.1. Materials

Poly(sodium 4-styrenesulfonate) (PSS, M_w = 70,000 Da), poly(allylamine hydrochloride) (PAH, M_w = 56,000 Da), poly(ethyleneimine) (PEI, branched, M_w = 25,000 Da), K_2PdCl_6, sodium citrate, sodium formate, and 4-nitrophenol were used as received from Sigma-Aldrich. Poly(acrylic acid) (PAA, M_w=5,000 Da) was purchased from Polysciences and was used without any further purification. Deionized water

(Milli-Q purification system, 18.2 MΩ·cm) was employed for membrane rinsing and preparation of polyelectrolyte or reaction solutions. The pH of the polyelectrolyte solutions was adjusted with dilute HCl or NaOH.

Anodisc alumina membranes with a pore size of 0.2 μm and a membrane thickness of 60 μm were purchased from Whatman. For pretreatment, these membranes were UV/O_3 cleaned (Boekel UV-Clean Model 1135500) with the feed side up for 15 min. Poly(ethersulfone) (PES) microfiltration (MF) flat-sheet membranes were purchased from Sterlitech Corporation (cat. number PES0225100). These membranes have a skin pore size of 0.2 μm and a membrane thickness of 110-150 μm. Prior to modification, about 30 mL of deionized water was passed through these membranes using the setup depicted in Figure 5.3. Figure 5.1 shows the SEM images of the skins and cross-sectional surfaces of the alumina and PES membranes.

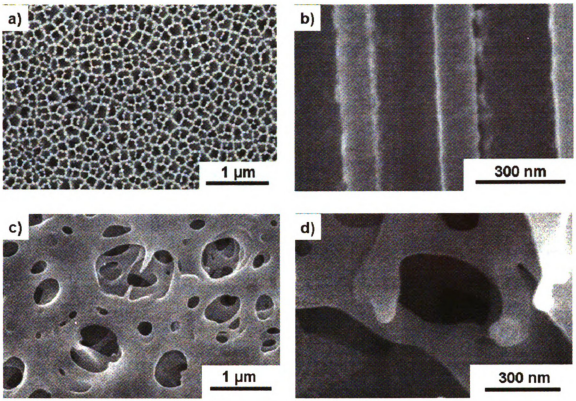

Figure 5.1. SEM images of alumina (a and b) and PES (c and d) flat-sheet membranes. Images (a) and (c) show skin layers, and images (b) and (d) are cross sectional views of the membranes.

5.2.2. Preparation of Citrate-Stabilized Pd Nanoparticles

The Pd nanoparticles were prepared using the well-established citrate reduction method.[3] In a 100 mL round-bottom flask equipped with a condenser, 50 mL of an aqueous 0.393 mM solution of potassium hexachloropalladate(IV) was heated to reflux. A 1% sodium citrate solution (6 mL) was added to the Pd solution, and the mixture was refluxed continuously for 4 h. The resulting dark brown nanoparticle solution was kept in an amber glass bottle and stored in a refrigerator until use. Prior to particle deposition,

the nanoparticle solution was diluted 4:1 with deionized water. TEM studies show that Pd nanoparticles prepared by this method have a diameter of 7 ± 1 nm (Figure 5.2)[16].

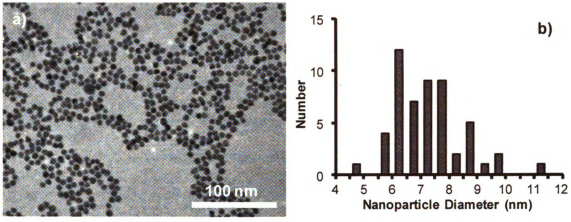

Figure 5.2. a) TEM image of citrate-stabilized Pd nanoparticles. b) Histogram of Pd nanoparticle diameters

5.2.3. Modification of Flat-Sheet Membranes

Both alumina and PES membranes were placed in an ultrafiltration cell (Amicon stirred cell 8010, Millipore, exposed membrane area of 3.1 cm^2) for modification and testing. A peristaltic pump (Cole-Parmer Masterflex C/L) attached to the permeate side of the cell pulled all the solutions through the membranes, and the flow rate was set between 3 and 4 mL/min (Figure 5.3). Deposition started with passage of 10 mL of 0.02 M PAA solution (pH adjusted to 4.5) for alumina membranes and 10 mL of 0.02 M PSS solution (no pH adjustment, pH 6.2) for PES membranes (polyelectrolyte concentrations are always given with respect to the repeating unit). Thirty mL of deionized water was then pumped through the membrane to remove any excess polyelectrolyte. Subsequently, 10 mL of 0.02 M PAH (pH adjusted to 4.5) or 0.02 M PEI (pH adjusted to 9) was passed through the membrane followed by another water rinse. Pd nanoparticles were then

loaded by passage of a citrate-stabilized Pd colloid solution (0.1 mM in Pd atoms) through the membrane until the permeate color changed from colorless to pale brown. (The volume of Pd colloid loading solution was about 50 and 100 mL for PAH-terminated and PEI-terminated films, respectively.) Finally, the coated membrane was rinsed with water and stored until use. All the polyelectrolyte solutions contained 0.5 M NaCl.

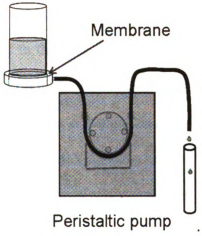

Figure 5.3. Apparatus employed for membrane modification and catalytic reactions.

5.2.4. Characterization of the Flat-Sheet Membranes

SEM images of bare and coated flat-sheet membranes were taken using a Hitachi S-4700 II field-emission scanning electron microscope (FESEM). For skin surface characterization, 5 nm of Au was sputter-coated (Pelco SC-7 auto sputter coater) on the surface before imaging, whereas for cross-sectional images, both the cross section and the skin surface were sputter coated with 5 nm of Au. Membrane cross-sections were prepared as described in chapter 2.

To determine the amount of Pd loading, the membrane was immersed in 1 mL of aqua regia (3 parts HCl and 1 part HNO_3) for 5 min, and this solution was then diluted

and analyzed for Pd by inductively coupled plasma optical emission spectroscopy (ICP-OES) (Varian 710-ES ICP Optical Emission Spectrometer).

5.2.5. Catalytic Reactions and Leaching Studies

The catalytic activities of the modified membranes were examined by reduction of aqueous 4-nitrophenol with HCOONa at room temperature. A solution containing 4-nitrophenol and HCOONa was passed through the membrane using a peristaltic pump as shown in Figure 5.3. Permeate samples were collected at specific time intervals, and the concentration of 4-nitrophenol in the feed and permeate solutions was determined from the solution absorbance at 400 nm.[1,17] (UV-Vis spectra were acquired with a Perkin-Elmer Lambda 40 spectrophotomer.) A typical reaction mixture contained 0.5 mM 4-nitrophenol and 0.05 M HCOONa, with a pH adjusted to 4.5 with dilute formic acid.

To determine the extent of catalyst leaching during the reaction, the amount of Pd in the feed and permeate samples was analyzed using ICP-OES. To qualitatively examine catalyst leaching, I examined the change in 4-nitrophenol concentration in the permeate solution (after exiting the membrane) over time. If leached catalyst is present in the permeate, the reaction should continue to take place after permeation to decrease the 4-nitrophenol concentration in the sample.

5.3. Results and Discussion

Figure 5.4 shows the structures of the polyelectrolytes investigated in this study. PSS is usually deposited first on polymeric membranes due to its hydrophobic interactions with polymer surfaces,[18,19] and because PAA does not adsorb as well on such substrates. In contrast, PAA binds strongly to alumina and serves as the initial layer in

porous alumina membranes. Comparing the polycations branched PEI and PAH, the branched PEI forms thicker films that have more binding sites for noble metal nanoparticles. Thus, films containing PEI have a higher catalyst loading than films containing PAH.

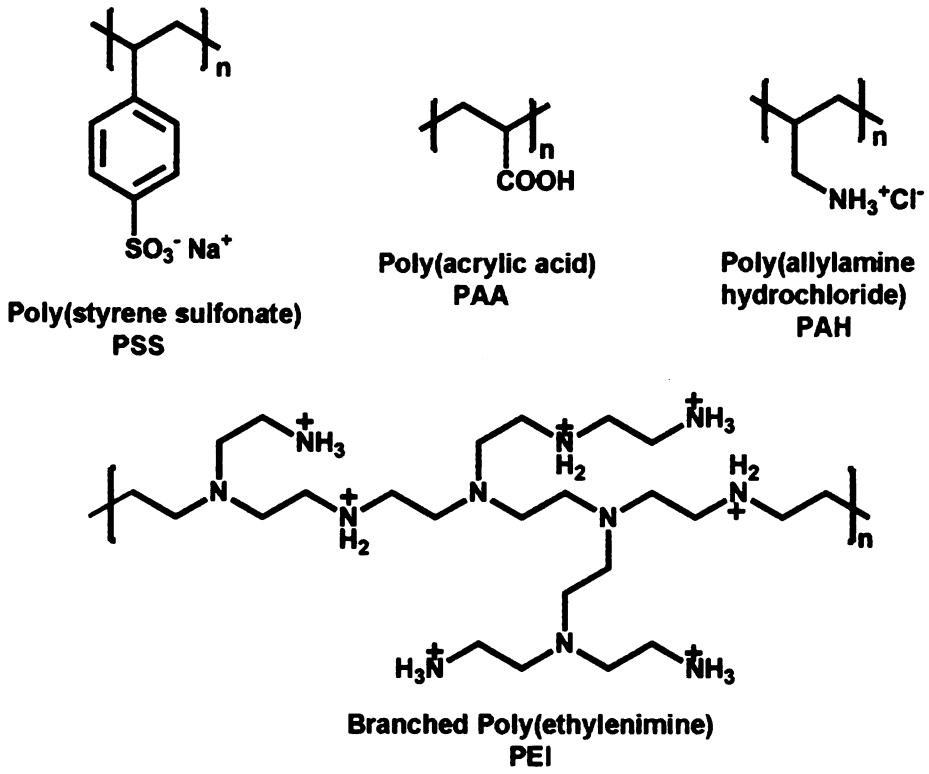

Figure 5.4. Structures of the polyelectrolytes used in this study.

5.3.1. SEM Characterization of Immobilized Nanoparticles

Figure 5.1 shows SEM images of bare alumina and PES membranes. Alumina membranes have standard cylindrical pore structures with a relatively uniform skin pore size distribution, whereas PES membranes have a layered structure and a relatively wide range of skin pore sizes (approximately 0.2-0.5 μm). Moreover, the PES membranes have a smaller porosity than alumina membranes. Although these two substrates differ in

structure, SEM images of the cross-sections of membranes coated with polyanion/PEI/Pd nanoparticle (PdNP) films show that Pd nanoparticles are loaded in the membrane pores of both materials (Figure 5.5). Due to the small size of Pd nanoparticles (7 nm diameter), some aggregation may occur in alumina membranes to give particles that are larger than expected. However, the low resolution of SEM and the sputter coating process could also cause particles to appear larger than their actual size. The density of Pd nanoparticles in PES membranes is not as high as that in alumina membranes, and it is difficult to characterize the small Pd particles in the PES membranes. However, the color of the PES membrane changes from white to dark brown after film deposition, confirming the loading of Pd nanoparticles. ICP-OES analysis also shows that the Pd loading in alumina and PES membranes is 320 μg and 390 μg, respectively. Taking into account the larger PES membrane thickness (110-150 μm) compared to alumina (60 μm), the Pd loading per cm^3 of membrane is lower in PES membranes than in alumina.

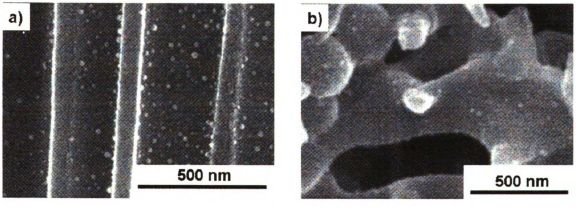

Figure 5.5. SEM images of cross-sections of flat-sheet membranes coated with polyanion/PEI/PdNP films. (a) alumina and (b) PES.

5.3.2. Catalysis with Pd Nanoparticle-Loaded Alumina Membranes

Guibal and coworkers extensively studied reduction of aqueous nitrophenol with HCOONa as the hydrogen donor.[20-22] According to their work, when using a chitosan-supported Pd catalyst, the most rapid nitrophenol reduction occurs at a pH between 3 and 4.[20] Thus, we began our studies by investigating the effect of feed pH on the rate of 4-nitrophenol reduction in modified membranes.

5.3.2.1. Effect of Feed pH on 4-Nitrophenol Conversion

pH is an important variable in catalytic reactions because it affects both the charge of the substrate and the dissociation of the hydrogen donor (HCOONa in this study). Without any adjustment, the pH of the reaction solution (0.5 mM 4-nitrophenol and 0.05 M HCOONa) is 6.2. Passage of this solution through a PAA/PEI/PdNP-coated alumina membrane at a flux of 0.027 mL cm^{-2} s^{-1} (residence time of 68 ms, assuming a 30% porosity) results in the reduction of only ~1% of the 4-nitrophenol. When the pH is adjusted to 4.5, however, passage through the membrane at the same flux yields >99.8% conversion of 4-nitrophenol, and the conversion remains essentially constant over a 5-h reaction period (Figure 5.6). By lowering the feed pH to 4.5, less charge on the citrate-stabilized nanoparticles may facilitate the adsorption of formate ions and 4-nitrophenol onto catalytic active sites and allow for a faster reaction.

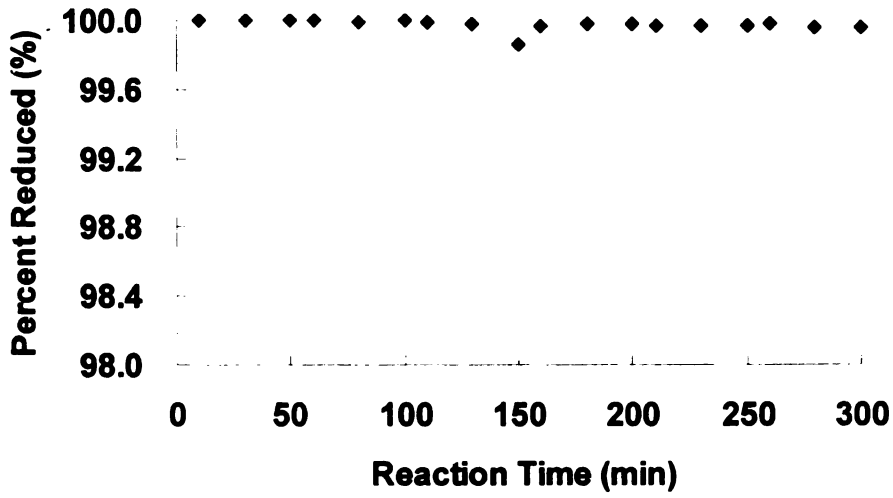

Figure 5.6. Percent reduction of 4-nitrophenol during passage of a 0.5 mM 4-nitrophenol, 50 mM HCOONa aqueous solution (pH adjusted to 4.5) through an alumina membrane coated with a PAA/PEI/PdNP film (flux = 0.027 mL cm^{-2} s^{-1}, residence time in the membrane of 68 ms).

In preliminary experiments with PES membranes, feed solutions at pH 4.5 and 3.8 gave similar conversions, but about 4.6% of the Pd was leached from a PSS/PEI/PdNP membrane at pH 3.8 over an 80-min permeation (0.5 mM 4-nitrophenol, 50 mM HCOONa, flux of 0.035 mL cm^{-2} s^{-1}), whereas only 2.2% of the Pd was leached from a similar membrane at a pH of 4.5 under the same conditions. Because the citrate ions become less charged at low pH, the Pd nanoparticles may be less stable and more subject to leaching at pH 3.8 than at pH 4.5. Thus, we employed a pH of 4.5 for all subsequent studies.

5.3.2.2. Dependence of 4-Nitrophenol Conversion on HCOONa Concentration

At a constant 4-nitrophenol concentration and pH, the percent reduction of 4-nitrophenol upon passage through a catalytic alumina membrane varies significantly with the concentration of HCOONa in the feed solution. Figure 5.7 shows that more than 99.5% of 4-nitrophenol is reduced when 20 mM HCOONa (40-fold excess) is present in the feed. In contrast, conversion is only ~70% when using 10 mM HCOONa (20-fold excess). To insure high rates of reduction, subsequent experiments were performed using 50 mM HCOONa.

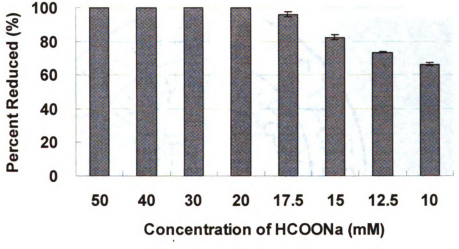

Figure 5.7. Effect of HCOONa concentration on the percent reduction of 4-nitrophenol during passage of a 0.5 mM 4-nitrophenol, HCOONa aqueous solution (pH adjusted to 4.5) through an alumina membrane coated with a PAA/PEI/PdNP film. (flux = 0.027 mL cm^{-2} s^{-1}, residence time in the membrane of 68 ms, conversion was measured after 5 min of permeation)

5.3.2.3. SEM Characterization of Deposit Formation on Alumina Membranes

As noted in the study of Au-catalyzed 4-nitrophenol reduction by $NaBH_4$ (chapter 4), deposits that form on the lumen surface of catalytic hollow fiber membranes might stem from oxidation of aminophenol.[20] Similar deposit formation occurs on the alumina membrane surface during the reduction of 4-nitrophenol with HCOONa. Figure 5.8 shows that stirring the solution above the membrane during the reaction may reduce the amount of material deposited. However, these deposits do not appear in SEM images of the membrane pores, where most of the catalyst is located. Nevertheless, plugging of membrane pores could decrease the available catalyst surface area.

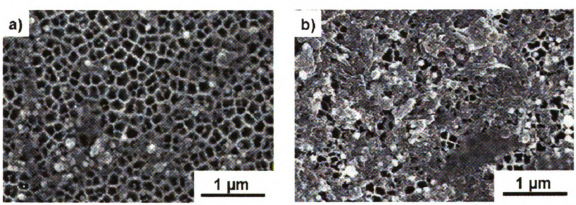

Figure 5.8. SEM images of the skin surfaces of PAA/PEI/PdNP-coated alumina membranes after their use in catalyzing the reduction of 4-nitrophenol by HCOONa (a) with stirring and (b) without stirring of the solution above the membrane. The reaction solution contained 0.5 mM 4-nitrophenol and 50 mM HCOONa, and permeation occurred at a flux of 0.021 mL cm^{-2} s^{-1} for 1 h.

5.3.3. Catalysis with Pd Nanoparticle-Loaded PES Membranes

As mentioned earlier, one advantage of the layer-by-layer (LBL) method is its applicability to different materials including ceramics and polymers. By using PSS as the

initial layer, polyelectrolyte/Pd nanoparticle film formation can take place in PES membranes as well as in porous alumina.

5.3.3.1. 4-Nitrophenol Reduction in PES Membranes Coated with PSS/PEI/PdNP Films

Figure 5.9 shows the percent conversion of 4-nitrophenol during passage through a PES membrane coated with a PSS/PEI/PdNP film. At the beginning of the experiment, 99% of the 4-nitrophenol is reduced, but the conversion decreases gradually to 97% after 1 h. This conversion decline could be due to either catalyst leaching or catalyst fouling.

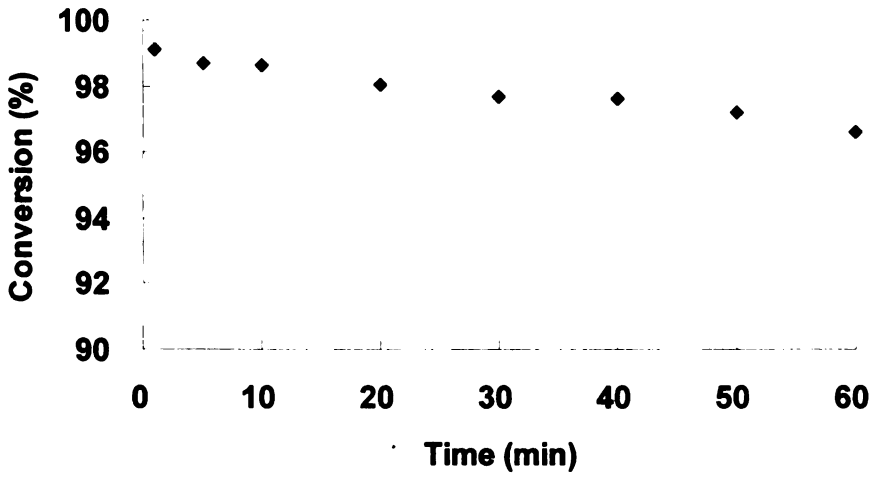

Figure 5.9. Percent reduction of 4-nitrophenol during passage of a 0.5 mM 4-nitrophenol, 50 mM HCOONa aqueous solution (pH adjusted to 4.5) through a PES membrane coated with a PSS/PEI/PdNP film (flux = 0.022 mL cm^{-2} s^{-1}, residence time = 173 ms, assuming 30% porosity).

5.3.3.2. Catalyst Leaching

The above results show that conversion declines over time and that at least some leaching of Pd occurs. Below we first discuss capping of films to minimize leaching along with qualitative and quantitative studies of leaching as a function of flow rate and film composition.

5.3.3.2.1. Use of a Capping Layer to Minimize Catalyst Leaching

One way to minimize catalyst leaching is to add a capping layer on the polyelectrolyte/PdNP films. Because the citrate-stabilized Pd nanoparticles are negatively charged, an additional polycation layer can be deposited to protect the nanoparticles. However, Figure 5.10 shows that conversion still declines dramatically with time during passage of 4-nitrophenol, HCOONa solutions through a PES membrane coated with a PEI-capped (PSS/PEI/PdNP/PEI) film. Almost complete conversion of 4-nitrophenol occurs in the first 5 minutes of the experiment, but a dramatic drop to 85% conversion follows in the next 10 min. We also examined the concentration of 4-nitrophenol in several permeate samples as a function of time elapsed since permeation through the membrane. For the permeate sample taken at 6 min of filtration, conversion increased from 92% to almost complete conversion after the sample sat for one day, which suggests that some Pd is present in the permeate to catalyze continued conversion of the 4-nitrophenol. Smaller increases in conversion with time after permeating through the membrane occurred for subsequent permeate samples. These results suggest that Pd leaching takes place even in the presence of a PEI capping layer, but leaching may be most extensive in earlier stages of permeation. We should note that in a control experiment, the concentration of 4-nitrophenol was constant with time (for at least 1 day) in formate-containing feed solutions.

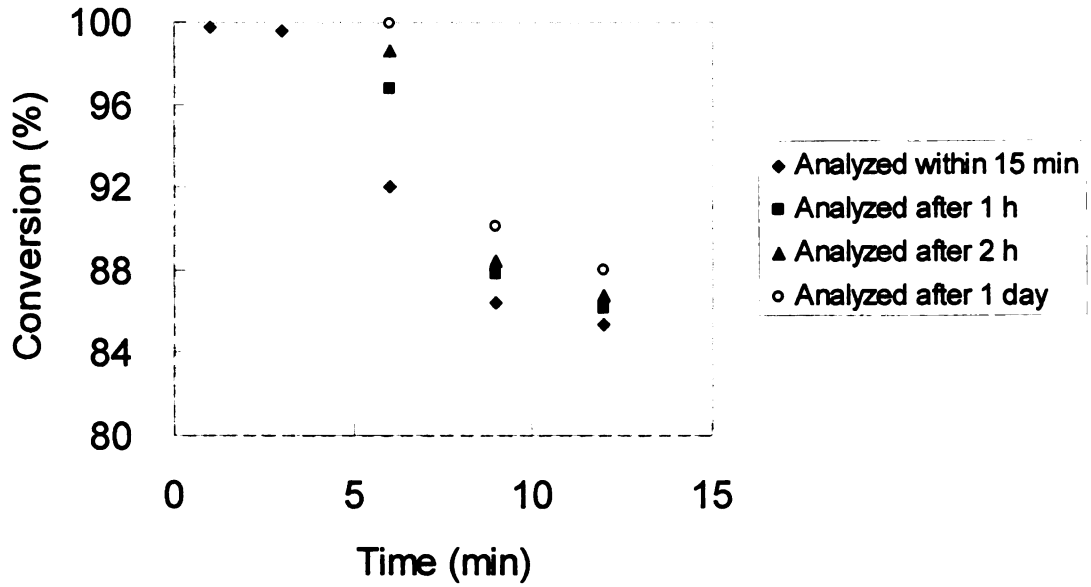

Figure 5.10. Conversion of 4-nitrophenol during passage of a 0.5 mM 4-nitrophenol, 50 mM HCOONa aqueous solution (pH adjusted to 4.5) through a PES membrane coated with a PSS/PEI/PdNP/PEI film (flux = 0.06 mL cm^{-2} s^{-1}, residence time = 67 ms). Samples were analyzed 15 min, diamonds; 1 h, squares; 2 h, triangles; and 1 day, open circles,,after passing through the membrane.

Figure 5.11 shows the conversion as a function of filtration time during passage of a 4-nitrophenol, HCOONa solution through a PES membrane coated with a PSS/PEI/PdNP/PAH film. The conversion, which is lower for this membrane than typical PSS/PEI/PdNP/PAH-coated PES membranes, perhaps because of defects, is essentially constant with permeate volume in this case. For permeate samples taken in the first 5 min, increases in conversion with the time elapsed prior to analysis suggest that there is some Pd in the permeate. However, after the first 6 min of permeation, no detectable changes in 4-nitrophenol concentration appear as a function of time elapsed

prior to analysis. This suggests minimal leaching occurs after 6 min of permeation. Comparison of Figures 5.10 and 5.11 suggests that the PAH capping layer more effectively prevents catalyst leaching than a PEI capping layer, but this conclusion needs further verification. In the following experiments, all polyelectrolyte/PdNP films are capped with a PAH layer.

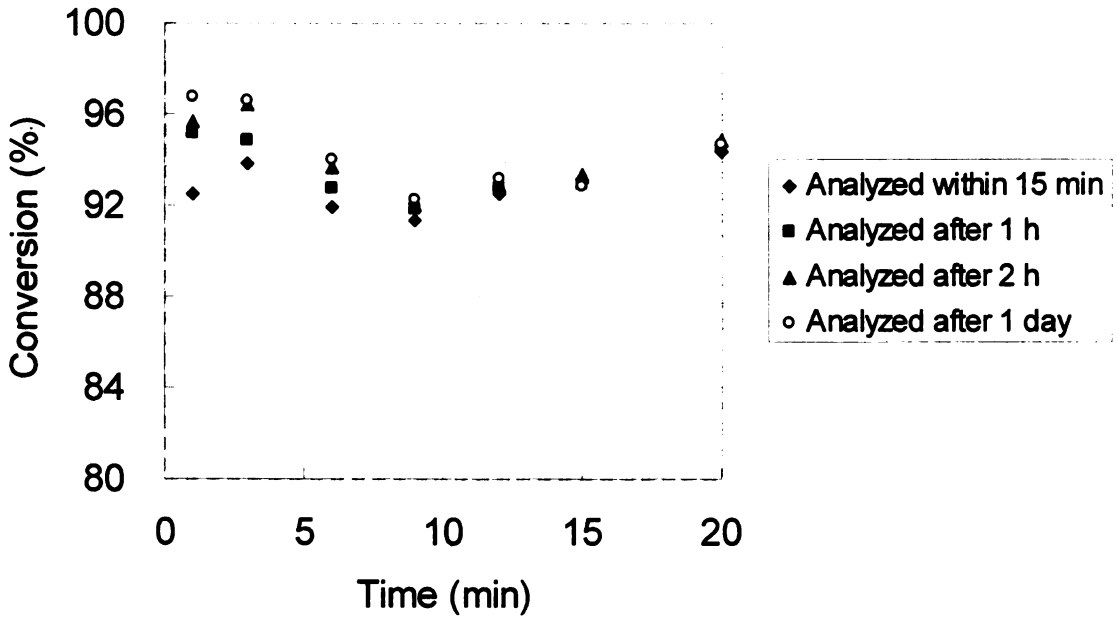

Figure 5.11. Conversion of 4-nitrophenol during passage of a 0.5 mM 4-nitrophenol, 50 mM HCOONa aqueous solution (pH adjusted to 4.5) through a PES membrane coated with a PSS/PEI/PdNP/PAH film (flux = 0.06 mL cm^{-2} s^{-1}, residence time = 67 ms). Samples were analyzed 15 min, diamonds; 1 h, squares; 2 h, triangles; and 1 day, open circles, after passing through the membrane.

5.3.3.2.2. Effect of Solution Flux and Feed Concentration on Catalyst Leaching

To confirm the ability of the PAH capping layer to minimize catalyst leaching, we carried out the reduction reaction at a lower flow rate using a PES membrane coated with

a PSS/PEI/PdNP/PAH film. Figure 5.12 shows that at the lower flux value, more than 99.5% of the 4-nitrophenol is reduced throughout a 1-h permeation, although there is a small conversion decline between 50 and 80 min of permeation. In comparison, a Pd-loaded PES membrane without a capping layer showed a 2% conversion decline in 1 h at an even lower flow rate (Figure 5.9). The comparison between Figure 5.9 and 5.12 suggests that use of PAH is capping layer is helpful to minimize Pd leaching and maintain a high catalytic activity. However, the differences in initial conversions for the two membranes complicate the comparison.

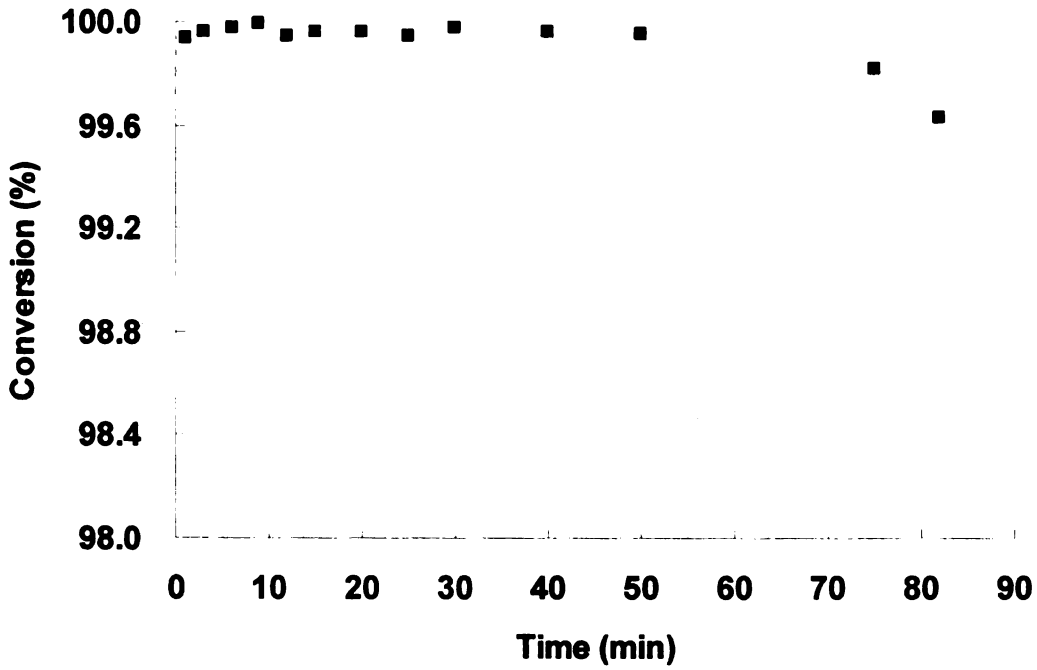

Figure 5.12. Percent reduction of 4-nitrophenol during passage of a 0.5 mM 4-nitrophenol, 50 mM HCOONa aqueous solution (pH adjusted to 4.5) through a PES membrane coated with a PSS/PEI/PdNP/PAH film (flux = 0.035 mL cm^{-2} s^{-1}, residence time =110 ms).

High fluxes might induce more catalyst leaching from the film. To better examine this effect, we increased the flux more than 3-fold relative to the experiment in Figure 5.12. Figure 5.13 shows the conversion change using the PSS/PEI/PdNP/PAH film-coated PES membrane at this high solution flux. Conversion remains more than 99.5% in the first 20 min, but then it drops drastically to as low as 30% in 50 min. ICP-OES analysis of permeate samples and the total loading of the membranes show that about 6.3% of Pd leaches out in this experiment (Figure 5.13) while only 2% Pd leaching is detected when the reduction is carried out at lower flux (Figure 5.12).

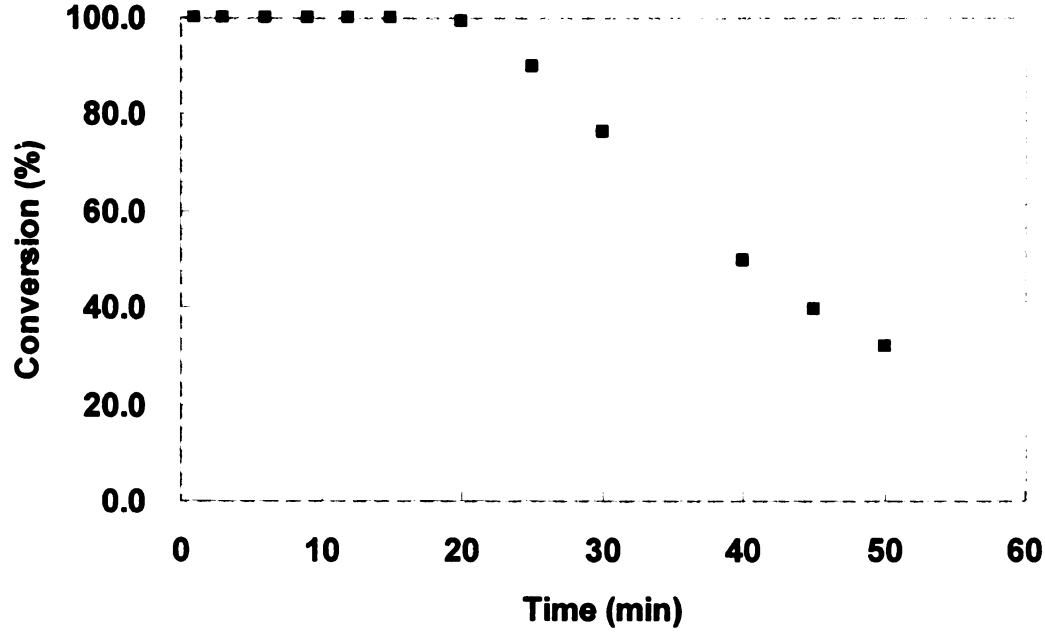

Figure 5.13. Percent reduction of 4-nitrophenol during passage of a 0.5 mM 4-nitrophenol, 50 mM HCOONa aqueous solution (pH adjusted to 4.5) through a PES membrane coated with a PSS/PEI/PdNP/PAH film (flux = 0.12 mL cm^{-2} s^{-1}, residence time =33 ms).

The high solution flux could result in greater shear forces that enhance catalyst leaching, but another possible explanation for decreases in catalytic activity is that at higher flux, more 4-nitrophenol is reduced and more catalyst fouling may occur. (In fact, leaching of 2 to 6% of the Pd may have only a minor effect on catalytic activity.) To differentiate between the effects of flux and fouling, we performed 4-nitrophenol reduction at a the flow rate used to obtain Figure 5.13 but with a feed that contains only 0.1 mM 4-nitrophenol with 100 fold excess HCOONa. Under these conditions, more than 99.6% of the 4-nitrophenol is reduced without any significant conversion decline over 45 min (Figure 5.14). This suggests that the primary reason for conversion decline is catalyst fouling from byproducts of 4-aminophenol and that fouling is a function of the amount of material reacted at the catalyst. However, comparison of the amount of Pd in the permeate solution and in the membrane after this experiment did indicate 8.7% Pd leaching with most leaching happened in the early stage of the experiment.

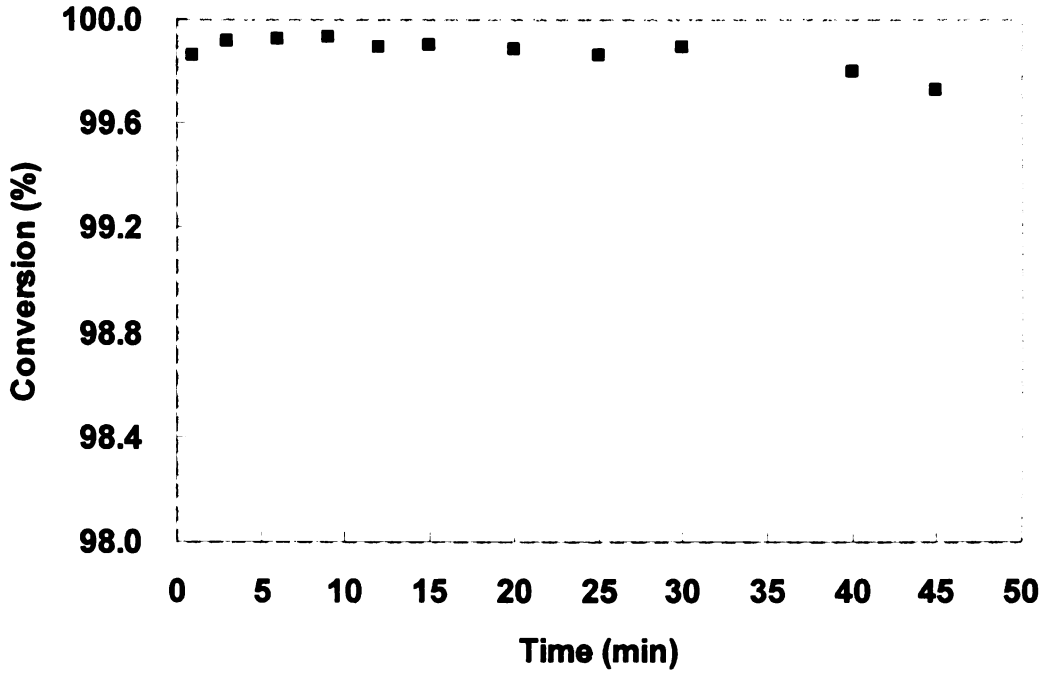

Figure 5.14. Percent reduction of 4-nitrophenol during passage of a 0.1 mM 4-nitrophenol, 10 mM HCOONa aqueous solution (pH adjusted to 4.5) through a PES membrane coated with a PSS/PEI/PdNP/PAH film (flux = 0.12 mL cm^{-2} s^{-1}, residence time =33 ms).

Figure 5.15 shows the conversion of 4-nitrophenol using a feed solution containing 0.1 mM 4-nitrophenol with 100 fold excess HCOONa at a high solution flux over a 3-h reaction period. Conversion remains essentially constant at >99.5% for 150 min and deceases to 85% in the last 30 min. Pd leaching mainly happens during the first 60 min and less than 2 ppb Pd is detected in the permate during the rest of the experiment. This result confirms that the conversion decline is not due to catalyst leaching. As mentioned above, we speculate that the conversion decline after 150 min is the result of

catalyst fouling by oxidation products of 4-aminophenol. The precipitous drop in conversion may occur as pores become fully occluded.

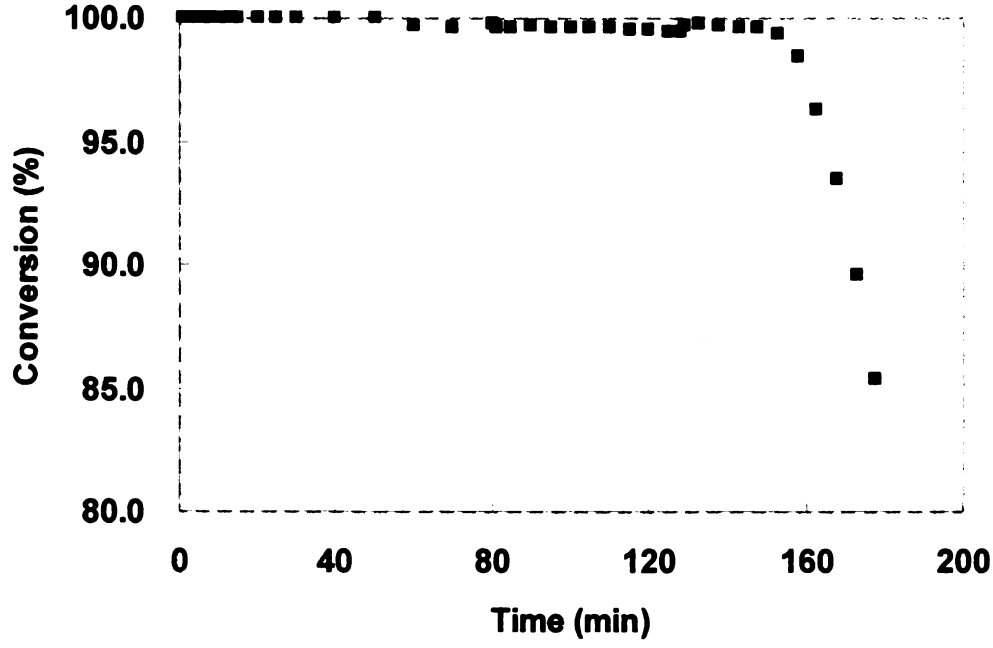

Figure 5.15. Percent reduction of 4-nitrophenol during passage of a 0.1 mM 4-nitrophenol, 10 mM HCOONa aqueous solution (pH adjusted to 4.5) through a PES membrane coated with a PSS/PEI/PdNP/PAH film (flux = 0.12 mL cm^{-2} s^{-1}, residence time =33 ms).

5.4. Conclusions

Layer-by-layer adsorption of polyelectrolytes and Pd nanoparticles in porous membranes yields catalytic reactors that are active in the reduction of 4-nitrophenol with HCOONa, which is a more cost-effective and environment friendly reagent than $NaBH_4$. This LBL method is applicable to both ceramic and polymeric materials, and the resulting membranes allow a high conversion of 4-nitrophenol to 4-aminophenol, but the catalytic

activity declines over time. When low concentrations of reactants pass through the membrane at relatively low flow rates, high catalytic activities can be maintained for several hours, but higher flow rates and 4-nitrophenol concentrations lead to more rapid conversion declines. The decline in conversion is probably due to catalyst fouling, which may stem from the oxidation aminophenol, as we noted earlier in the study of Au-catalyzed reduction of 4-nitrophenol with $NaBH_4$.

5.5. References

(1) Dotzauer, D. M.; Dai, J.; Sun, L.; Bruening, M. L. *Nano Lett.* **2006**, *6*, 2268-2272.

(2) Dotzauer, D. M.; Bhattacharjee, S.; Wen, Y.; Bruening, M. L. *Langmuir* **2009**, *25*, 1865-1871.

(3) Dokoutchaev, A.; James, J. T.; Koene, S. C.; Pathak, S.; Prakash, G. K. S.; Thompson, M. E. *Chem. Mater.* **1999**, *11*, 2389-2399.

(4) Dotzauer, D. M.; Abusaloua, A.; Miachon, S.; Dalmon, J.-A.; Bruening, M. L. *Appl. Catal., B* **2009**, *91*, 180-188.

(5) Feng, Z.; Yan, F. *Surf. Interface Anal.* **2008**, *40*, 1523-1528.

(6) Goulet, P. J. G.; dos Santos, D. S.; Alvarez-Puebla, R. A.; Oliveira, O. N.; Aroca, R. F. *Langmuir* **2005**, *21*, 5576-5581.

(7) Puniredd, S. R.; Yin, C. M.; Hooi, Y. S.; Lee, P. S.; Srinivasan, M. P. *J. Colloid Interface Sci.* **2009**, *332*, 505-510.

(8) Soler, L.; Macanás, J.; Muñoz, M.; Casado, J. *Int. J. Hydrogen Energy* **2007**, *32*, 4702-4710.

(9) Brieger, G.; Nestrick, T. J. *Chem. Rev.* **1974**, *74*, 567-580.

(10) Johnstone, R. A. W.; Wilby, A. H.; Entwistle, I. D. *Chem. Rev.* **1985**, *85*, 129-170.

(11) Basu, B.; Das, P.; Das, S. *Mol. Diversity* **2005**, *9*, 259-262.

(12) Rajagopal, S.; Spatola, A. F. *J. Org. Chem.* **1995**, *60*, 1347-1355.

(13) Zoran, A.; Sasson, Y.; Blum, J. *J. Mol. Catal.* **1984**, *26*, 321-326.

(14) Wiener, H.; Blum, J.; Feilchenfeld, H.; Sasson, Y.; Zalmanov, N. *J. Catal.* **1988**, *110*, 184-190.

(15) Wiener, H.; Blum, J.; Sasson, Y. *J. Org. Chem.* **1991**, *56*, 4481-4486.

(16) Dotzauer, D. M., Ph. D Dissertation, Michigan State University, 2009.

(17) Pradhan, N.; Pal, A.; Pal, T. *Colloids Surf., A* **2002**, *196*, 247-257.

(18) Malaisamy, R.; Bruening, M. L. *Langmuir* **2005**, *21*, 10587-10592.

(19) Ouyang, L.; Malaisamy, R.; Bruening, M. L. *J. Membr. Sci.* **2008**, *310*, 76-84.

(20) Vincent, T.; Guibal, E. *Langmuir* **2003**, *19*, 8475-8483.

(21) Guibal, E.; Vincent, T. *J. Environ. Manage.* **2004**, *71*, 15-23.

(22) Vincent, T.; Guibal, E. *Environ. Sci. Technol.* **2004**, *38*, 4233-4240.

Chapter 6

Summary and Future Work

This dissertation investigates two applications of functional membranes prepared with layer-by-layer (LBL) adsorption: ion separations and catalysis. Chapters 2 and 3 describe high-flux nanofiltration (NF) membranes that selectively remove multivalent ions in the presence of monovalent ions, and the formation of these membranes through LBL adsorption of polycations and polyanions allows tuning of separations through control over the terminating layer. Deposition parameters such as number of bilayers and the pH and ionic strength of the polyelectrolyte deposition solutions can be varied to optimize cation or anion separations. The best membranes prepared in these studies exhibit both higher fluxes and higher selectivities than commercially available NF membranes. Chapters 4 and 5 discuss catalytic membrane reactors that contain a high density of well separated metal nanoparticles deposited by LBL adsorption of polyelectrolytes and metal nanoparticles. This adsorption method occurs with substrates of different geometries (hollow fiber and flat sheet membranes) and various noble metal nanoparticles including Au and Pd. Hollow fiber membrane reactors loaded with Au nanoparticles show high catalytic activity in the reduction of 4-nitrophenol with $NaBH_4$, and >99% initial conversion of 4-nitrophenol to 4-aminophenol by HCOONa also takes place in flat sheet membranes containing Pd nanoparticles. However, a slight conversion decline over time appears in both hollow fiber and flat sheet membranes. This conversion decline probably stems from catalyst fouling by byproducts of 4-aminophenol oxidation.

Although polyelectrolyte multilayer films (PEMs) on ultrafiltration supports show promising NF properties, there are still several challenges to overcome in this area. Because electrostatic interactions hold the layers together, the film structure is sensitive to changes in solution pH or ionic strength.[1-3] Release of polymer material and even hole formation occur upon dramatic changes in pH or ionic strength.[3,4] One way to overcome this instability is to incorporate covalent bonding between different layers in the film. Several studies reported formation of covalently linked PEMs through UV- or heat-induced cross-linking.[5-7] Perhaps the biggest challenge in utilizing PEMs is that their formation involves many adsorption and rinsing steps. The use of spin- and spray-coating methods could potentially speed up the film formation process[8-10] and facilitate the commercial application of PEMs.

Because Donnan exclusion plays an important role in ion separations with NF membranes, increasing the charge density at the surface of PEMs improves their ion-transport selectivities. One way to increase surface charge is to prepare the terminating polyelectrolyte layer in a deposition solution of high ionic strength.[11-13] Another approach is to introduce net, fixed charge into the PEMs by partial derivatization of polyelectrolytes with photolabile functional groups that photolyze to charged species.[14] While the underivatized ionic functional groups allow for formation of PEMs through electrostatic interactions, postdeposition UV irradiation of partially derivatized films results in the formation of fixed-charge sites that are not charge compensated by a neighboring polyelectrolyte. Such sites may greatly increase cation or anion selectivities.

This thesis describes preliminary work on developing catalytic membrane reactors through LBL adsorption of polyelectrolytes and metal nanoparticles. One important

advantage of the LBL method is its ability to control the catalyst location in a tubular membrane.[15] In a gas-liquid reaction, localization of the catalyst at the interior of a tubular membrane (Figure 6.1) can increase catalytic activity. The combination of hollow fiber membranes, whose geometry provides a high surface area to volume ratio, with catalyst localization in the fiber may further enhance the region of gas-liquid-catalyst contact to facilitate gas-liquid reactions.[16-18]. Such a membrane reactor system might be useful in applications including hydrogenation and oxidation reactions.[19-21]

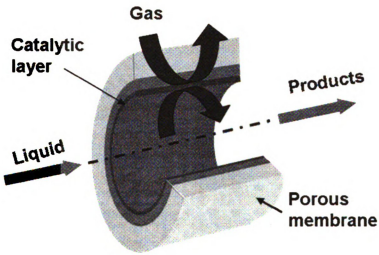

Figure 6.1. Schematic diagram of a gas-liquid contactor in a hollow fiber membrane.

Several recent studies utilized star polymers with globular architecture and multiple arms in LBL assembly.[22,23] Due to their unique mechanical properties and significantly higher degree of functionality compared to linear analogues, star polymers can serve as an inexpensive alternative to dendrimers for stabilizing catalytic metal nanoparticles.[24-27] Because the thickness of LBL films of star polymers is comparable to

that of conventional PEMs,[23] their high charge density make these materials promising in forming highly selective membranes in ion separations.

Overall, the versatility of LBL assembly should allow for formation of a wide range of membrane compositions to further improve both catalytic and NF membranes. However, issues of stability and the economic feasibility of the LBL procedure must be addressed.

References

(1) Itano, K.; Choi, J.; Rubner, M. F. *Macromolecules* **2005**, *38*, 3450-3460.

(2) Ladhari, N.; Hemmerl, J.; Haikel, Y.; Voegel, J.-C.; Schaaf, P.; Ball, V. *Appl. Surf. Sci.* **2008**, *255*, 1988-1995.

(3) Mjahed, H.; Voegel, J.-C.; Senger, B.; Chassepot, A.; Rameau, A.; Ball, V.; Schaaf, P.; Boulmedais, F. *Soft Matter* **2009**, *5*, 2269-2276.

(4) Dejeu, J.; Diziain, S.; Dange, C.; Membrey, F.; Charraut, D.; Foissy, A. *Langmuir* **2008**, *24*, 3090-3098.

(5) Ma, N.; Wang, Y.; Wang, Z.; Zhang, X. *Langmuir* **2006**, *22*, 3906-3909.

(6) Dai, J.; Jensen, A. W.; Mohanty, D. K.; Erndt, J.; Bruening, M. L. *Langmuir* **2001**, *17*, 931-937.

(7) Wu, G.; Shi, F.; Wang, Z.; Liu, Z.; Zhang, X. *Langmuir* **2009**, *25*, 2949-2955.

(8) Schlenoff, J. B.; Dubas, S. T.; Farhat, T. *Langmuir* **2000**, *16*, 9968-9969.

(9) Lee, S.-S.; Hong, J.-D.; Kim, C. H.; Kim, K.; Koo, J. P.; Lee, K.-B. *Macromolecules* **2001**, *34*, 5358-5360.

(10) Bruening, M.; Dotzauer, D. *Nat. Mater.* **2009**, *8*, 449-450.

(11) Stanton, B. W.; Harris, J. J.; Miller, M. D.; Bruening, M. L. *Langmuir* **2003**, *19*, 7038-7042.

(12) Malaisamy, R.; Bruening, M. L. *Langmuir* **2005**, *21*, 10587-10592.

(13) Ouyang, L.; Malaisamy, R.; Bruening, M. L. *J. Membr. Sci.* **2008**, *310*, 76-84.

(14) Dai, J.; Balachandra, A. M.; Lee, J. I.; Bruening, M. L. *Macromolecules* **2002**, *35*, 3164-3170.

(15) Dotzauer, D. M.; Abusaloua, A.; Miachon, S.; Dalmon, J.-A.; Bruening, M. L. *Appl. Catal., B* **2009**, *91*, 180-188.

(16) Israni, S. H.; Nair, B. K. R.; Harold, M. P. *Catal. Today* **2009**, *139*, 299-311.

(17) Peirano, F.; Vincent, T.; Quignard, F.; Robitzer, M.; Guibal, E. *J. Membr. Sci.* **2009**, *329*, 30-45.

(18) Lebedeva, V. I.; Gryaznov, V. M.; Petrova, I. V.; Volkov, V. V.; Tereshchenko, G. F.; Shkol'nikov, E. I.; Plyasova, L. M.; Kochubey, D. I.; van der Vaart, R.; van Soest-Verecammen, E. L. J. *Kinet. Catal.* **2006**, *47*, 867-872.

(19) van der Vaart, R.; Lebedeva, V. I.; Petrova, I. V.; Plyasova, L. M.; Rudina, N. A.; Kochubey, D. I.; Tereshchenko, G. F.; Volkov, V. V.; van Erkel, J. *J. Membr. Sci.* **2007**, *299*, 38-44.

(20) Caro, J.; Caspary, K. J.; Hamel, C.; Hoting, B.; Kolsch, P.; Langanke, B.; Nassauer, K.; Schiestel, T.; Schmidt, A.; Schomacker, R.; Seidel-Morgenstern, A.; Tsotsas, E.; Voigt, I.; Wang, H.; Warsitz, R.; Werth, S.; Wolf, A. *Ind. Eng. Chem. Res.* **2006**, *46*, 2286-2294.

(21) Sirkar, K. K.; Shanbhag, P. V.; Kovvali, A. S. *Ind. Eng. Chem. Res.* **1999**, *38*, 3715-3737.

(22) Connal, L. A.; Li, Q.; Quinn, J. F.; Tjipto, E.; Caruso, F.; Qiao, G. G. *Macromolecules* **2008**, *41*, 2620-2626.

(23) Kim, B.-S.; Gao, H.; Argun, A. A.; Matyjaszewski, K.; Hammond, P. T. *Macromolecules* **2009**, *42*, 368-375.

(24) Yoo, H.-S.; Watanabe, T.; Hirao, A. *Macromolecules* **2009**, *42*, 4558-4570.

(25) Hirao, A.; Watanabe, T.; Ishizu, K.; Ree, M.; Jin, S.; Jin, K. S.; Deffieux, A.; Schappacher, M.; Carlotti, S. *Macromolecules* **2009**, *42*, 682-693.

(26) Hirao, A.; Matsuo, A.; Watanabe, T. *Macromolecules* **2005**, *38*, 8701-8711.

(27) Zheng, Q.; Pan, C.-Y. *Macromolecules* **2005**, *38*, 6841-6848.

MICHIGAN STATE UNIVERSITY LIBRARIES
3 1293 03063 1505